Renewable Materials from Renewable Resources

Guangmao Tian

Doctor of Philosophy

University of York

Chemistry

September 2015

Abstract

Renewable resources related to biomass, waste materials and recycled materials are an important concept in the principles of green chemistry, development of biorefineries and sustainability development. This thesis reports the repurposing of renewable resources which included wheat straw, biomass ash, waste cardboard (paper) and paper de-inking residues (DIR) to extract, synthesize and produce potentially high value chemicals, materials and composites.

Biosilicate solutions were successfully extracted from biomass ash including wheat straw ash and miscanthus ash with aqueous potassium hydroxide solutions. Systematic analyses had been applied on the extraction of biosilicate solutions to obtain different types of silicate solutions for further applications of binder and mesoporous materials. Biosilicate solutions extracted from miscanthus ash were utilized as binders to make bioboards, whilst biosilicate solutions extracted from wheat straw ash were utilized as a silica resource to synthesize biobased mesoporous materials, namely bio-MCM-41 and bio-SBA-15. N_2 porosimetry analysis revealed that mesoporous silica made from biosilicate solutions gave a surface area of bio-MCM-41 of >1000 $m^2\,g^{-1}$ and a surface area of >800 $m^2\,g^{-1}$ for bio-SBA-15. XRD, SEM and TEM analyses for both bio-MCM-41 and bio-SBA-15 revealed significant ordering pores, structure and the hexagonal arrays. Different kinds of renewable resources including wheat straw, pea pod waste and paper de-inking residue with the binder of biosilicate solutions and other chemical additives such as protein and starch were processed to bioboards. Also, wheat straw powder was added into cardboard/paper sheets to decrease the cost of paper manufacture and to improve mechanical properties. De-waxed wheat straw cardboard/paper sheets was successfully incorporated in to paper pulp to give a tensile index of 30-34 Nm/g similar with respect to conventional cardboard paper (tensile index of 30-32 Nm/g). A brief study to elicit sugars to the surface of cardboard/paper thus producing an *in-situ* sticky surface using low temperature microwave irradiation was conducted. Although it's not conclusive, an aqueous fraction was expelled that contains organic matter (based on C-H stretch absorption bands noted in FT-IR), which may be due to sugars.

List of Contents

List of Figures

List of Tables

Acknowledgements

Firstly, I would like to thank Dr. Avtar S. Matharu for his wise and scrupulous supervision through my PhD study in York. During the four years' research, Dr. Avtar S. Matharu lead, encouraged, motivated, helped and inspired me in various field. He gave me great help, encouragement and patience when my father met an accident in 2014. I do appreciate all opportunities to attend different international conferences, training courses and the experiences working with industries that he provided. I appreciate Professor James Clark for providing the opportunity to carry out my research in Green Chemistry of Excellence Centre. Especially, I would like to thank Dr Duncan J. Macquarrie for his suggestions, guidance and comments on my PhD work.

Thanks must also go to Chris Mortimer and Dr Mario de Bruyn for the training and setup of hot-press. I would like to thank Dr. Pedro Aguiar for his help with solid-state NMR, Dr. Helen Parker for her help with ICP-MS and Dr. Meg Stark for her help with SEM and TEM. I would also like to thank Dr. Rob McElroy and Dr. Peter Hurst for the help with pre-treatment of biomass and ash. Thanks to Paul Elliott and Dr. Hannah Briers for their technical assistance in the last four years.

I would like to thank Cheng Ding, Tengyao Jiang, Yuan Yuan and Zhanrong Zhang for the help with my research in the past five years.

Finally to my parents (Father: Gaowen Tian; Mother: Xiqian Wu), wife (Xiaofei Yu) and children (Zongye Tian and Yuyao Tian). Thank you very much for your love and support that allowed me to get this point. Thank you very much for everything you had done for me.

Author's Declaration

I hereby declare that all the work presented in this thesis is my own, except some of the results acknowledged. This work has not previously been presented for an award at this, or any other, University. All sources are acknowledged as References.

Chapter 1: Introduction

1.1 Thesis scope and contextualisation

This thesis aims to develop potentially new bio-based or bio-derived materials and application from (bio) renewable waste, by-product or under-utilised resources. Opportunities from four main resource types are investigated, often inter-related within composites:

i. Wheat straw as the main aggregate for bioboards (at times blended with pea pod wastes) and as a minor component in new re-cycled paper formulations;

ii. Wheat straw and miscanthus ash as the main source of biosilicate binder and mesoporous silica (bio-MCM-41 and bio-SBA-15), respectively;

iii. Waste cardboard/paper as a source of *in-situ* bioadhesive via low temperature microwave processing, and;

iv. De-inking residue (DIR) as the main aggregate for bioboards.

Waste reduction or minimisation is a global grand challenge. With increasing global population, urbanisation and accessibility to *disposable* consumer goods, solid waste generation is estimated to exceed 11 million tonnes per day by 2100.[1] Food and horticultural waste are major contributors to global waste; 1.3 billion tonnes of food is wasted per annum.[2] Today, Mexico City's Bordo Poniente and Shanghai's Laogang receive more than 10,000 tonnes of waste per day. Globally, the estimated 2,000 waste incinerators are full to capacity adding to increased air (gaseous and airborne particulate matter) and land pollution (ash disposal).[1] Accumulation at landfill sites and decomposition of general uncollected waste contributes to the environmental burden through the release of methane gas, which is 23 times more potent than CO_2 as a greenhouse gas.

The UK generates in excess of 100 million tonnes of carbon-containing municipal, commercial and industrial solid waste. The 2014 “House of Lords Science and Technology Committee Third Report “Waste or resource? Stimulating a bioeconomy” highlights a significant market for renewable chemicals, already estimated $57bn worldwide and forecast to rise to $83 billion by 2018.[3] The Chemistry Growth Partnership’s, “Chemistry at Work" sector strategy reports that utilising biomass or waste as a raw material benefits of £8 billion and potential to grow the gross value added (GVA) of the sector from £195 billion to £300 billion by 2030.[3] The EU bioeconomy (not restricted to waste feedstocks) has a turnover of nearly €2 trillion, employs more than 22 million people, predominantly in rural areas and often in SMEs, and represents 9% of total employment in the EU. In addition, each euro invested in EU-funded bioeconomy research and innovation is estimated to trigger €10 of value added in bioeconomy sectors by 2025.[4]

1.1.1 Green Chemistry

"Green Chemistry is the utilisation of a set of principles that reduces or eliminates the use or generation of hazardous substances in the design, manufacture and application of chemical products."[5]

With the issues of environmental pollution, risk of human health and the consumption of materials and resources, green processes and green products has been a great awareness to the public. The popularity of Green Chemistry also has grown rapidly in last few years. The Twelve Principles of Green Chemistry (listed below), as outlined in 'Green Chemistry: Theory and Practice'[5], have been established to promote sustainable chemistry research and development.

1. It is better to prevent waste than to treat or clean up waste after it has been created.
2. Synthetic methods should be designed to maximize the incorporation of all materials used in the process into the final product.
3. Wherever practicable, synthetic methods should be designed to use and generate substances that possess little or no toxicity to human health and the environment.
4. Chemical products should be designed to effect their desired function while minimizing their toxicity.
5. The use of auxiliary substances (e.g., solvents, separation agents, etc.) should be made unnecessary wherever possible and innocuous when used.
6. Energy requirements of chemical processes should be recognized for their environmental and economic impacts and should be minimized. If possible, synthetic methods should be conducted at ambient temperature and pressure.

7. A raw material or feedstock should be renewable rather than depleting whenever technically and economically practicable.
8. Unnecessary derivatization (use of blocking groups, protection/ deportation, temporary modification of physical/chemical processes) should be minimized or avoided if possible, because such steps require additional reagents and can generate waste.
9. Catalytic reagents (as selective as possible) are superior to stoichiometric reagents.
10. Chemical products should be designed so that at the end of their function they break down into innocuous degradation products and do not persist in the environment.
11. Analytical methodologies need to be further developed to allow for real-time, in-process monitoring and control prior to the formation of hazardous substances.
12. Substances and the form of a substance used in a chemical process should be chosen to minimize the potential for chemical accidents, including releases, explosions, and fires.

These principles will be applied as much as possible in this thesis. Especially, most of the raw materials used in this project are waste products (principle 7) and the products synthesised from this project will have higher value than original materials (principle 9). Utilisation of biomass, agriculture residue, waste materials and low value resource represents an excellent opportunity and development for next generation resource in chemical industries. in 2011 by Pike Research reported a value of $2.98 billion for green chemistry markets with the potential value of the market expected to reach $98.5 billion at 2020.[6] Novel applications and products based on the 12 principles of green chemistry[1] (waste as a resource, bio-based or renewable materials) could save the chemical industry approximately $65.5 billion by 2020.

1.1.2 The Biorefinery Concept

The definition or concept of Biorefinery is "an integrated factory to process crops (biomass) in to "refined" fractions". A biorefinery provides an alternative and sustainable approach for energy and chemical needs. Also, in the biorefinery, parts of recycled and refined materials are reused in other process to reduce the waste and increase the value of materials. A simple schematic diagram of a possible wheat straw biorefinery as applicable to the work in this thesis is shown in Figure 1.1.

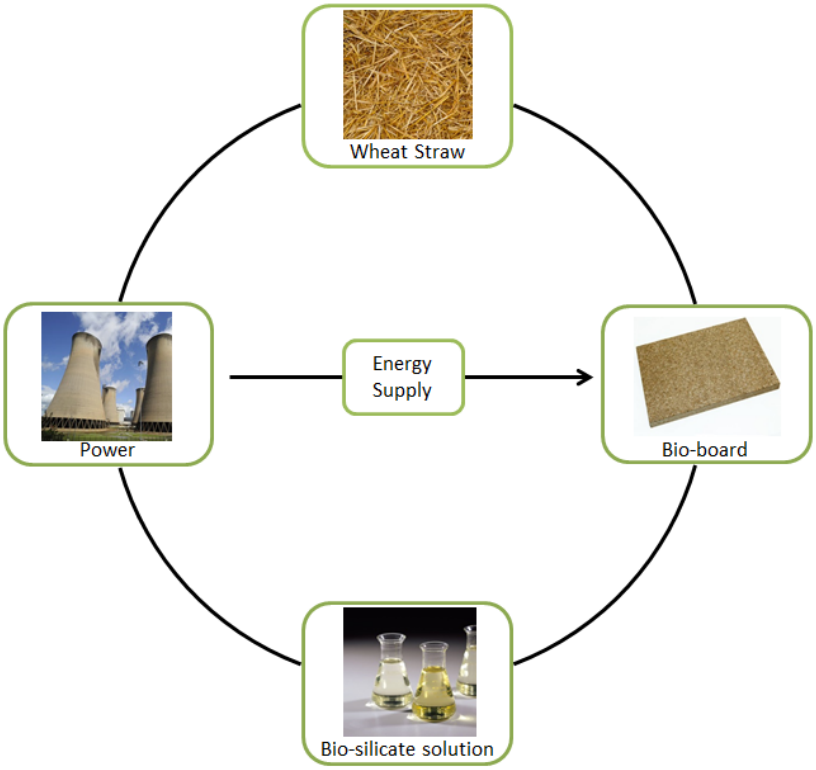

Figure 1.1 Schematic diagram showing a simple Biorefinery process from agricultural waste (wheat straw) to chemicals, boards and energy

The UK generates approximately 12 million tonnes of agricultural straws, namely wheat, miscanthus and barley.[7] According to the statistics at 2008, cereal and oilseed straw is concentrated in the Eastern parts of UK.[8] About 70% of wheat straw and 55% of winter barley straw is mostly produced in the Yorkshire, the Humber region, East Midlands, Eastern Regions and South East Regions.[8] About 57% of spring barley straw is produced in the North and South East of Scotland, Eastern Regions and the South West Regions of England.[8] Allowing for the current straw use in livestock and other industries, there would be approximately 3 million tonnes annual cereal straw surplus concentrated in the East of England. In 2011, UK wheat productions had an average level of 7.7t/ha with the area grown of 1,969,382ha.[9, 10] According to the estimate in 2011, and 100% dry weight wheat at harvest contained three parts: 51% of grain, 43% of stem and leaves materials and 6% chaff. In the stem and leaves materials, there were 60% straw materials can be collected for further applications.[9, 10]

Ely Power Station, the first straw fuelled power station in UK[11] produces over 270 GWh of renewable energy each year.[12] Consequently, Ely Power Station generates about 3,000 tonnes of fly ash and 10,000 tonnes of bottom per annum.[11] Thus, agricultural straw serves an important biorefinery feedstock as exemplified in Figure 1.1, whereby an agricultural waste product such as wheat straw is combusted for renewable energy and the resultant ash serves as a feedstock for biosilicate solution, a bio-derived binder. Combination of the latter with virgin wheat straw affords a bioboard or renewable article/product. This process suggests a sustainable, low-cost, low-toxic & low-risk novel approach for chemistry research and industry. For further applications of biomass ash, the advances on preparation of silica and carbon derived materials from ash are shown in Figure 1.2. It is suggested that bio-silica in biomass ash can also be recycled and reused for preparing high value chemicals and materials, such as SiO_2, Si_3N_4, $SiCl_4$ and SiC. In addition, porous carbon materials can be fabricated from bio-mass ash as well.[13]

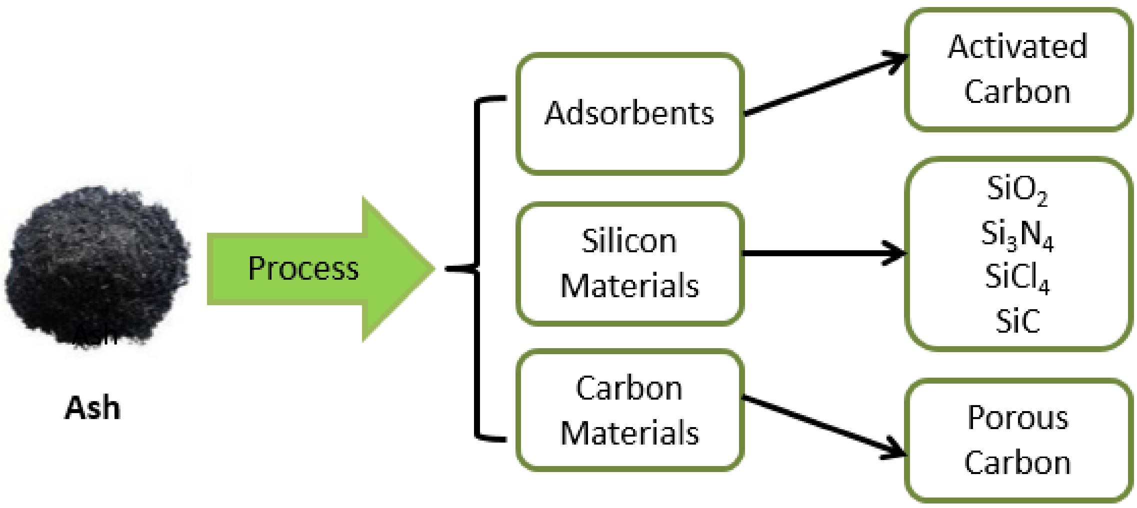

Figure 1.2 Alternative applications of bio-mass ash[13]

1.2 Wheat straw characterization

Wheat straw comprises two parts: stem and leaves (Figure 1.3). The stem is composed of node (5 wt%) and internode (68 wt%), and the leaf comprises approximately 20 wt%.

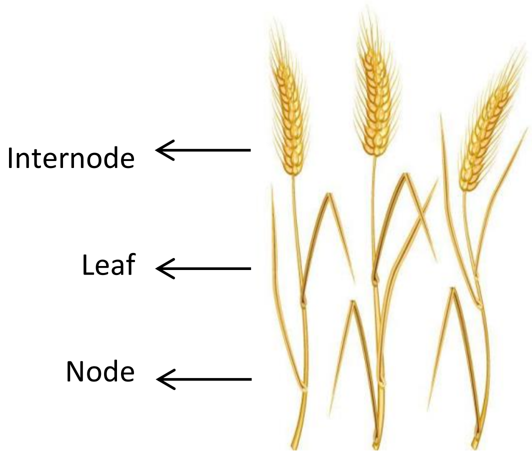

Figure 1.3 Structure of wheat straw

Wheat straw, rich in fibre, is essentially provides structure and rigidity to the whole plant.[14] The chemical proportion of different parts in straw is different. Internodes and leaves have much more cellulosic matter than nodes which are rich of lignin.[15] As the surfaces of leaves contain a waxy layer and inorganic substances, leaves contain much more ash composition after combustion than other parts of straw. Silicon/silica is the major inorganic component in the ash (35.84 wt%).[8] Table 1.1 gives an example of chemical composition of wheat straw.[15, 16]

Table 1.1 Chemical compositions in wheat straw

	Internodes	**Nodes**	**Leaves**
Lignin (%)	18.90	23.22	17.48
Cellulose (%)	71.24		56.95
Ash (%)	5.93		12.06

Cellulose as the major structural chemical of cell wall in plants is a linear homogeneous polysaccharide with the formula $(C_6H_{10}O_5)n$, which based on β-1, 4-D-glucopyranose repeat units. The average degree of polymerization variously estimated in the range of 3,000 to 15,000 depending on different resource.[17] The properties of cellulose approximately depend on its degree of polymerization as the glucose units make up the molecule of cellulose. Cellulose from woody materials does not have a special high molecular weight, which the typical chain lengths are between 300 and 1,700 units. And some of non-wood materials usually have the highest molecular weight of cellulose. For example, cotton cellulose has chain lengths ranging from 800 to 10,000 units.[18] Cellulose from plant is usually mixed with hemicellulose, lignin, pectin and other substances, while bacterial cellulose is much more pure, which has high moisture content and high tensile strength due to its high chain length.[13]

It is also reported by Mckean and Jacobs[19] that the carbohydrate contents and other chemicals in wheat straw will be influenced by location, growing conditions, years, genetics and varieties. The chemical composition based on different locations and years are shown in Table 1.2. The cellulosic content can vary about ±6%, lignin approximately ±4%, ash approximately ±5%, but with no significant variation in silica and/or other components.[16-20]

Table 1.2 Chemical compositions in wheat straw based on different locations and years[19]

	Pakistan 1991	**Illinois 1948**	**India 1988**	**Norway 1992**	**American 1987**	**Denmark 1987**
Holocellulose	58.5					72.9
α-cellulose	33.7	34.8		29.0-35.0	39.9	41.6
Hemicellulose	25.0	27.6	28.9	26.0-32.0	28.2	31.3
Lignin	16.0-17.0	20.1	23.0	16.0-20.0	16.7	20.5
Ash	7.5-8.5	8.1	10.0	4.0-9.0	6.6	3.7
Silica-Silicate	4.5-5.5		6.3	3.0-7.0		2.0

1.2.1 Current applications of wheat straw

The current applications of wheat straw, as summarised in Table 1.3, range from bio-fuels to biocomposites.

Table 1.3 Current applications of wheat straw in industries

Applications	Details
Bio-fuel	Straw could be alternative resources to produce bio-gas or alcohol after certain fermentation. Also, the straw as a carbon energy source is developing rapidly in many research area, such as bio-butanol[20], ethanol and Briquet[21]. The new generation energy will reduce the demand of fossil oil and coal.
Paper	Straw as a cellulose based material which similar with woody material could be the resources for paper industry.[19]
Construction Material	Wheat straw can be a raw material to making low-density particleboard[22] which is widely used in construction materials, furniture and insulation material.
Power Station Resources	Dried wheat straw as a renewable material could be pressed to brick and transfer to power station for energy produce.[11]

1.3 Characterization of Ash Residue from bio-mass combustion

The various inorganic components in the ash content can be observed in agricultural residue and other biomass residues (Table 1.4).[23] As the human factors influence on the growth of annual plants such as irrigation and fertiliser usage, annual plants have higher content for most of inorganic species in comparison to wood.[24] In particularly, the alkali content in annual plants is much higher than the woody and coal sources. Additionally, silica and potassium are the two major components in ash residue for all of the agricultural residues, excluding rape straw. The mixture of inorganic components in each material affects both the combustion properties of the fuel and the design and operation of combustion systems.

The stoichiometric equation for the combustion of biomass by the basic empirical formula for cellulose can be represented as below:

$$(C_6H_{10}O_5)_n + 6nO_2 \longrightarrow 6nCO_2 + 5nH_2O$$

Thermogravimetric analysis has been used to verify the stages of biomass combustion.[21] At the beginning the of the combustion, an initial mass loss during 120 °C is caused by evaporation of the moisture content along with high-energy volatiles. As the temperature increase to 180—375 °C, the solid lignocellulose materials begin to decompose and devolatilize to release organic compounds that will burn in gas phase.[25] This step is similar with respect to conventional pyrolysis. At high temperatures (375°C – 525°C), the residual chars combust at a slower rate in an oxygen-rich atmosphere.[25]

1.3.1 Current applications of ash residues from bio-mass combustion

Agricultural products have attracted wide attention for renewable energy generation and for the ash residue post large-scale combustion. Many agricultural products, by-products such as oil and extracts, and agricultural waste materials such as rice husk ash and wheat straw ash are considered as alternative resources for preparing high value chemicals or products. With the large-scale utilisation of wheat straw and other herbaceous biomass, a significant quantity of new waste will be produced, including fly ash and bottom ash. In large scale combustions tests on wheat straw, it is found that wheat straw could produce as much as 12% ash by weight of the wheat straw, including 72 wt% bottom ash and 28 wt% fly ash in initial ash.[26] The fly ash contains potassium, sodium, sulfates chlorides and phosphates, whilst the bottom ash is rich in silica or silicates.[26, 27]

The current cited alternative applications for biomass ashes are fertiliser or soil amendment in agriculture and construction by partly replacing cement or as an aggregate in road building.[28] The landfill of biomass ash is considered invaluable approach to reduce fertiliser usage and recycle the nutrients such as phosphorus, potassium, magnesium and calcium from plant. Nutrient is also the most important nutrients for plants but it will be totally lost during combustion. Although landfill of biomass ash is not an efficient and valuable method, it is the primary disposal approach for agricultural residues nowadays.[29] The large majority of research on the reutilization of ash has been carried out on wood ash with returning the ash residues to forest soils, particularly in the US, Sweden, Finland and Denmark.[30] It is suggested the development of valuable chemicals in ash for recycling the forest floors.[30] In addition, ash residues are also considered as potential liming agents to reduce acidity in soils.[31] The large majorities of coal fly ash have led to the development as a standard additive in concrete as a pozzolan.[32] It is approximately 6.7 million tonnes of coal fly ash were used as pozzolan in the US in 1994.[27] A pozzolan is a kind of siliceous material that will react with calcium hydroxide in the presence of water to form a material with binding properties.[33] However, fly ash from biomass does not meet this application, due to the high alkali and chloride concentrations and lower alumina levels. On the other hand, several agricultural ash residues such as rice husk ash[34], sugarcane ash[35], palm oil fuel ash[35], and wheat ash, could be used as an additive to concrete.

Table 1.4 Inorganic components in different kinds of ash residue[39]

Residue Type		Ash (wt%)	SiO_2	Al_2O_3	Fe_2O_3	CaO	MgO	Na_2O	K_2O	SO_3	P_2O_5	Cl
Wheat Straw	USA[24]	12.8	35.8	2.5	1.0	4.7	2.5	10.5	18.4	5.5	1.5	14.7
	China[36]	10.0	36.9	8.0	6.3	8.1	3.0	9.2	17.4	4.5	2.0	
	Denmark[37]	4.8	35.3	1.1	0.1	10.2	2.4	0.5	30.1	6.2	2.6	3.4
	Spain[37]	5.7	64.0	0.3	0.2	5.4	1.8	0.1	17.0	1.8	1.6	2.8
Other straw in UK	Winter barley[37]	6.9	25.2	0.2	0.1	6.9	2.2	5.1	40.2	5.1	1.9	6.9
	Spring barley[37]	5.7	37.2			12.5	1.0	0.9	17.8	2.7	1.4	1.4
	Oat straw[37]	3.8	15.2	0.3	0.1	26.5	3.3	4.5	17.4	6.4	6.7	0.8
	Rape straw[37]	2.7	2.4	4.2	1.6	48.7	3.1	0.2	15.2	3.8	1.4	0.5
	Rice straw[24]	20.9	72.3	0.1	0.3	2.1	2.1	2.7	11.8	1.1	1.8	4.1
	Cotton straw[36]	7.4	17.7	10.8	2.4	9.0	7.3	6.8	30.2	5.8	4.3	4.9
Other Agricultural waste in the world	Maize[37]	7.1	33.0	3.7	1.6	17.0	4.4	0.4	22.0	1.7	1.9	5.4
	Sugarcane[24]	8.5	42.6	23.2	16.2	3.0	2.0	0.6	3.0	0.5	1.3	0.1
	Switch grass[24]	3.8	62.8	0.3	0.9	6.2	1.7	0.4	11.7	1.5	4.2	0.1
Wood	Wood fuel[24]	4.5	37.5	14.1	0.6	7.6	17.0	3.6	1.4	2.2	6.0	2.2
	Red Oak[38]	1.2	38.3	8.1	7.6	12.8	1.0	0.4	8.6	1.8	1.0	<0.01
Coal	Eastern Kentucky[38]	7.6	51.6	32.5	4.5	1.1	0.4	0.2	1.3	1.3	0.3	2.3

1.4 Wood based panels

Wood based panels are the necessary part of office and home design in daily life with huge production every year. For example, in 2013, production and import of wood based panels was in the region 3 million m^3 and 2.9 million m^3, respectively in the UK.[40] Whilst for China comparative figures are staggering: production, 177 million m^3 comprising approximately 62.57 million m^3 of fibreboard, 18.93 million m^3 of particle board, 92.51 million m^3 of plywood and 3.03 million m^3 of veneer sheets.[41] The details of the quantity of wood based panels shown are shown Figure 1.4 and Figure 1.5.

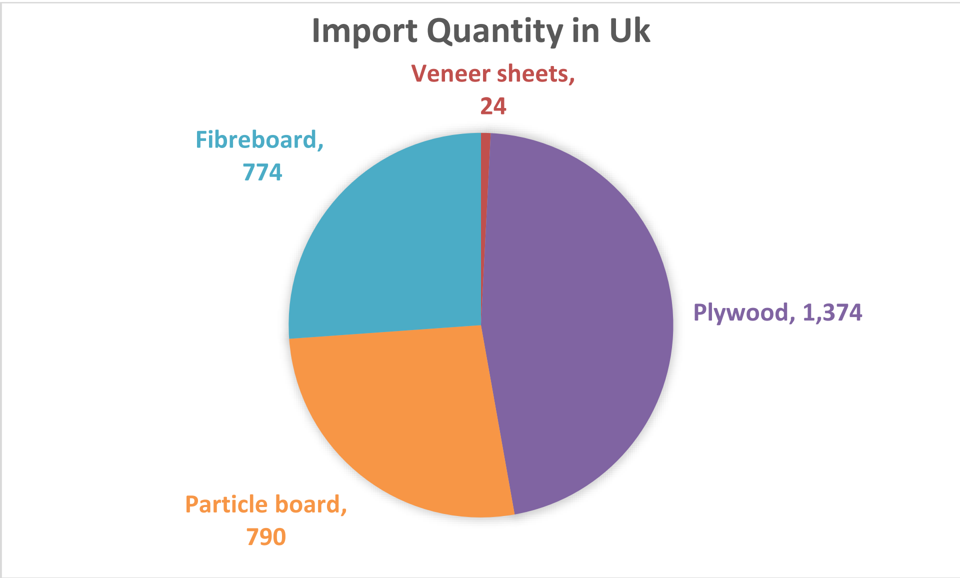

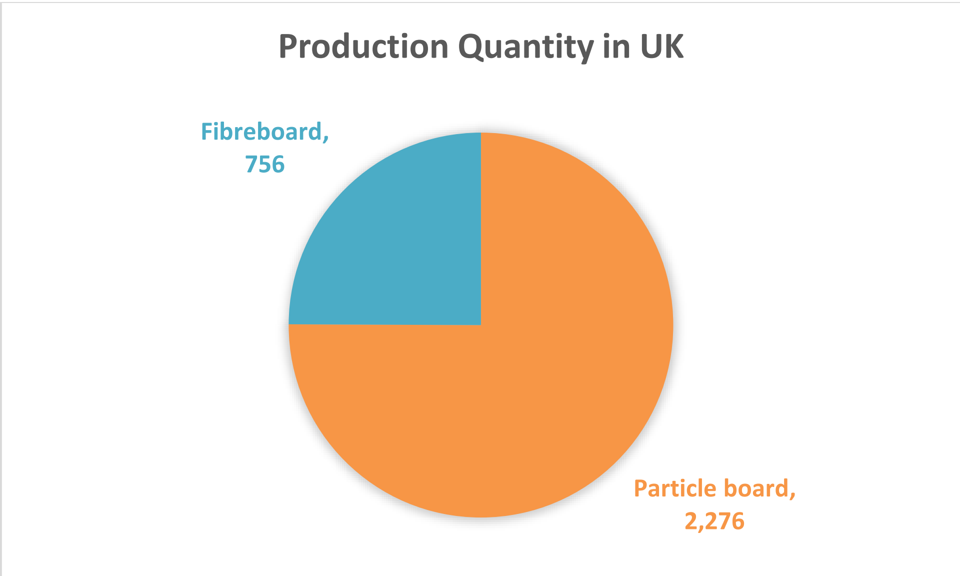

Figure 1.4 Distribution of wood-based panelling production and import quantity in the UK in 2013 (x 1000 m^3)[40]

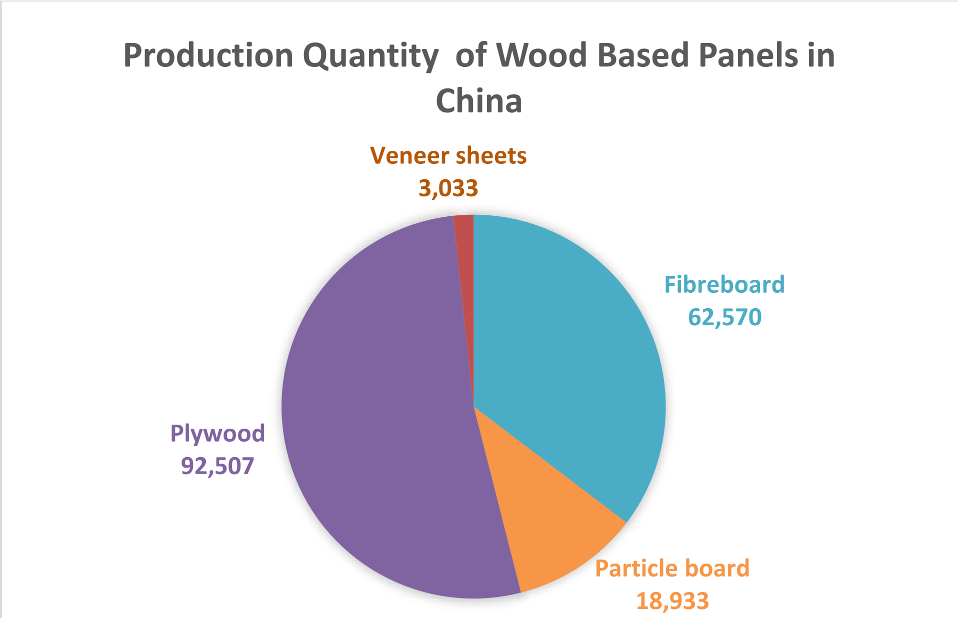

Figure 1.5 Distribution of wood-based panelling production in China in 2013 (x 1000 m^3)[41]

Plywood, fibreboard and particleboard are the three major types of wood based panels used in UK, which take more than 90% of the total usage. In particularly, fibreboard and particleboard are the only two products that produced in UK.

Particleboard could be defined as a "sheet material manufactured from small pieces of wood or other ligno-cellulosic materials (e.g. chips, flakes, splinters, strands, shreds etc.) agglomerated by use of an organic binder together with one or more of the following agents: heat, pressure, humidity, a catalyst, etc".[23, 40] Fibreboard is defined as "a panel manufactured from fibres of wood or other lignocellulosic materials with the primary bond deriving from the felting of the fibres and their inherent adhesive properties. Bonding materials and/or additives may be added. It is usually flat pressed but may also be moulded."[23, 40]

The manufacturing processes for fibreboard which take the medium density fibreboard as a typical example, and particleboard are shown in Figure 1.6.[23] The general process of MDF and particleboard are similar, but the MDF process requires fine fibres by pulping.

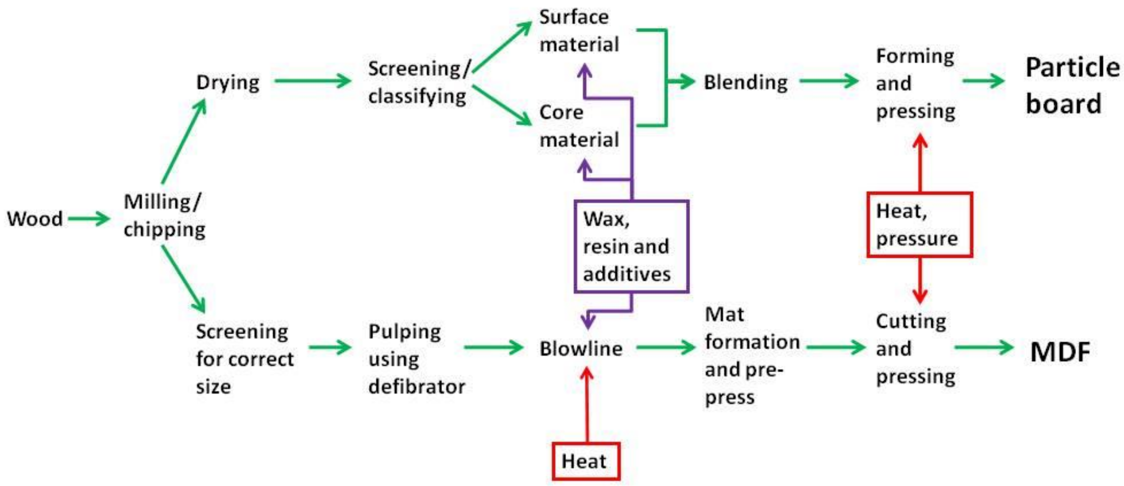

Figure 1.6 Major steps in the manufacture of particleboard and MDF[23]

There also might be some toxic chemicals existing as resin and additives are introduced, which will bring restrictions on the application. For example, the California Air Resources Board (CARB) approved an airborne toxic control measure (ATCM) to reduce formaldehyde emissions at 26/04/2007 in United States (USA)[42], which is used as binder in wood-based panels. The airborne toxic control measure aimed at wood-based products, including hardwood plywood (HWPW), particleboard (PB), medium density fibreboard (MDF), and also furniture and other finished products made with composite wood products. "For manufacturers of HWPW, PB, and MDF, compliance with emission standards specified in the ATCM must be verified by using a third-party certifier approved by CARB. Third-party certifiers are required to ensure that manufacturers of composite wood products verify compliance with the applicable emissions standards under the ATCM for their manufactured products."[42]

In addition, the process of making bio-based fibre board in industry could also divided into wet method (fibre distribution in water) and dry method (fibre distribution in air) based on Figure 1.6.[43] Wet processing boards have more than 20% moisture content at the forming stage, while dry processing boards have less than 20% moisture content at the forming stage.[43] Additionally, both wet processing boards and dry processing boards could be classified by their density. Approximately, boards with a density more than 900 kg/m^3 are hardboards (HB) in wet processing boards, and boards with a density between 400 kg/m^3 and 900 kg/m^3 are medium boards (MD). As dry processing boards are always produced under heating and pressure with the additive of binder, most of dry processing boards have a density ≧ 450 kg/m^3. Dry processing boards could also be classified by density: hard fibre boards (HDF) with the density higher than 800 kg/m^3, ultra-light medium fibre boards with the density between 450 kg/m^3 and 550 kg/m^3, light MDF with the density between 550 kg/m^3 and 650 kg/m^3, and medium fibre boards (MDF) with the density between 650 kg/m^3- 800 kg/m^3.[43]

1.4.1 Binder in board manufacture

Urea formaldehyde (UF shown in Figure 1.7) is the frequently-used binder for over 90% of particleboard and many other wood-based panels due to the strong bonds.[44] However, formaldehyde has been identified as a 'probable carcinogen' by the International Agency for Research on Cancer.[45] It is harmful to eye, nose and respiratory which can cause contact dermatitis.[46] Therefore UF has a significant health risk to people working in the board manufacturing industries. In addition, free formaldehyde released from manufactures has resulted that many countries applied strict limits on formaldehyde release from composite boards.[42] Also, urea formaldehyde is made from fossil fuel sources.[47] The large usage of urea formaldehyde in board manufacture has given great pressure on the dwindling fossil fuel resources.[48]

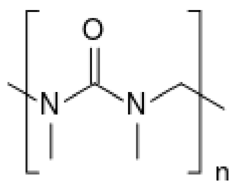

Figure 1.7 Urea Formaldehyde

As the wide applications of UF boards, low toxic or non-toxic chemicals that could get reaction with free formaldehyde are tried to be introduced into UF boards to eliminate the risk. For example, phenol is expected to be the additive to get reaction with formaldehyde (Figure 1.8). But the modification of free formaldehyde from board is also very hard. Based on this assumption, tannin-phenol formaldehyde resins as binder in board manufacture has been investigated. Based on this research, wood board with tannin-phenol formaldehyde resins has less free formaldehyde than normal UF board.[9]

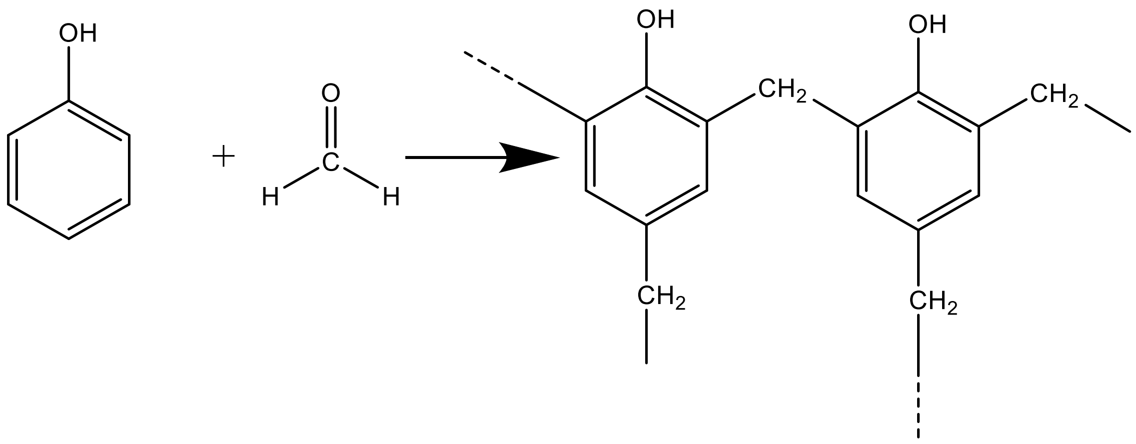

Figure 1.8 Reactions phenol/formaldehyde

Also, environmentally-friendly raw materials are expected to have the similar effect to eliminate the free formaldehyde. For examples, tea leaves which have rich polyphenols, tannins, proteins and amino acids are expected as additives to UF boards. These chemicals in tea leaves are supposed to trap or react with the free formaldehyde.[49]

Another alternative binder for board process is silicate binders which have been utilised in cardboard packaging and foil laminate.[50] Silica binders are inorganic, polymeric, alkaline silica based materials containing silica (SiO_2), alkali material (Na_2O or K_2O) and water. In manufacture process of silicate, the silica and alkali materials are fused at a very high temperature of 1200 ^{0}C and the resultant glass can be converted into liquids, or hydrous or anhydrous powders. Silicate binder could be considered as a kind of film binder or a kind of chemical binder depend on different kinds of silicate, combined materials and which kind of the final products that are expected. The mass ratio between SiO_2 and Na_2O (or K_2O) is a very important property to determine the final silicate binder. This property will influence the solubility, viscosity and reactivity of silicate binder.[51, 52] Silicate binders have many advantages than the traditional UF binders. In the silicate binder systems, Volatile Organic Compounds (VOCs) such as UF would be completely eliminated. They also have a high tensile strength, strong water, bacteria and heat resistant abilities. But the silicate binders have high energy cost as the heating temperature around 1200 ^{0}C in traditional process.

In the binder system, hydrogen bond and synthetic adhesive are considered as the major reason for binding.[53] Most of the adhesives are completely distributed on the surface of fibre, also a fraction of adhesive penetrates into the porous cell wall.[53, 54] The approximately adhesion theories of the UF resin bonding is that UF resin is anchored into the cell wall structure of the fibre.[53, 54] After hot-pressing, the UF resins bridge spread between different fibres and set the final structure of boards.

1.5 Background of adhesion

In order to bond two or more materials as one kind of material or one kind of composite, there need to be adhesive bond between these materials which can allow materials to reform as one. Also, the materials, adhesive and adhesive bond must be able to resist the external stresses and strains to constitute a composite. Adhesion is the tendency for the surfaces or particles' dissimilar materials to cling together. The forces that generate adhesion have several types.[55]

1.5.1 Adhesion theories-- Chemical bond

Chemical bonding (covalent bond, ionic bond and hydrogen bond), diffusion, adsorption, Van der Waals interaction, molecular interactions and mechanical interlocking are mainly mechanisms of adhesion. A covalent bond is consisted by a pair of electrons shared between two atoms.[56-59] When covalent materials are brought into intimate contact, one material probably expect the bonding across the interface that is similar to the bonding within another material. In addition, most covalent solids are extremely hard and have a high elastic modulus.

Ionic bonds are formed whenever one or several electrons are transferred from one atom to another. Electron transfer results in the formation of negative and positive ions. It is also to be expected that coulombic attraction of unlike ions form the ionic bonds.[60-63] When metals combine with non-metals, metals tend to form ionic bonds by the attraction for their valence electrons.

Hydrogen can exist both as cation and anion. The hydrogen or proton results from the removal of the only electron. On the other hand, the negative hydrogen ion is formed by the fragmentary protection of the positively charged nucleus by the single electron in neutral atom. In the negative hydrogen ion, the imperfect shielding will result in continuously shifting dipole. Then there was a weak tendency to get another electron by ionic attraction. With this property of attraction, the hydrogen atom can bridge two negative ions. Then the hydrogen bond formed.[56-59, 64] Hydrogen bond is very important to adhesion of polymers, especially there certain polar atoms present certain capability of forming hydrogen bond.

1.5.2 Non-chemical bond mechanism

The diffusion always presents in the entanglement of polymer chains in solutions or melt. Self-diffusion and inter-diffusion are the two major theory of this adhesion. In self-diffusion, adhesive will weave into the adherent. In addition, there is a cooperative movement of entanglement and chain reputation. For the inter-diffusion, polymers will cross the interface to result in adhesion. Van der Waals forces are some kind of secondary bonds, which also can result interatomic attraction. It presents between molecules or within molecules when chemical bonds have not formed between atoms.[55]

Molecule interaction is a kind of non-dispersive force. It require a short range or specific interactions (<2 nm) between materials. Molecule interaction generally presents in hydrogen, polar chemicals, acid and base. Mechanical interlock is a “hammer and nail” like approach. Glue or resins flow into pores if the surfaces and get physically stuck by polymerization or crystallization.

1.6 Silica characterisation

Silicon dioxide also named silica is one of the most abundant minerals presents in many different phases in nature, such as plants and soils. Common crystalline phases of silica in nature include quartz, tridymite and cristobalite are always formed with Q^4 tetrahedral crystal structures.[65] The soluble silica in plants which have a strong ability to accumulate silica have a higher concentration than that in the soil.[23] The ability of silica accumulation appears to be highly dependent on the different level phylogenetic position of the plant, particularly presents in land plants and monocot angiosperms, such as grass.[23] This kind of plants includes the major agricultural plants such as rice, wheat and other important plants. Studies have shown a various accumulation ability of silica in these plants: rice >> wheat > triticale > sorghum > rye > maize > barley.[66] These plants will accumulate silica in the form of silicic acid by the roots. Then the silicic acid is transported to the xylem and to the shoot, stem and leaves by the transpiration stream, where it is concentrated due to evaporation and polymerisation.[23] The reason for strong "absorption" of the transpiration stream is that the silicon concentration is higher in older tissues, leaves and the shoot than in the stem (Table 1.5).[67]

Table 1.5 Percentage of silica in different parts of the wheat plant[67]

Wheat organ	**SiO_2 (%)**
Culm/stem	1.5 ± 0.2
Leaf sheath	5.8 ± 0.9
Leaf blade	5.7 ± 1.4
Rachis	1.1
Influorescence	3.8 ± 0.9
Bulk	2.3 ± 0.3

1.6.1 Silica depolymerisation

The depolymerisation of silica is caused by the solubilisation of silica, which has a reverse reaction appeared. This reaction is spontaneous in water and is influenced by alkaline or different pH conditions.[68] The mechanism of this reaction is shown in Figure 1.9.[68]

$$SiO_{2(s)} + 2H_2O_{(l)} \rightleftharpoons Si(OH)_{4(aq)}$$

Under basic conditions, it starts with nucleophilic attack of OH^- to increase the coordination number whilst decrease the potential Si-O bond strength.[69] This initial variation will break some Si-O bonds. At the beginning of the silica depolymerisation, this step will continues repeat which would release much more free $Si(OH)_4$. The $Si(OH)_4$ groups are then desorbed from the surface of silica resulting further dissolution.[70] On the other hand, silica solubilisation will be reduced by preventing re-polymerisation of silicic acid. On the contrary, silica solubilisation would increase by an ester-like mechanism at acidic pH.[68] In addition, the rate of silica depolymerisation is also depend on the adsorption of Si-O^- groups on silica surfaces.[71] The concentration of these groups on silica surface is influenced by silica surface area, pH and ionic strength.[72] In Figure 1.8a, depolymerization of silica at alkaline conditions initiated by a nucleophilic attack by OH- followed by breakage of a Si-O bonds. Repeating this step twice results in the release of a free silicic acid. In Figure 1.9b, depolymerization of silica at acidic conditions might progress by an ester-like mechanism, due to the partial double bond character of the Si-O bond.

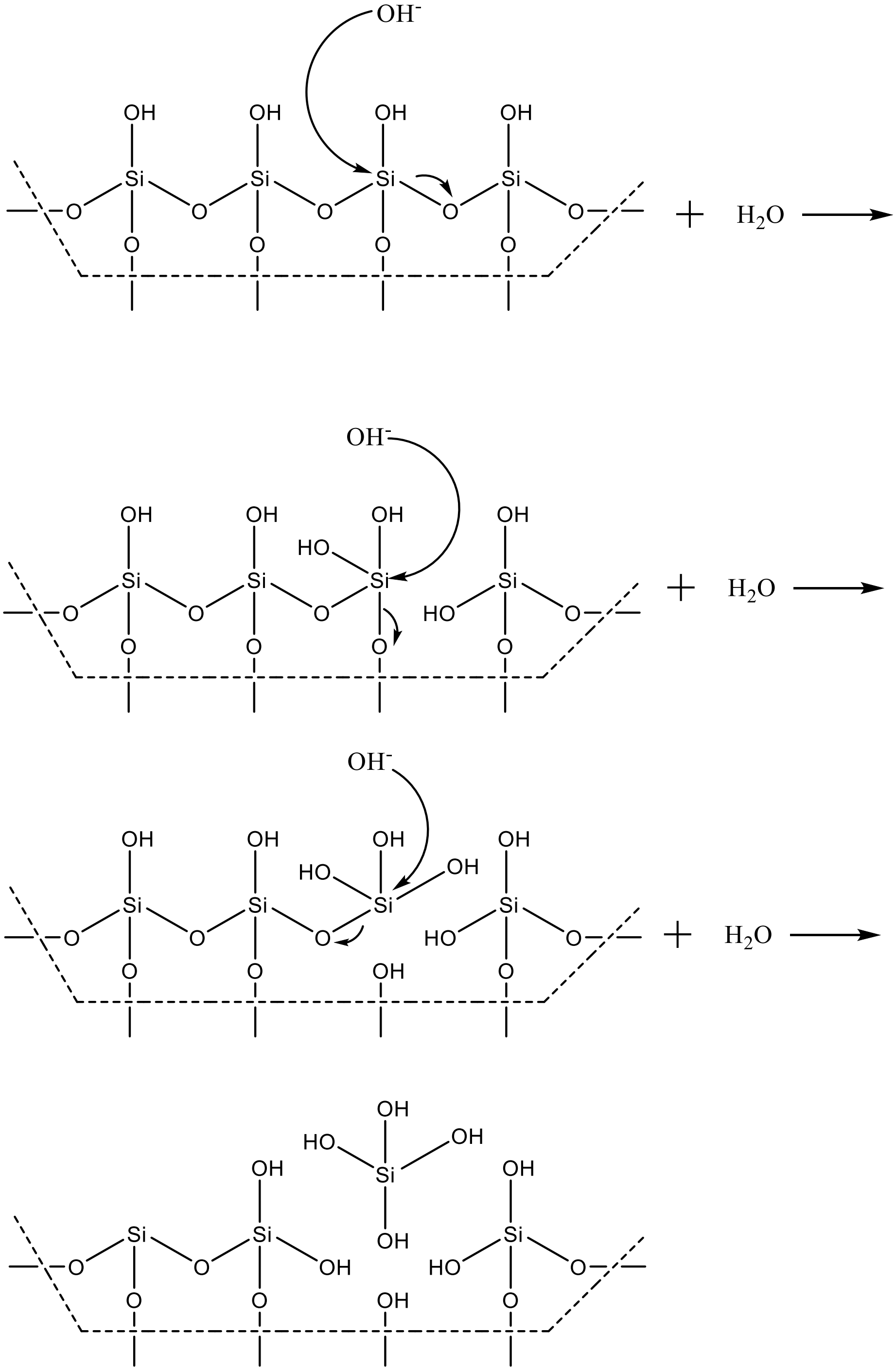

(a)

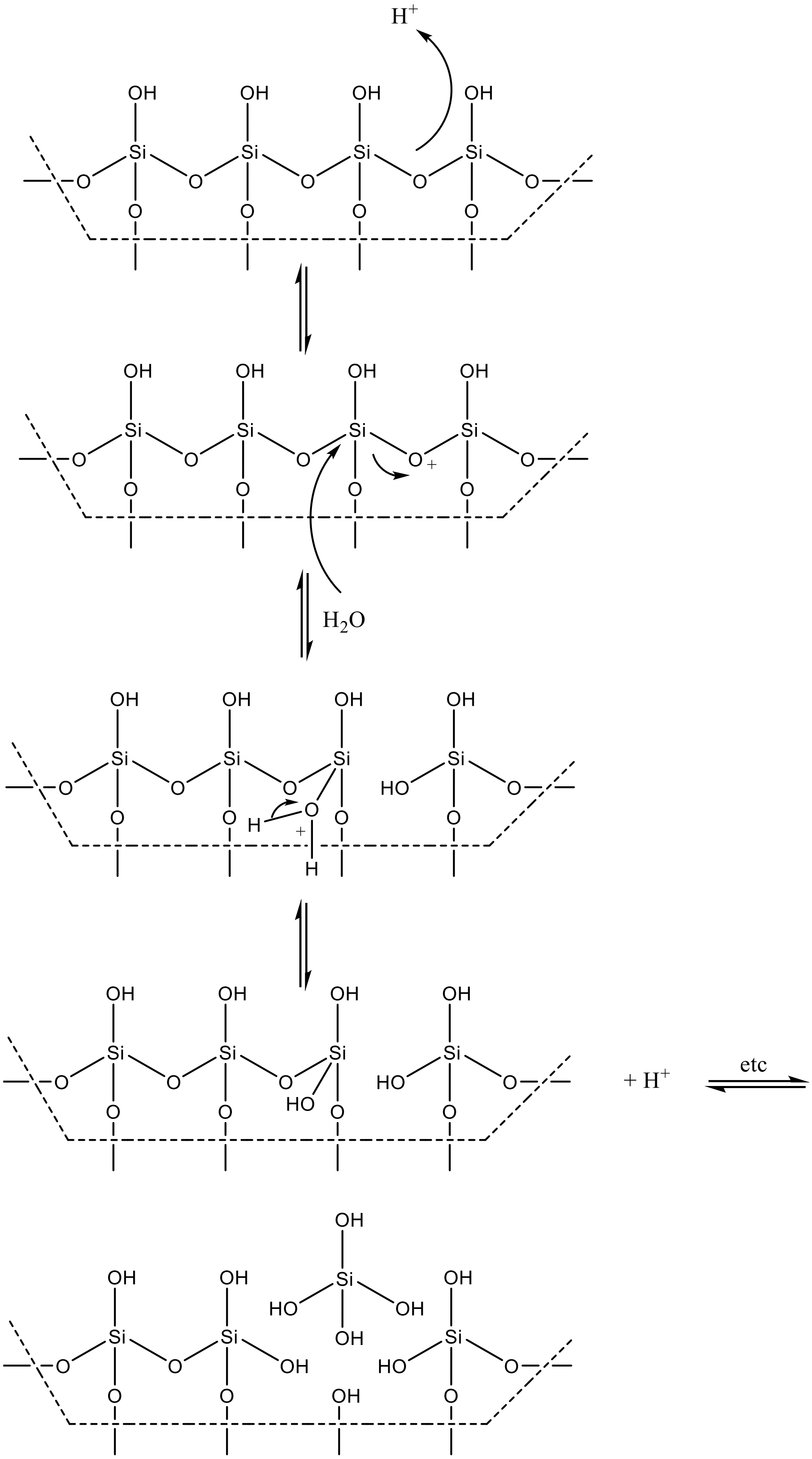

(b)

Figure 1.9 The proposed scheme for depolymerization of silica based[68]

1.7 Characterisation of alkali silicate

Alkali silicates are solutions or solids with silicate anions and alkali metal cations. Alkali silicate can be presented as M_2SiO_3 or $xSiO_2$:M_2O, which M could be Li, Na or K. With different mass ratio between SiO_2 and M_2O, the properties of alkali silicate are quite different. And this ratio could be controlled during preparing process. This various property will give the alkali silicate a wide application. Alkali silicate will form different silicate structure in aqueous phase. It has been reported that the species of silicate are compact and form tetrahedral structure with each other in dynamic equilibrium.[81] The mechanism of condensation is still be studied recently. But it is believed that the silicate is catalysed by hydroxyl ions.[73] The approximate mechanism suggested that a two-step condensation reaction with silicic acid via a five-coordinate reaction intermediate stabilised by three strong hydrogen bonds caused by loss of water (Figure 1.10).[74] The species in aqueous phase will become stable with the combination between anionic species and alkali cation.

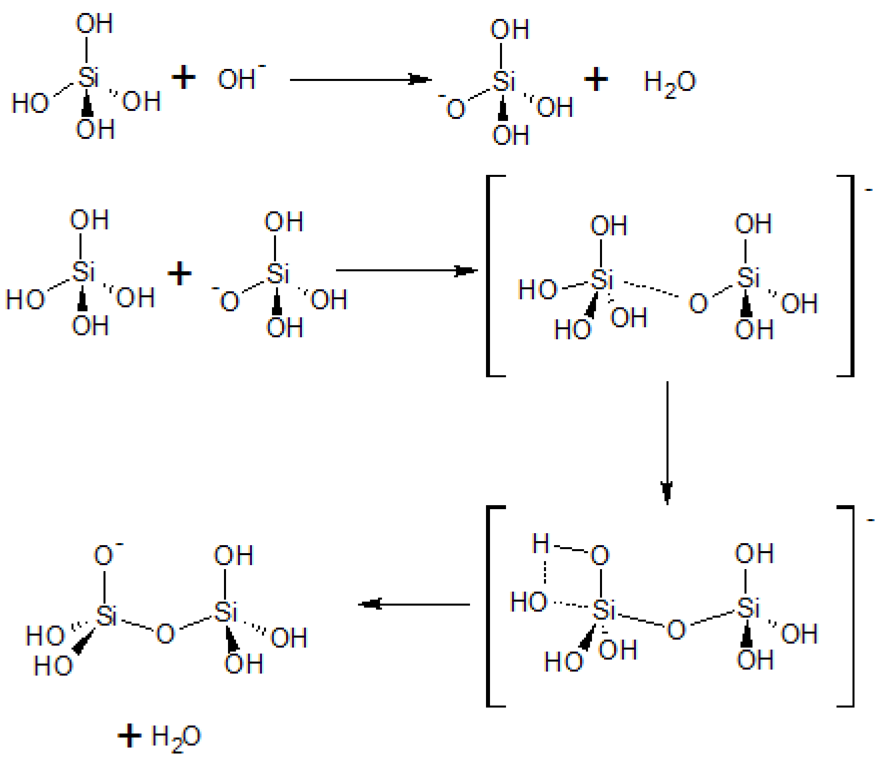

Figure 1.10 Approximately mechanism for the condensation of silicic acid[74]

1.7.1 Mechanism of silicate solution bonding

The mechanisms for silicate solution cure or bond have two major approaches: Evaporation of water (dehydration) and Chemical setting mechanism. The two processes could work separately or together. In addition, chemical setting is generally been used for improving film moisture resistance, reducing setting time and increasing bond strength.

As water evaporates from silicate solution, the solutions become sticky and viscous. It has been report by PQ corporation[75] that the viscosity increases to 20 poises with a weight loss of 6% by evaporation for certain sodium silicate solution. When the weight loss of water achieves 14%, the viscosity of solution is around 40,000 poises. Then further dehydration results in a final hardened state. Heat is always been used for accelerating the cure process. However, heating too quickly will probably cause steam to form within the film, resulting in bubble or expand after the steam released.

For chemical setting or cure, silicate solution can react with a variety of acidic or soluble metal compounds. With the neutralization by acidic chemicals, silicate solution will polymerize and result in a gel. There are some common agents for chemical cure, included: mineral and organic acid, carbon dioxide and salt. In addition, multivalent metal compounds can form coating or bond with reacting with silicate solution to get precipitation of insoluble metal silicate compounds.

1.7.2 Lab-scale preparation of potassium silicate solutions

Alkali silicate is the binder used in this study. Potassium silicate was extracted from power station bottom ash. This reaction was carried out at a temperature in the range 180^{o}C -200^{o}C for 24 hours reflux.[12, 39] The reaction is shown below:

$$SiO_2 + 2KOH \underset{24h}{\overset{180^oC\text{-}200^oC}{\rightleftharpoons}} K_2SiO_3 + H_2O$$

This ash is mostly amorphous silica which is reactive around 180^{o}C with KOH solution to yield sodium silicate. A viscous and colourless potassium silicate solution is obtained after filtration of the reacted slurry (consisting of residue digested ash, potassium silicate, water and free sodium hydroxide).

After extraction, potassium silicate solutions were collected. During the solution, SiO_3^{2-} ion is the major form of silica. Silicate particles are hydrated as shown below:

$$K_2SiO3 \bullet 5H_2O \rightleftharpoons K_2SiO_2(OH)_2 \bullet 4H_2O$$

After hot-pressing, most of the water content in silicate solution will be evaporated. The anhydrous potassium silicates then have a significant change. Silica group are no longer discrete in the composite. A chain polymeric anion composed of corner shared [SiO_4] tetrahedral structure is formed in the composite. This is also the process of silicate cure. Then fibre particles will be combined together by anhydrous silicates. With the additions of probable hydrogen bond and Van der Waals force, the bioboards are well bonded.

1.7.3 ^{29}Si NMR analysis of silicate

Engelhardt *et al* developed a Q^i description by ^{29}Si NMR to identify the silicate species and silicic polymerisation in solutions.[76] Q^0 represents a silicate structure which the silicon atom is not connected to other silicon atoms through an oxygen bridge. Q^2 indicates two silicon atom connections. Q^3 indicates three silicon atom connections, while Q^4 indicates that a silicon atom that is connected to four other silicon atoms at each tetrahedral linkage (Figure 1.11)[23]. Also ^{29}Si NMR peaks suggested the difference in Q^i species in aqueous phase (Table 1.6).[77]

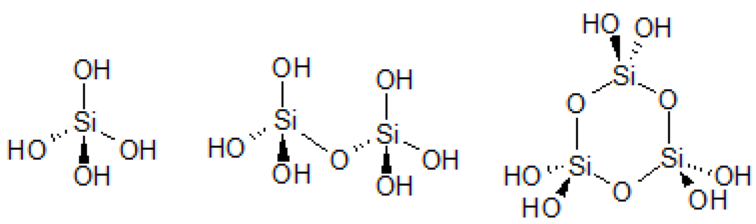

Q^0 Q^1 Q^2

Figure 1.11 The structure of silicate species in aqueous phase identified by ^{29}Si NMR[23]

Although ^{29}Si NMR could approximately indicate different silicate species in aqueous phase, it is still hard to identify specific structure in the silicate solutions due to the similitude between different species and the low abundance of ^{29}Si which prevents the visibility of ^{29}Si-^{29}Si coupling.[23] With different concentrations of silicate solution, cation type, pH and mass ratio, the different integrated peak of Q^i intensities will also change.[77-79] This conclusion suggests a novel research approach of silicate structure by ^{29}Si. Also, the degree of polymerisation in silicate solution will be decreased with the decreasing concentration of solution.[77]

Table 1.6 Assigned ^{29}Si NMR shifts for silicate species with different connectivities in solution[77]

Q^i connectivity	-δ(ppm)
Q^0	~ 72
Q^1	~ 79
$Q^2_{(3R)}$ (cyclic trimer)	~ 82
$Q^2_{(4R)}$ and $Q^3_{(3R)}$ (three ring)	~ 87 – 92
$Q^3_{(4R)}$ (four ring)	~ 96 – 98
Q^4	~ 108 (broad)

1.7.4 Infrared analysis of silicate solution

IR is another feasible method to characterise the silicate solutions. The major infrared absorption bands of silicon in silicate solutions are found between 1250 and 700 cm^{-1} with a strong wide band due to asymmetric Si-O-Si stretching vibrations, which usually appeared around 1000 cm^{-1}.[23] Bass and Turner have summarized the differences of IR spectra with different silicate structure in silicate solutions observed by ^{29}Si NMR.[78] The results is shown at Table 1.7.[78] It is suggested that higher wavenumber silicate solution will have much more complex structure.

The major absorption bands of silicate solutions will also shift with different concentration of the alkali silicate.[80] (This situation was observed in this thesis: the aqueous ATR/FT-IR spectra showed the major peak without a high frequency shoulder, shifted to lower wavenumbers with decreasing concentration or increasing alkali content – see later).[80]

Table 1.7 Bass and Turner's assignments of components silicate infrared peak to different silicate structures[78]

Assignment	Wavenumber (cm^{-1})
SiO- small anions	850-900
Monomer + dimer	910-950
Linear Q^1	965-985, 995-1005
SiO^- cyclic anions	1010-1020
$Q^2_{(3R)}$ rings	1020-1050
$Q^3_{(3R)}$, $Q^2_{(4R)}$ rings, linear Q^2	1030-1070
$Q^3_{(4R)}$ rings	1050-1120
Polymer	1100-1300

1.7.5 Mesoporous silica

Since the early 1990s, silica derived molecular sieves with mesoporous pore structures have been synthesised.[81, 82] In 1992, scientists at Mobil Oil synthesised the first mesoporous material, MCM-41 (Mobil Composition of Matter number 41) (MCM-41), comprising regular arrays of uniform channels (between 16-100 Å depending on synthesis conditions).[81, 82] These mesoporous materials present similar advantages of zeolites such as thermal stability, high surface areas, and shape selective catalysis. With the addition of larger pores, this material would engage the number of molecules and chemical reactions that would be catalysed by mesoporous silica. Molecular sieve type silica materials have a wide range of applications such as catalysts and catalyst supports, adsorbents and separation materials.[83-86] Thereafter, in 1998, the Santa Barbara Amorphous type material (SBA-15) with large pore diameter (4.6 nm—30 nm) and thicker walls than the MCM-41 family was produced.[87, 88]

Chapter 2: Biosilicate solution from biomass ash and the applications of biosilicate solution

2.1 Introduction

The first part of this chapter introduces and discusses the extraction of biosilicate solution from biomass ash. This includes the analysis performed on the extraction of biosilicate solution to obtain different kinds of silicate solutions as potential biosilicate binders.

The second part focuses on production of *advanced* materials, namely mesoporous bio-MCM-41 and bio-SBA-15 from biosilicate solution. The feasibility of biosilicate solution as an alternative resource is explored in different analytical approaches.

Industrial-scale combustion of biomass produces two types of ash: bottom ash and fly ash (Figure 2.1). In this thesis bottom ash from miscanthus and wheat straw incineration undertaken at Ely Power Station, England, was used as renewable feedstock for silica/silicate leaching.

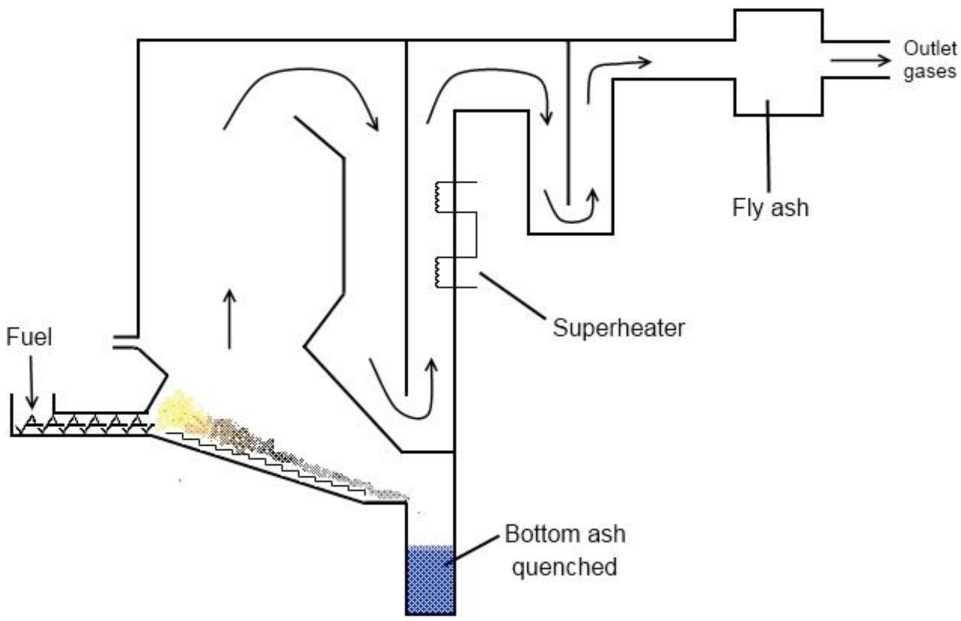

Figure 2.1 Diagram of the combustion process at a power station[12]

The common elemental composition of these ashes was shown in Table 2.1. Miscanthus (bottom) ash and wheat straw (bottom) ash had similar elemental composition except that the former had higher sulfur, phosphorus and magnesium content and lower potassium and calcium content than the latter (wheat straw bottom ash).

Table 2.1 ICP-MS (Inductively coupled plasma mass spectrometry) analysis of miscanthus (bottom) ash and wheat straw (bottom) ash. Elemental composition in wt%

Element	Miscanthus (bottom) Ash	Wheat Straw (bottom) Ash
Na	0.166	0.199
Mg	0.666	0.494
Al	0.133	0.138
Si	0.018	0.018
P	0.665	0.346
S	0.772	0.665
K	6.671	7.919
Ca	2.673	4.483
Cu	0.002	0.002
Zn	0.005	0.005

2.2 Alkali silicate solution extraction from miscanthus (bottom) ash

Biosilicate solution was extracted from miscanthus (bottom) ash (<125 µm) by using aqueous potassium hydroxide (KOH) solution. A series of studies were introduced into this part to develop the application of biosilicate solution as a binder, which included: extraction time (reflux time); concentration of alkali, and; the volume of alkali solution in the extraction. Two different concentrations of potassium hydroxide (KOH) solution (3M and 5M) and different reflux times (24 h, 18 h, 12 h and 6 h) were investigated to develop a kinetic study of the silicate extraction from miscanthus (bottom). The majority of the silica present in the ash can be extracted under these conditions, forming silicate solutions of varying mass ratios (K_2O: SiO_2). The details of these samples are shown in Table 2.2 and Table 2.3, where K120 is commercial silicate solution obtained from PQ Corporation, England.

Table 2.2 Analysis of biosilicate solutions from miscanthus (bottom) ash using 125 ml 5M KOH solution. K120 (commercial potassium silicate solution) is also analysed with biosilicate solutions by the same method

5 M-aqueous KOH (75 g Ash, 35 g KOH, 125 ml H_2O at 187 °C)								
	pH	Density (g/cm^3)	Solid Content (g/ml)	Solid Content (wt%)	K_2SiO_3 content (wt%)	Concentration (g/ml)		K_2O : SiO_2
						K_2O	SiO_2	
K120	14.00	1.5961	0.9468	59.32%	51.74%	0.3038	0.5220	1:1.72
24 h	14.04	1.3243	0.4568	34.49%	29.25%	0.1857	0.2018	1:1.09
18 h	14.03	1.3311	0.4387	32.96%	28.25%	0.1793	0.1967	1:1.10
12 h	14.12	1.3629	0.4845	35.55%	30.43%	0.2014	0.2160	1:1.07
6 h	14.20	1.3595	0.4870	35.82%	30.42%	0.2028	0.2108	1:1.04

Table 2.3 Analysis of biosilicate solutions from miscanthus (bottom) ash using 208 ml 3 M-aqueous KOH solution. K120 (commercial potassium silicate solution) is also analysed with biosilicate solutions by the same method

3 M-aqueous KOH (75 g, Ash, 35 g KOH, 205 ml H_2O at 187 °C)								
	pH	Density (g/cm^3)	Solid Content (g/ml)	Solid Content (wt%)	K_2SiO_3 content (wt%)	Concentration (g/ml)		K_2O : SiO_2
						K_2O	SiO_2	
K120	14.00	1.5961	0.9468	59.32%	51.74%	0.3038	0.5220	1 :1.72
24 h	13.82	1.2193	0.3097	25.40%	22.92%	0.1333	0.1463	1:1.10
18 h	13.87	1.2205	0.3028	24.81%	22.43%	0.1302	0.1435	1:1.10
12 h	13.84	1.2296	0.3048	24.79%	22.71%	0.1333	0.1460	1:1.10
6 h	13.93	1.2495	0.2892	23.15%	21.71%	0.1340	0.1373	1:1.02

The data from titration and the measuring of density indicated that different extraction conditions did not have significant influence on the physico-chemical properties of extracted silicate solutions. Although the concentrations of KOH solution were different, the mass ratio of K_2O: SiO_2 was almost the same (1.07-1.10). Extraction with 3 M-aqueous KOH were marginally better and more stable than with 5 M-aqueous KOH. A reduction in extraction time, e.g., 6 h, elicited the least amount of silicate. As the moisture (water) content in biosilicate solutions was much higher than commercial silicate solution (K120), the mass ratio and densities of biosilicate solution were lower than K120. As expected 3 M-aqueous KOH extracted samples had lower pH than any other samples. On the other hand, 5 M-aqueous KOH extracted samples had similar pH with commercial silicate solution. Long extraction times (24 h, 18 h and 12 h) gave silicate solutions with similar pH and density for both 5 M- and 3 M-aqueous KOH, but the pH increased for the 6 h reaction. Again, the latter was due to incomplete extraction and thus presence of *free* alkali in the solution. The effect of time does not change significantly the properties of silicate solution and for further analysis the time was fixed in 18 h so as to ensure complete dissolution.

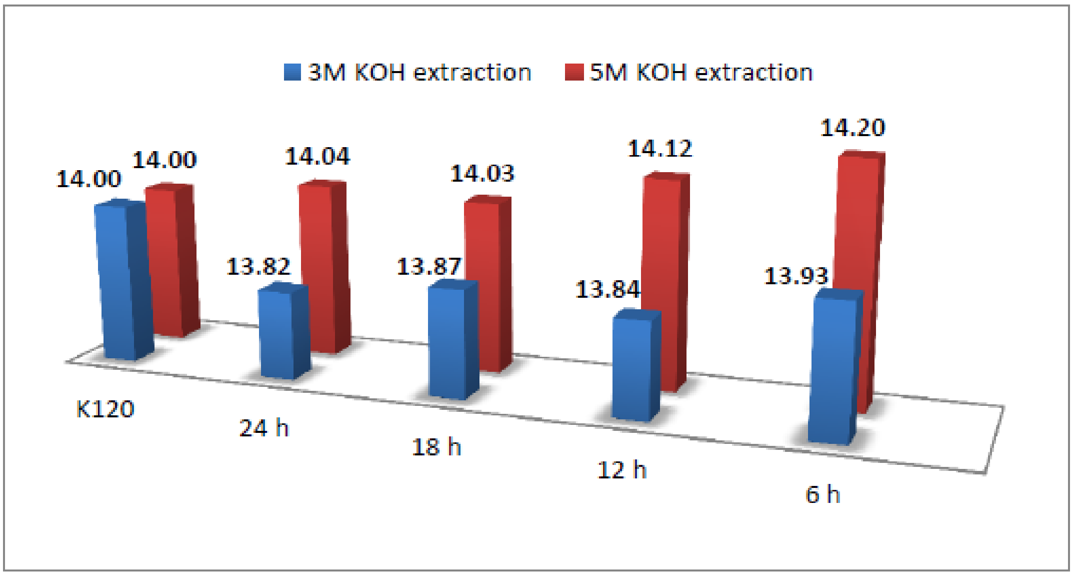

Figure 2.2 pH of biosilicate solution under different extraction time

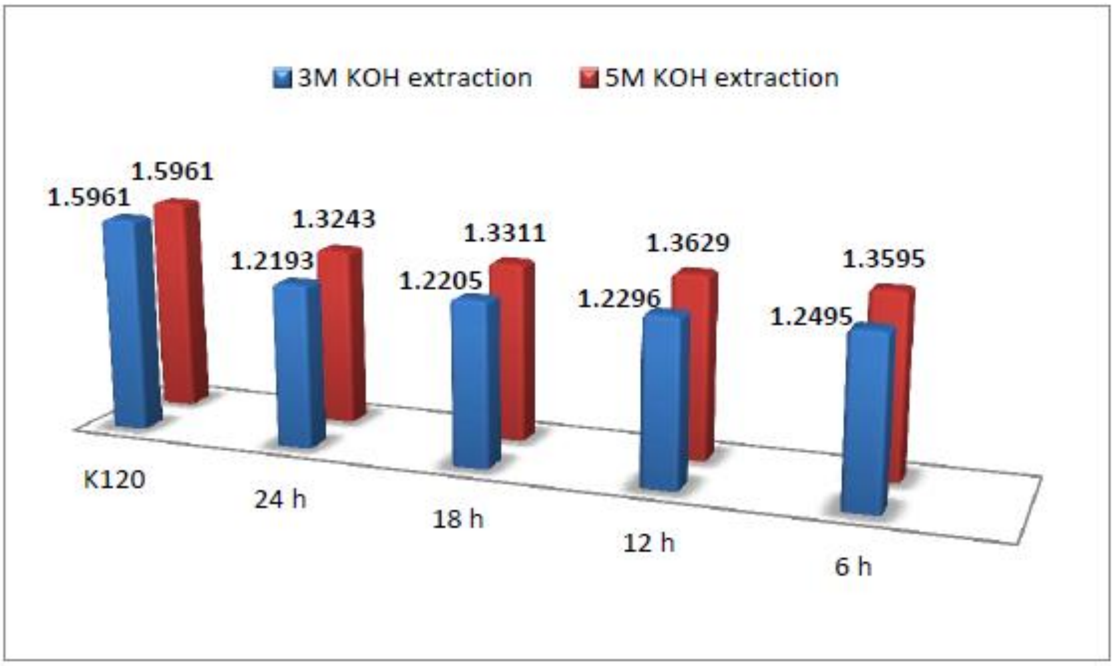

Figure 2.3 Density of biosilicate solution (g/ml) under different extraction time

2.2.1 Effect of alkali concentration

The effect of potassium hydroxide concentration was tested at two different concentrations (3 M and 5 M) at reflux for 18 h in a fixed volume of potassium hydroxide solution (125 ml).

For the mass ratio, 3 M-aqueous KOH extracted samples gave much better results than the corresponding 5 M-aqueous KOH extracted samples. The increase in potassium oxide (K_2O) leached in turn increased the pH of the silicate solution. It also can be found that the density, solid content and concentration were decreased with the concentration of KOH decreasing.

Table 2.4 Comparison between biosilicate solution and commercial product. K120 (commercial potassium silicate solution) is also analysed with biosilicate solutions by the same method

	pH	Density (g/ml)	Solid Content (wt%)	Concentration (g/ml)		$K_2O : SiO_2$
				K_2O	SiO_2	
K120	14.00	1.5961	59.32	0.3038	0.5220	1 : 1.72
Biosilicate (5 M KOH)	14.03	1.3311	32.96	0.1793	0.1967	1 : 1.10
Biosilicate (3 M KOH)	13.16	1.1251	14.39	0.0588	0.0805	1 : 1.37

2.2.2 Different volume of 3 M-aqueous KOH solution in extraction

In order to study the influence of the volume used in the extraction, 6 different volumes of solution were tested. The extraction time was fixed at 18 h and 3 M-aqueous KOH solution was used in these experiments. According to the results shown in Table 2.5, the mass ratio of SiO_2: K_2O decreased as the volume of solutions increased. The tendency of silica concentration and potassium concentration were different than the total concentration. The K_2O concentration increased gradually as the concentration of KOH increased with a final concentration fixed around 0.13 g/ml. The SiO_2 concentration would reach maximum when a volume of 208 ml was used. Therefore, these results suggested that maximum extraction of silicate extraction would be using 3 times more by the weight of the hydroxide solution than ash. The mass ratio of K_2O: SiO_2 was gradually decreased with higher volume of solutions.

Table 2.5 The effect of different volume of 3 M-aqueous KOH solution after 18 h extraction.

	pH	Density (g/ml)	Solid Content (wt%)	Concentration (g/ml)		$K_2O : SiO_2$
				K_2O	SiO_2	
K120	14.00	1.5961	59.32	0.3038	0.5220	1 : 1.72
Biosilicate 100 ml	12.54	1.1569	19.16	0.0791	0.1180	1 : 1.49
Biosilicate 125 ml	13.16	1.1251	14.39	0.0588	0.0805	1 : 1.37
Biosilicate 208 ml	13.87	1.2205	24.81	0.1302	0.1435	1 : 1.10
Biosilicate 290 ml	14.06	1.2074	24.57	0.1375	0.1264	1 : 0.92
Biosilicate 370 ml	14.07	1.1835	22.44	0.1302	0.0950	1 : 0.73
Biosilicate 400 ml	14.30	1.1930	21.92	0.1316	0.0900	1 : 0.68

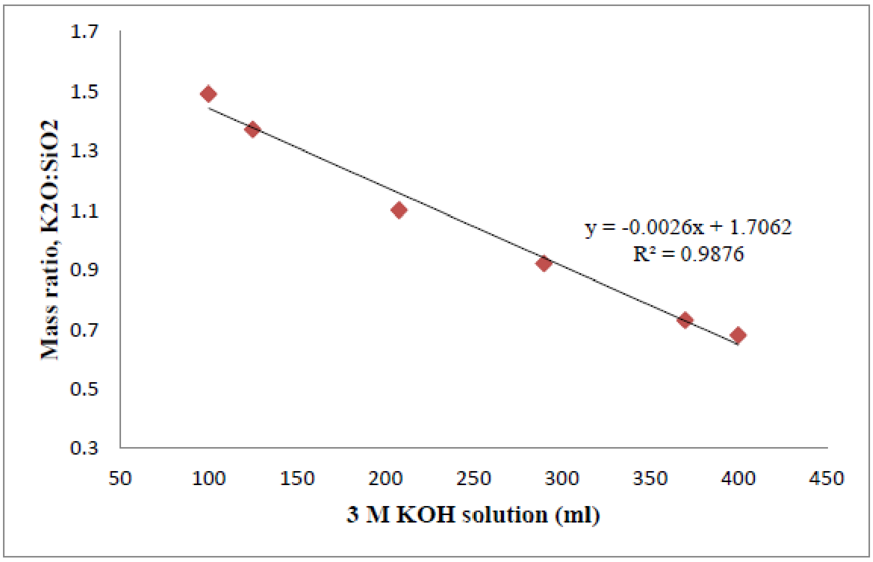

Figure 2.4 The connection between mass ratio (K_2O: SiO_2) and the volume of KOH

2.2.3 IR correlation of silicate solution

The silica/silicate content can be measured directly by titration but the end-point is troublesome to identify and the procedure is very time-consuming procedure. An IR method was employed whereby the intensity and area of the IR absorbance bands of silica (1250-650 cm^{-1}) were monitored; increased in intensity with increasing concentration of the solution.

It was decided to test the hypothesis that the silica concentration could be analysed by studying the changing absorbance band. Firstly, commercial K120 was diluted to different concentrations (5, 10, 20, 30 and 50% of the original concentration), ATR-IR spectra recorded (Figure 2.5). The absorption bands for silica/silicate are enlarged for clarity as shown in Figure 2.5 and Figure 2.6.

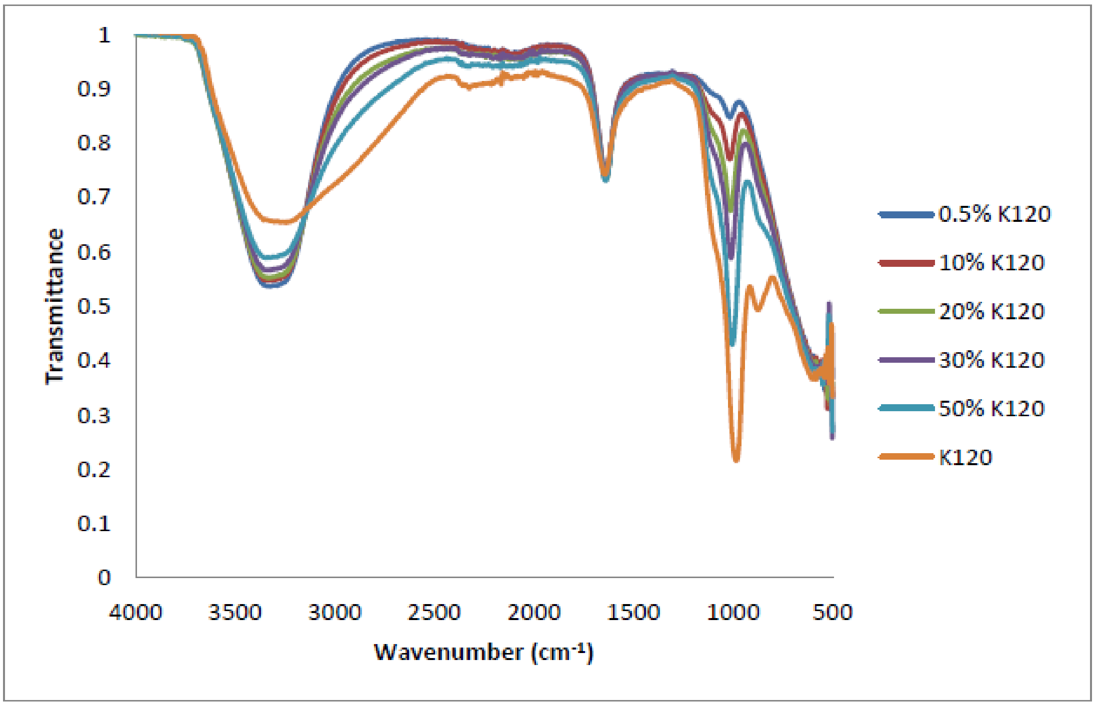

Figure 2.5 Stacked infrared spectra of K120 solution at various concentrations relative to the original solution

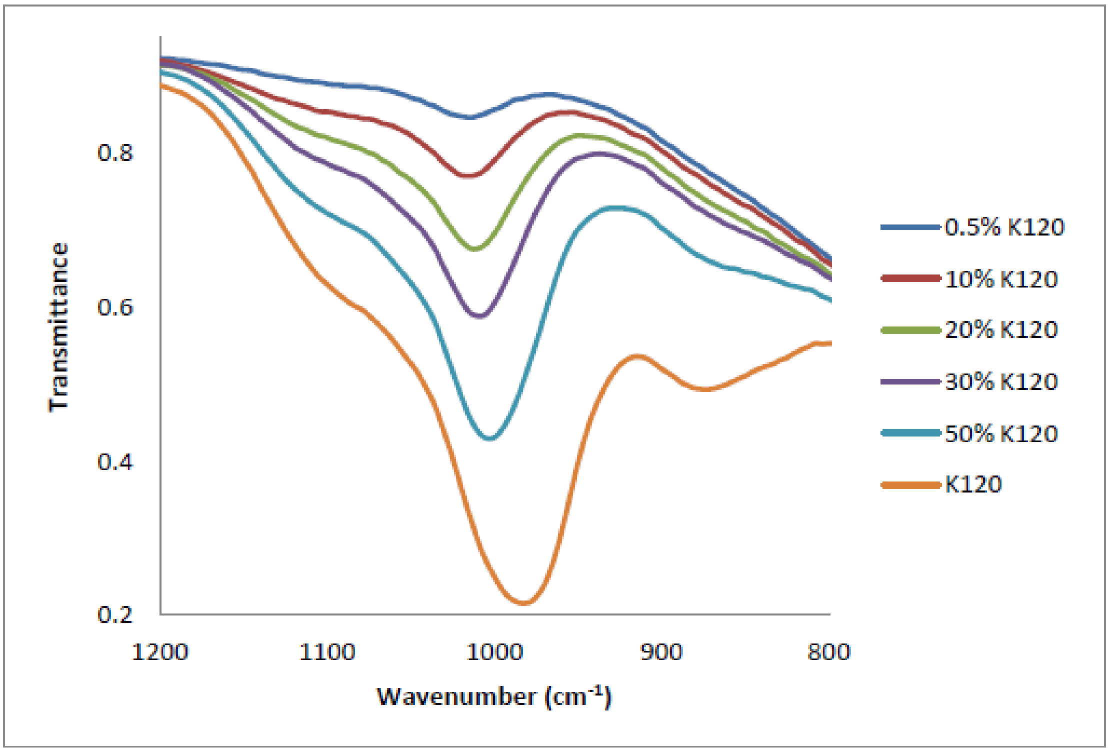

Figure 2.6 Expanded Infrared spectra showing silica/silicate absorption bands

Three main bands were found in solid silica, the strongest absorbance band centred around 1070 cm^{-1} (with a high frequency shoulder at 1200 cm^{-1}), 810 and 457. The most intense mode was correlated to the asymmetrical stretching of the Si-O-Si bond. The absorbance band at 810 cm^{-1} was characterised as symmetrical stretching or bending of the Si-O-Si bond, and the last absorbance band is assigned to rocking or bending of the bridging O-atom. However, the main absorbance in the silicate solution appeared at lower wavenumbers, between 1010-977 cm^{-1}, and the location of maximum absorption moves to lower frequency. The band shapes also changed with dilution. Although the curve fit shows bands below 850 cm^{-1}, the strong absorption of water was a strong negative influence on the determination of band location and area. Therefore, the main band was the target in this study. When the area of the silicate band around 1200-650 cm^{-1} was studied, a strong linear correlation with the silicon concentration was noted. This data indicated that using the IR integral method was an alternative method for the analysis of the silica concentration of potassium silicate solutions.

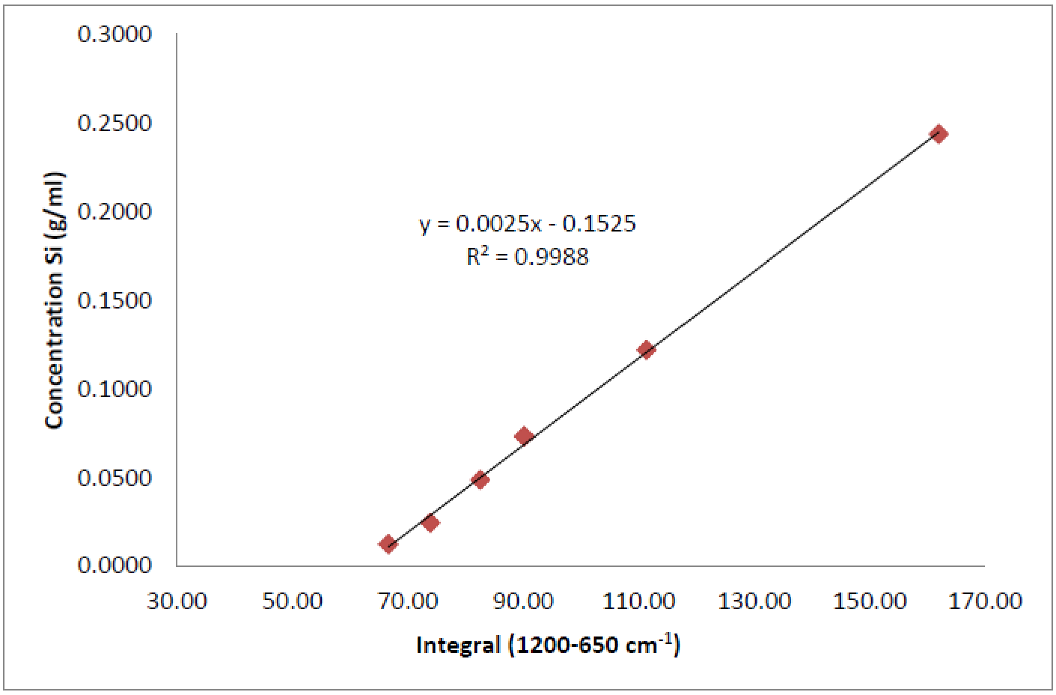

Figure 2.7 Correlation between the concentration of silicon measuring by titration and the IR integral

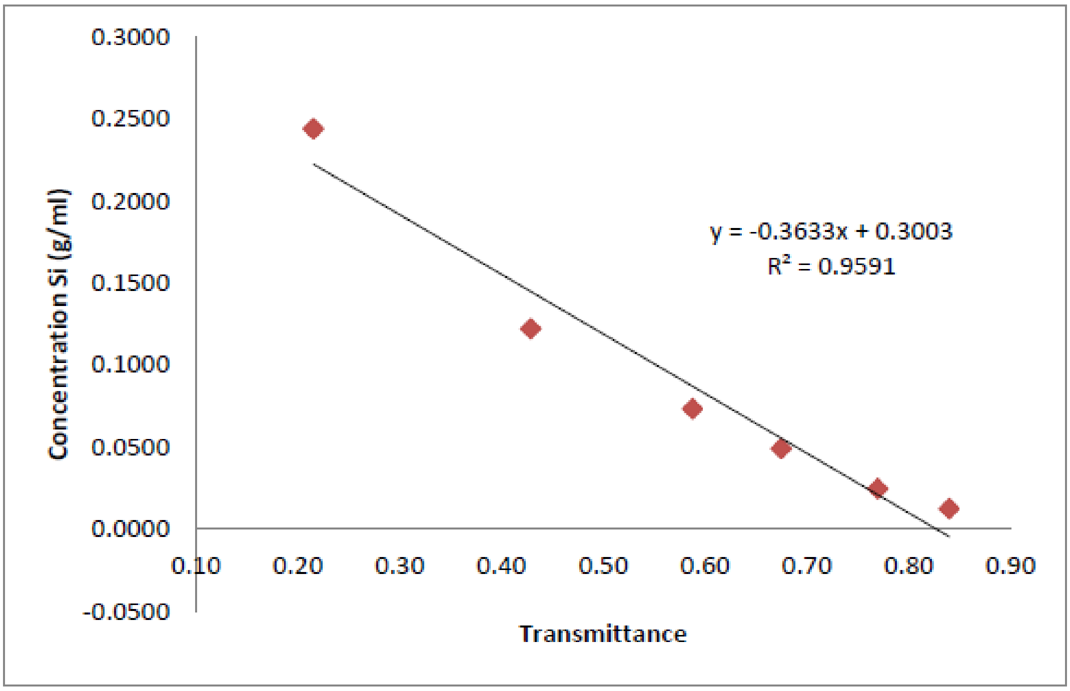

Figure 2.8 Correlation between the concentration of silicon measuring by titration and the IR transmittance

During this study, another correlation was found between the transmittance and the silicon concentration (SiO_2). Accordingly, these result suggested that both of the methods are valid.

After this initial study, the silicate solutions extracted by different volumes of 3 M-aqueous KOH were studied to verify these results. The IR method was applied and the results were compared with the silicon concentration found by titration. When the silicon concentration was studied for extraction with different volumes of potassium hydroxide solution, similar results for both methods were noted. The data suggests that IR is efficient method and reliable method for the estimation of silicate concentration.

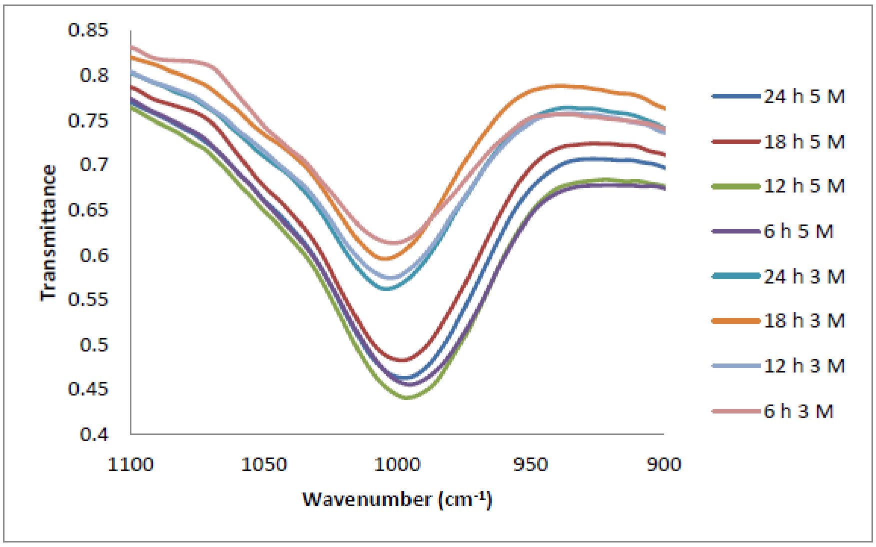

Figure 2.9 IR of the biosilicate solution (3M—208ml & 5M—125ml KOH extraction)

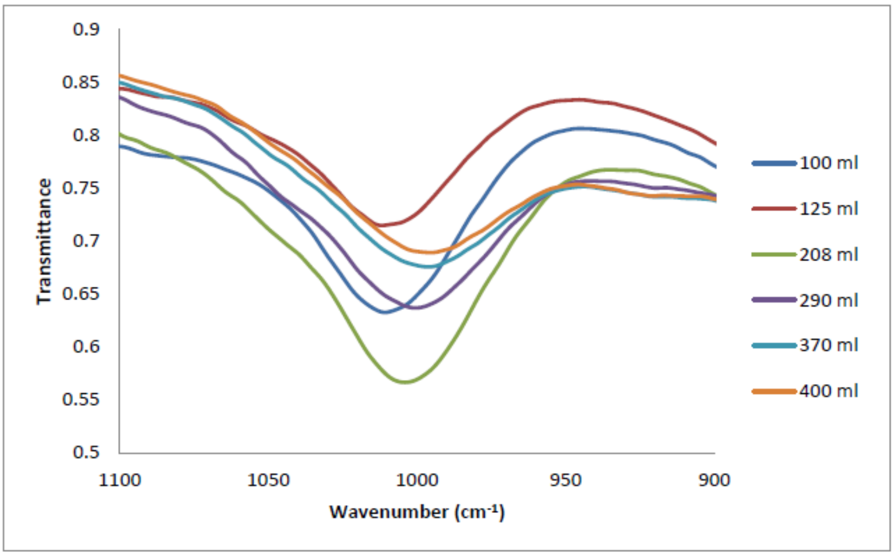

Figure 2.10 IR of the biosilicate solution extracted by different volumes of 3 M-aqueous KOH solution (reflux for 18 h)

Table 2.6 Comparison of Si concentration between titration and IR calibration in 3 M—208 ml and 5 M—125 ml KOH extraction

Biosilicate	[Si] by Titration (g/ml)	S	[Si] by IR (g/ml)		S
			X=transmittance	X=area	
			Y=-0.3633X+ 0.3003	Y = 0.0025X – 0.1525	
3M—6 h	0.0641	±0.1	0.0775	0.0714	±0.01
3M—12 h	0.0681	±0.1	0.0916	0.0836	±0.01
3M—18 h	0.0670	±0.1	0.0840	0.0680	±0.01
3M—24 h	0.0683	±0.1	0.0961	0.0831	±0.01
5M—6 h	0.0984	±0.1	0.1348	0.1240	±0.01
5M—12 h	0.1008	±0.1	0.1401	0.1282	±0.01
5M—18 h	0.0918	±0.1	0.1250	0.1035	±0.01
5M—24 h	0.0942	±0.1	0.1345	0.1183	±0.01

Table 2.7 Comparison of Si concentration between titration and IR calibration in 3 M—18h KOH extraction

Biosilicate (ml)	[Si] by Titration (g/ml)	S	[Si] by IR (g/ml)		S
			X=transmittance	X=area	
			Y=-0.3633X+ 0.3003	Y = 0.0025X – 0.1525	
100	0.0551	±0.1	0.0704	0.0648	±0.01
125	0.0376	±0.1	0.0442	0.0424	±0.01
208	0.0670	±0.1	0.0944	0.0810	±0.01
290	0.0590	±0.1	0.0683	0.0695	±0.01
370	0.0443	±0.1	0.0548	0.0655	±0.01
400	0.0420	±0.1	0.0499	0.0627	±0.01

2.3 Alkali silicate solution extraction from wheat straw (bottom) ash

Potassium silicate solution was extracted from wheat straw (bottom) ash that contained large particles and powder. Ideally, ash powder (<125 μm) was used as raw material for biosilicate solution extraction, which had to be milled prior to use. It had be proved that large particles of ash which were also named as original bottom ash could be used as feedstock for biosilicate extraction thus avoiding the need for milling.

After 24 h reflux, low concentration of silicate was extracted from these ashes. The concentration of silicate was shown in Table 2.8. In the extraction of wheat straw ash, different concentration of potassium hydroxide also had some influence on the yield or concentration of final extract, especially in ash powder extraction. For example, 5 M-aqueous KOH solution extracted more silicate than 3 M-aqueous KOH solution in the two types of ash extraction. Ash powder (<125 μm) was easily affected by different concentration of potassium hydroxide solution. With the increasing of the KOH concentration, the yield of silicate (K_2SiO_3) and the concentration of 'SiO_2' in solution was gradually increased. The same was also noted for miscanthus ash (bottom) extraction which discussed in Chapter 2.2. On the other hand, concentration of aqueous KOH solution had relatively small impact on the extraction of large particles ash. The differences between 3 M-aqueous KOH solution and 5 M-aqueous KOH solution were minor or could be regarded as within experimental error. Moreover, ash powder (<125 μm) could have higher concentration of silicate solution than large particles of ash in both 3 M- and 5 M-aqueous KOH. But concentration of silicate solution from large particles was still comparable with samples from ash powder (<125 μm). The differences of biosilicate concentration between large particles and ash powder (<125 μm) extraction were still acceptable, which was around ±0.02.

Table 2.8 Details of biosilicate solution extracted from wheat straw (bottom) ash. L means 'large particles of ash', S means ash powder (<125 μm)

1st and 2nd samples were extracted by 3M KOH solution; 3rd and 4th samples were extracted by 5M KOH solution

Biosilicate Solution	Ash size	Concentration	Concentration of SiO_2 (g/ml)	
			Titration	IR
1st	L	3M KOH	0.040	0.054
2nd	S		0.054	0.055
3rd	S	5M KOH	0.067	0.113
4th	L		0.045	0.062

2.4 Synthesis of Mesoporous MCM-41 (bio-MCM-41) from wheat straw (bottom) ash

From the early 1990s, silica derived molecular sieves with mesoporous structures of short range order have been synthesised.[81, 82] These materials offer advantages such as thermal stability, high surface areas, and shape selective catalysis. These mesoporous materials are synthesised using various template techniques and can have many applications such as catalysis and drug delivery.[89, 90] Molecular sieve type silica materials have a wide range of applications including as catalysts and catalyst supports, as adsorbents and particularly in CO_2 adsorption, and in separation. In 1992 a new family of materials were synthesised by scientists at Mobil known as MCM-41.[81, 82] They were the first mesoporous materials containing regular arrays of uniform channels (between 16-100 Å depending on synthesis conditions) to be synthesised via the calcination of silicate gels in the presence of surfactants.

2.4.1 Porosimetry of bio-MCM-41 from biosilicate solution

Porosimetry is an analytical technique which can characterise the material's surface structure and pore structure. In this section, N_2 porosimetry was introduced to identify the pore structure and surface area of mesoporous silica. The isotherm can be produced which examines the adsorption of nitrogen on the surface of a material by varying the partial pressure of nitrogen in a nitrogen/helium mixed atmosphere.[91] Adsorption is defined as the strictly physical effect of enrichment of one or more components in an interfacial layer.[124] Nitrogen porosimetry, thus, uses the inherent ability of nitrogen to condense on the surface and in the pores of a structure and also desorb.

Figure 2.11 shows the six types of adsorption isotherms classified by IUPAC. The most relevant isotherms for this section are Types I, II, and IV, which relate to microporous, nonporous, and mesoporous materials, respectively.[91]

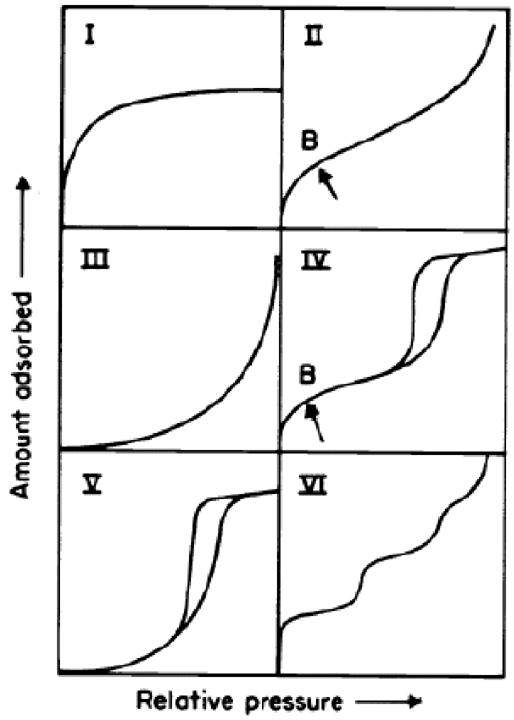

Figure 2.11 The six types of adsorption isotherm

The Type II isotherm which often refers to a non-porous material, gives information on the monolayer capacity (amount of adsorbate which can be accommodated in a single molecular layer of 1 g of the solid) of that solid. This information can be used to calculate the surface area by multiplying the number of molecules adsorbed by the area taken up by each molecule.[91] The pore size definitions by IUPAC are shown in Table 2.9.

Table 2.9 Pore size definitions. 1 nm = 10^{-9} m

	Pore Width (nm)
Micropore	Less than 2
Mesopore	Between 2 and 50
Macropore	More than 50

Microporous materials, represented by the Type I isotherm, adsorb a high volume of nitrogen at very low relative pressure. In the microporous materials, the potential field from neighbouring pore walls will overlap as the pore width is only few nanometres.[91]

This will result an enhancement of the interaction energy between solid material and gas molecule. Then the pores will be filled at a very low relative pressure.[91] Mesoporous materials have a Type IV isotherm (Figure 2.12) which follows a similar tendency to the microporous materials (Type II isotherm) at low relative pressure. But Type IV isotherm has a setting point 'C' that the isotherm will rise upwards until at higher pressures, then slope decreases.[91]

There are two stages adsorption of nitrogen in a mesoporous material. At first, a monolayer of the adsorbate is formed across the surface. It relates to the initial rise in volume adsorbed of its isotherm. The secondary step is caused by Capillary Condensation and is defined as a transformation of a vapour to a liquid in a pore. The Capillary Condensation occurs at a pressure which is lower than the saturation vapour pressure when there exists a concave meniscus in the pore. The radius of the capillary is replaced by the pore radius minus the thickness of the adsorbed film.[92] In the pore, the initial monolayer acts as a seed for the condensation to take place. When the adsorbate evaporates, the process spontaneously occurs once the relative pressure is low enough to change the meniscus.

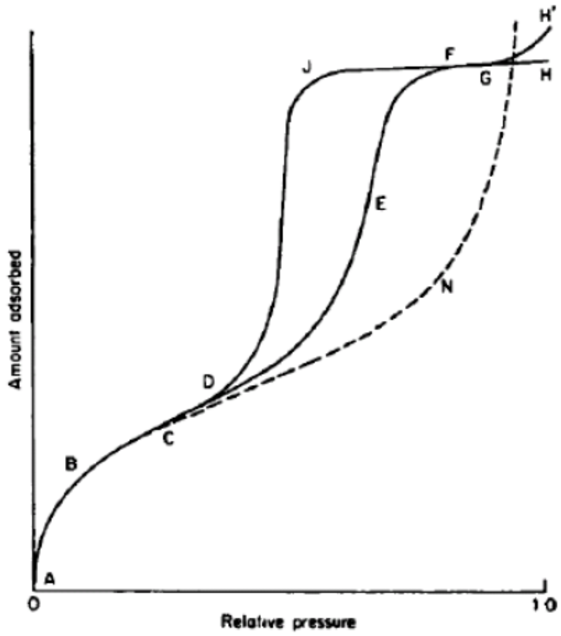

Figure 2.12 Type IV isotherm line from reference[91]

The process of hysteresis occurs only in some kinds of pore types. For a cylindrical pore which is closed at one end, the condensation begins at that end to form a hemispherical meniscus which then expands to the end of the pore. The process of evaporation then starts at the pore face and continues to the end of the pore. These processes occur at the same relative pressures. So the hysteresis loop is not appeared. If a cylindrical pore open at both sides, the condensation occurs from the film on the walls and a cylindrical meniscus is formed until the pore is full whereas a hemispherical meniscus is formed on evaporation. Since this difference in meniscus affects the core radius of the pore, these two processes occur at different relative pressure and this creates the hysteresis loop.

All mesoporous silica synthesised in this thesis showed extremely high surface areas, in a range of 1000—1600 $m^2\,g^{-1}$, pore volumes of 1.04--1.39 $cm^3\,g^{-1}$, and pore diameters of 2.67—3.81 nm. These values were comparable with the results summarized by Dr Emma Cooper[12], who used commercial alkali silicate and other kinds of silica sources (Table 2.11).

Table 2.10 Surface area values from porosimetry of MCM-41

Si Source	**BET Surface Area ($m^2\,g^{-1}$)**	**Pore Volume ($cm^3\,g^{-1}$)**	**Average Pore Diameter (nm)**
1st Biosilicate	1057	1.04	3.02
2nd Biosilicate	1354	1.26	2.86
3rd Biosilicate	1071	1.32	3.81
4th Biosilicate	1613	1.39	2.67
K120[7]	1010	0.80	3.20

Table 2.11 Surface area values from porosimetry summarized by Dr Emma Cooper[12]

	BET Surface Area ($m^2\,g^{-1}$)	Pore Volume ($cm^3\,g^{-1}$)	Average Pore Diameter (nm)
Rice Hull Ash[93]	1100	0.869	2.95
Sodium Silicate[93]	1180	0.91	2.95
Coal Fly Ash[94]	1149	0.6	not given
Coal Fly Ash[94]	953	0.9	not given
Coal Fly Ash[94]	996	0.7	not given
Power Plant Bottom Ash[95]	847	0.7	3.0

Porosimetry results of bio-MCM-41 which used K120 and biosilicate (wheat straw) solution as silicon source were shown in Table 2.10. The lowest surface area of WSA-MCM-41 (MCM-41 made from wheat straw bottom ash) was around 1000 $m^2\,g^{-1}$. Moreover, a surface area of 1600 $m^2\,g^{-1}$ could be achieved WSA-MCM-41. Also, the pore volume and average pore diameter were higher than literature data. Biosilicate from both types of ash was reasonable to produce mesoporous silica; the bio-MCM-41 with the largest surface area was from large particles ash synthesized.

The typical isotherm for the four types of materials is shown in Figure 2.13, Figure 2.14, Figure 2.15 and Figure 2.16. The isotherm for WSA-MCM-41 (3 M-aqueous KOH extraction from large particles, Figure 2.13) isotherm, gave a steep increase of nitrogen adsorption around 0.3—0.4 relative pressure with an adsorption of 140 $cm^3\,g^{-1}$. This inflexion in the isotherm was related to mesopores with a small range of sizes.[78] Also, there was no significant increase in adsorption at the start of the isotherm meaning virtually no microporosity. A Type H4 hysteresis loop was observed probably indicative of narrow mesopores open at both ends.[78] The second WSA-MCM-41 (3 M-aqueous KOH extraction from wheat straw ash powder, Figure 2.14) had the similar type of isotherm with respect to the first WSA-MCM-41, but larger scale of adsorption ($cm^3\,g^{-1}$). The fourth WSA-MCM-41 had much more centralized mesopore structure (Figure 2.16), whilst the third WSA-MCM-41 (Figure 2.15) had much more steep increase than other types of MCM-41.

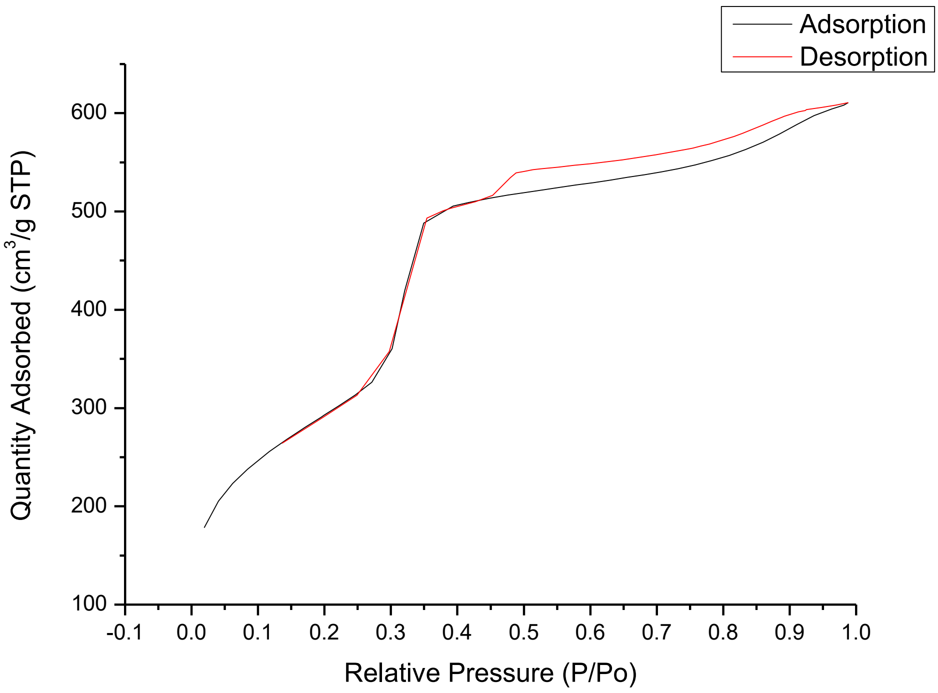

Figure 2.13 N_2 Adsorption/ Desorption Isotherm for WSA-MCM-41 (biosilicate from 1st extraction)

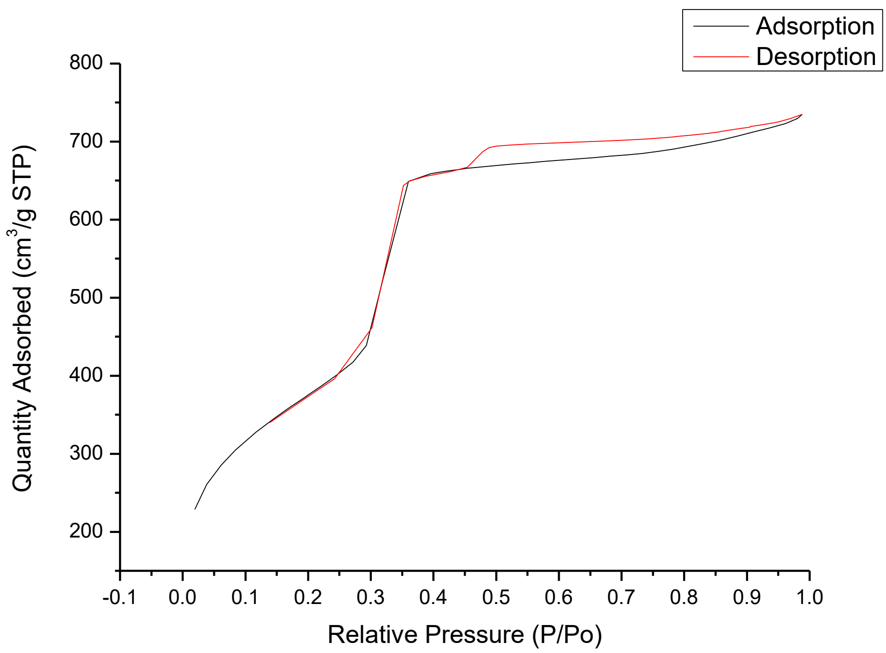

Figure 2.14 N_2 Adsorption/ Desorption Isotherm for WSA-MCM-41 (biosilicate from 2nd extraction)

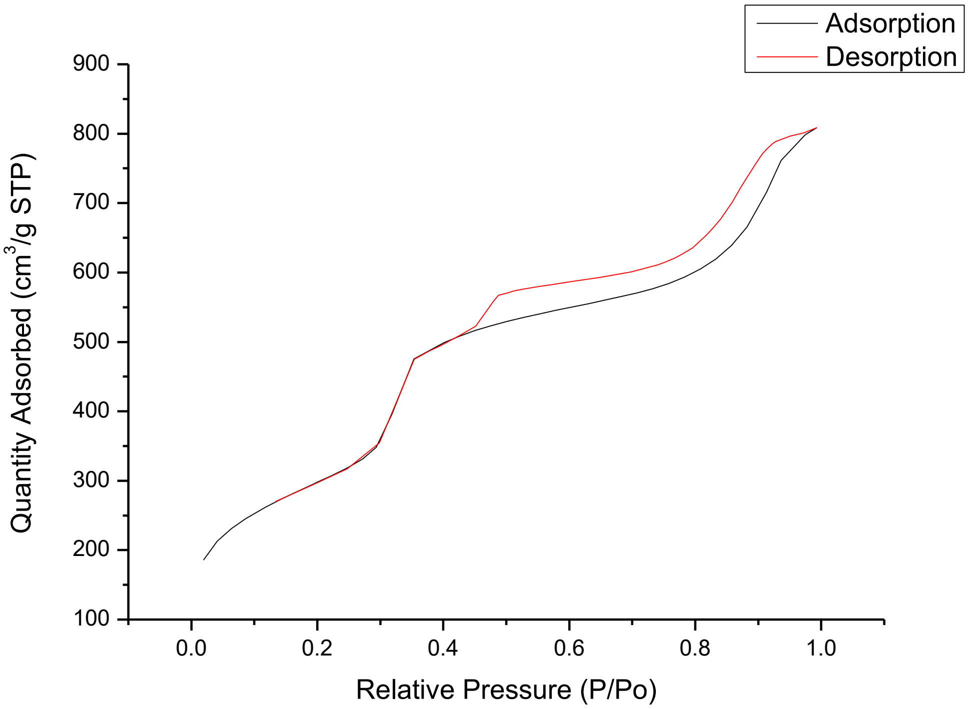

Figure 2.15 N_2 Adsorption /Desorption Isotherm for WSA-MCM-41 (biosilicate from 3rd extraction)

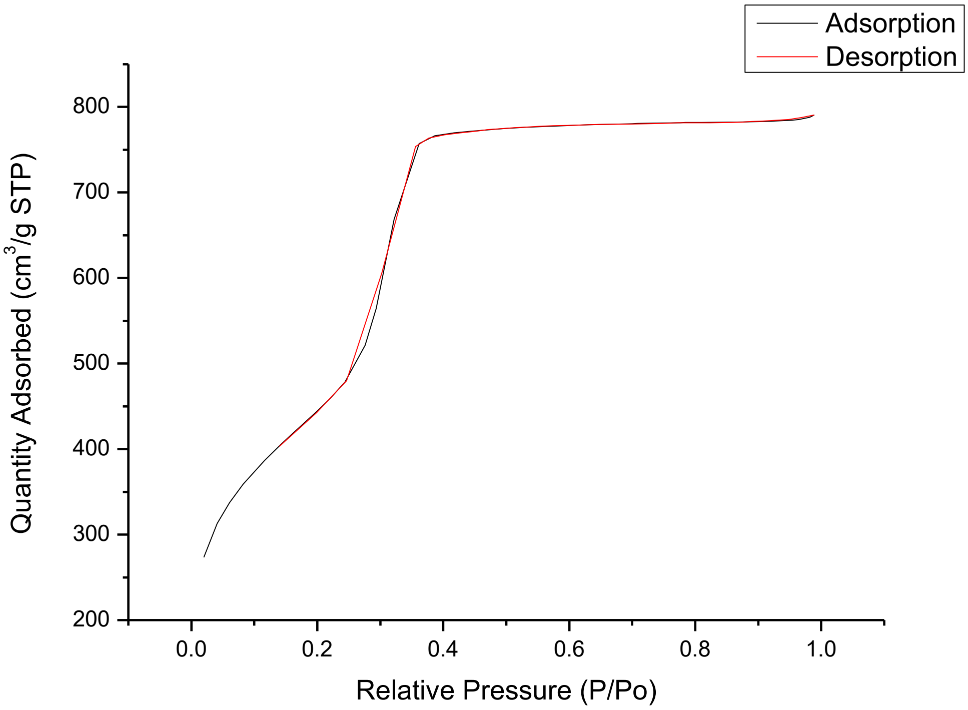

Figure 2.16 N_2 Adsorption /Desorption Isotherm for WSA-MCM-41 (biosilicate from 4th extraction)

The pore size distributions of WSA-MCM-41 (synthesized by biosilicate solutions) were shown in Figure 2.17. The pore size distribution of WSA-MCM-41 revealed one or two symmetric, and significant peaks, corresponding to pores in the range of 2 – 4 nm. Typically, MCM-41 should have one significant peak in the pore size distributions. For example, 4th WSA-MCM-41 just had one significant peak (shown in Figure 2.17) in the pore size distribution, which suggested that the 4th WSA-MCM-41 possessed a narrow pore range between 2nm and 3nm. But for 1st, 2nd and 3rd WSA-MCM-41, they had one strong peak and a minor peak in the pore size distribution (<5 nm), indicating there were two types of pore in the mesoporous materials (approximately 2.6 nm and 3.5 nm).

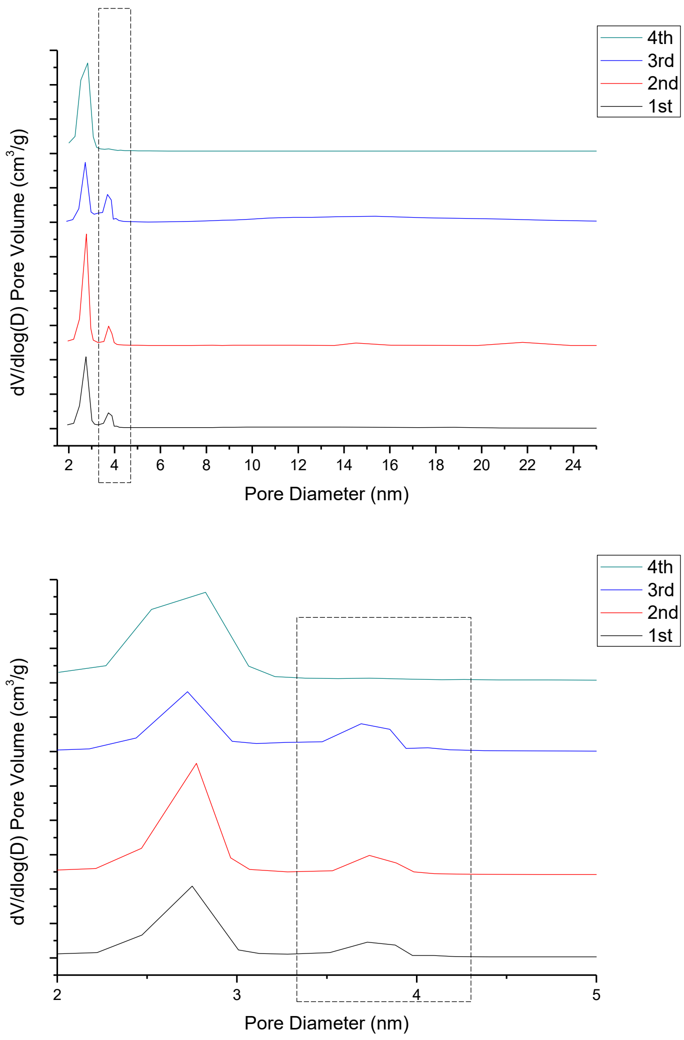

Figure 2.17 BJH adsorption pore size distribution for WSA-MCM-41. (Silicon source extracted from wheat straw bottom ash)

2.4.2 X-Ray diffraction analysis (XRD)

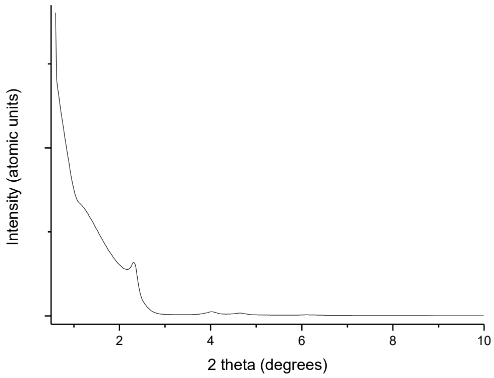

1st WSA-MCM-41

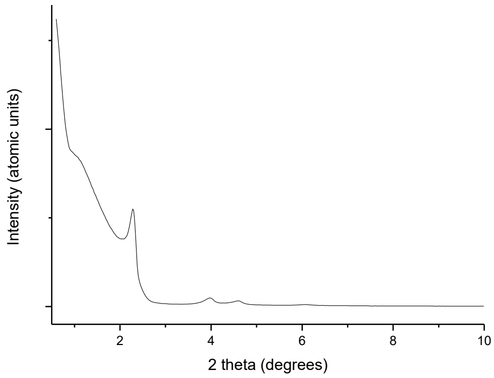

2nd WSA-MCM-41

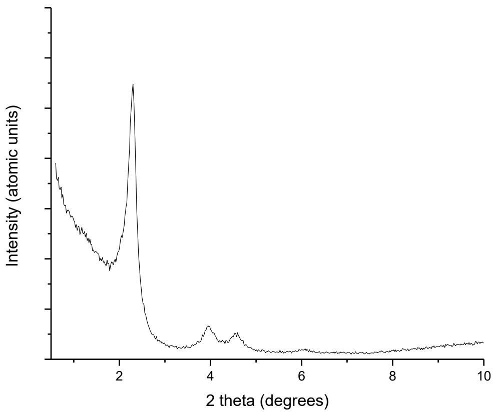

3rd WSA-MCM-41

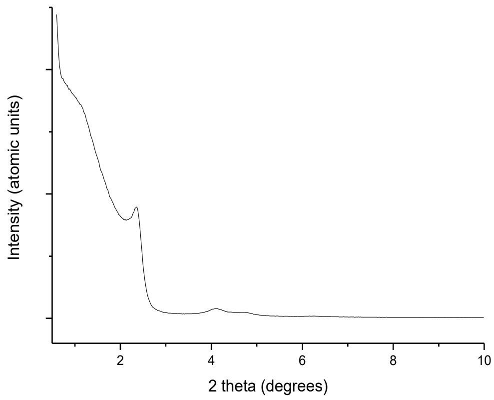

4th WSA-MCM-41

Figure 2.18 XRD analysis of MCM-41 synthesized with biosilicate solution (wheat straw bottom ash)

XRD spectra for all materials revealed one significant 2θ peak between 2 and 3 suggesting the presence of crystallinity and order. Also, there was one tiny shoulder of low intensity at the low 2θ. The XRD pattern of 3rd WSA-MCM-41 revealed relatively strong peaks compared to other samples, which indicated high crystalized structure inside.

2.4.3 Transmission electron microscopy (TEM) and scanning electron microscope (SEM)

Transmission Electron Microscopy (TEM) is an efficient method to image structures at high magnifications. TEM images of bio-MCM-41 prepared were shown in Figure 2.19 and

Figure 2.20, which clearly show the tube structure characteristic of a typical mesoporous materials. Normally, the surface of the tube structure was easily found and the transection of the tube structure which shown as hexagonal arrays is minority. The pore diameter measured by TEM (3.5 nm) was similar to porosimetry data (3.8 nm).

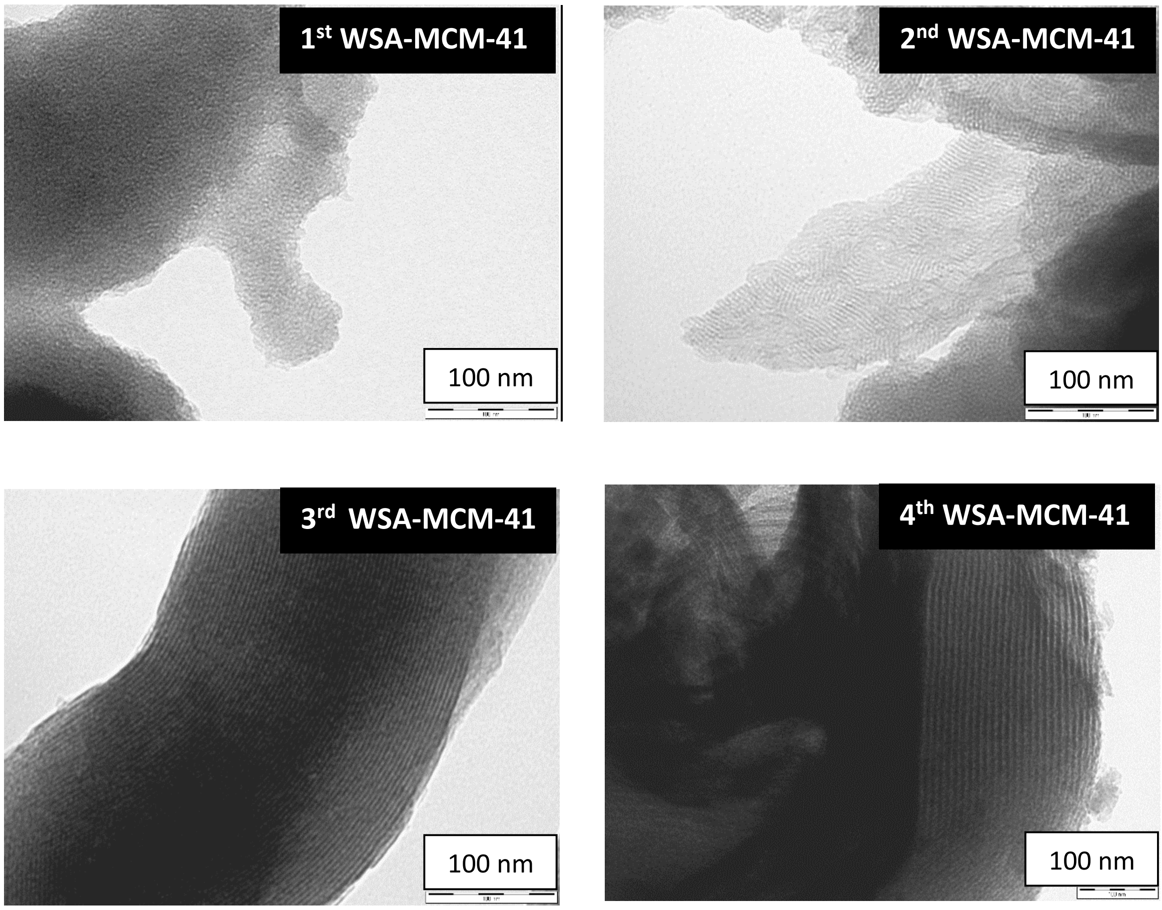

Figure 2.19 TEM of four types of WSA-MCM-41

The hexagonal pore arrangement was clearly observed in the 3rd WSA-MCM-41 for which, its SEM displayed a characteristic random and approximately spiral arrangement.

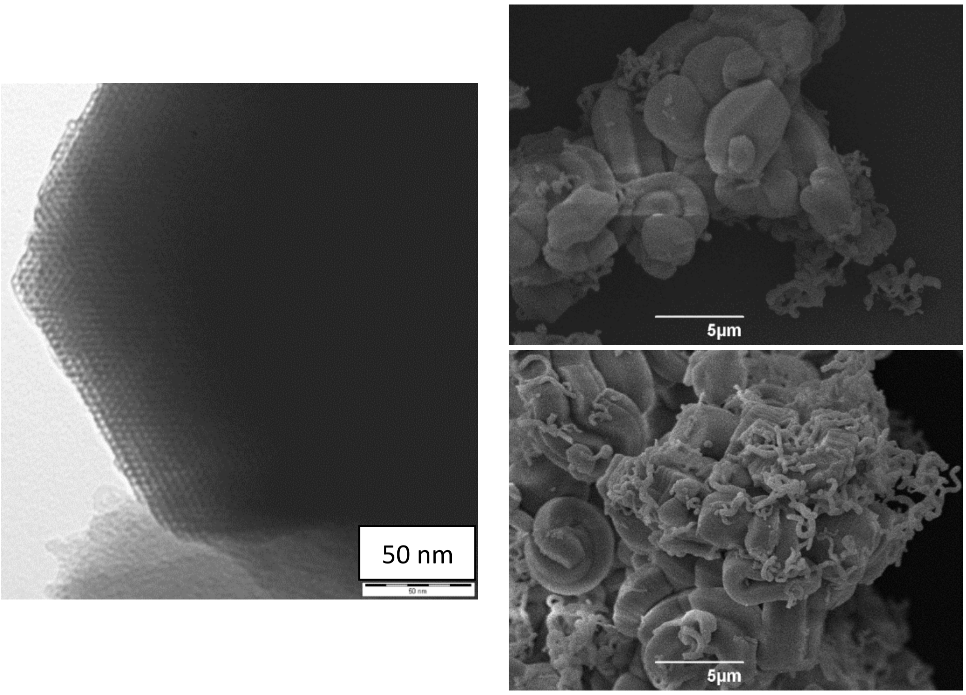

Figure 2.20 Hexagonal pore arrangement of 3rd WSA-MCM-41 in TEM (Right); and SEM images of 3rd WSA-MCM-41 (Left)

2.4.4 Solid-state nuclear magnetic resonance (Solid-State NMR)

Solid-State NMR spectroscopy plays an important role in characterization of mesoporous materials. Initially, MAS NMR of ^{29}Si was used to provide the information of structure, relative concentration, location of silicon and variously functionalized group in mesoporous silica. There are three major types of connections in mesoporous silica, which include siloxane bridges $(SiO)_4Si$ (also named Q_4, resonance around -110 ppm), single silanol $(SiO_3)SiOH$ (Q_3, resonance around -100 ppm) and geminal silanol $(SiO_2)Si(OH)_2$ (Q_2, resonance around -90 ppm). The results of solid-state ^{29}Si NMR for WSA-MCM-41 shown in Figure 2.21 and Figure 2.22.

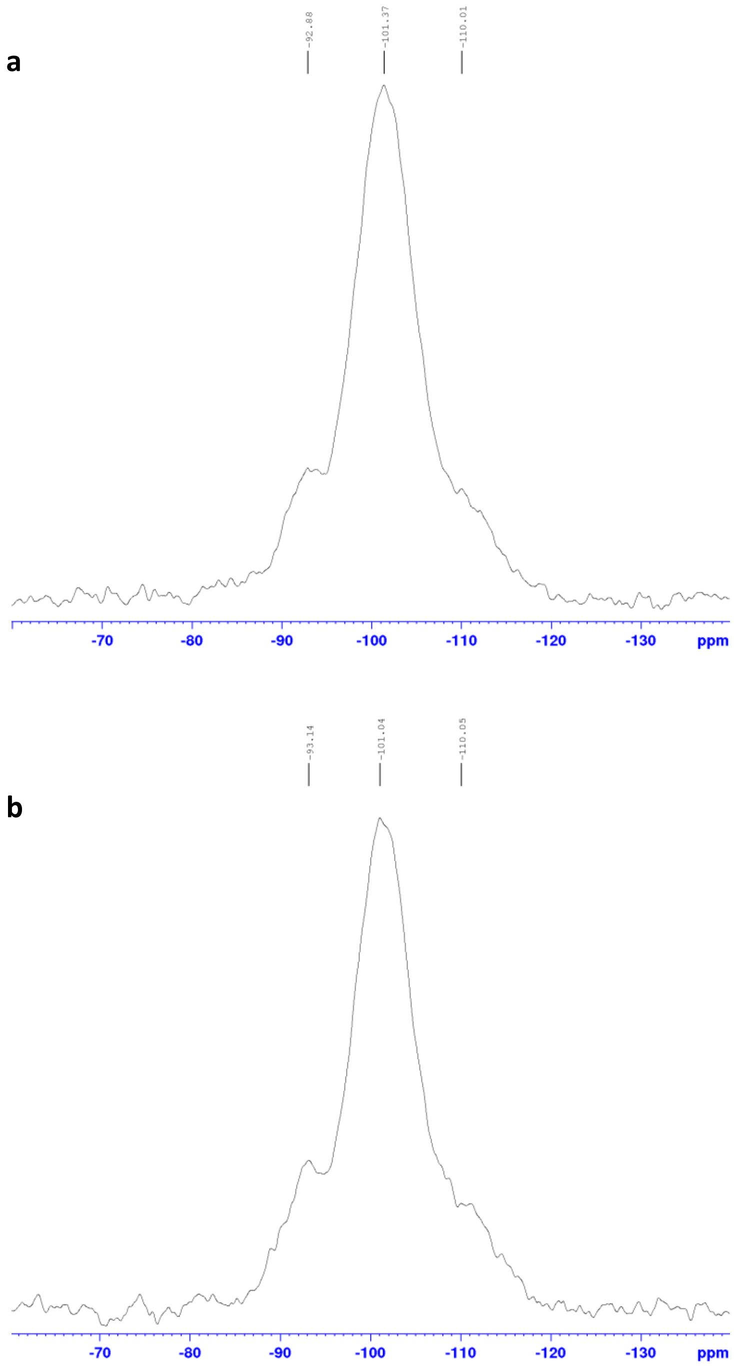

Figure 2.21 Solid-state ^{29}Si NMR for 1st WSA-MCM-41 (a) and 2nd WSA-MCM-41 (b)

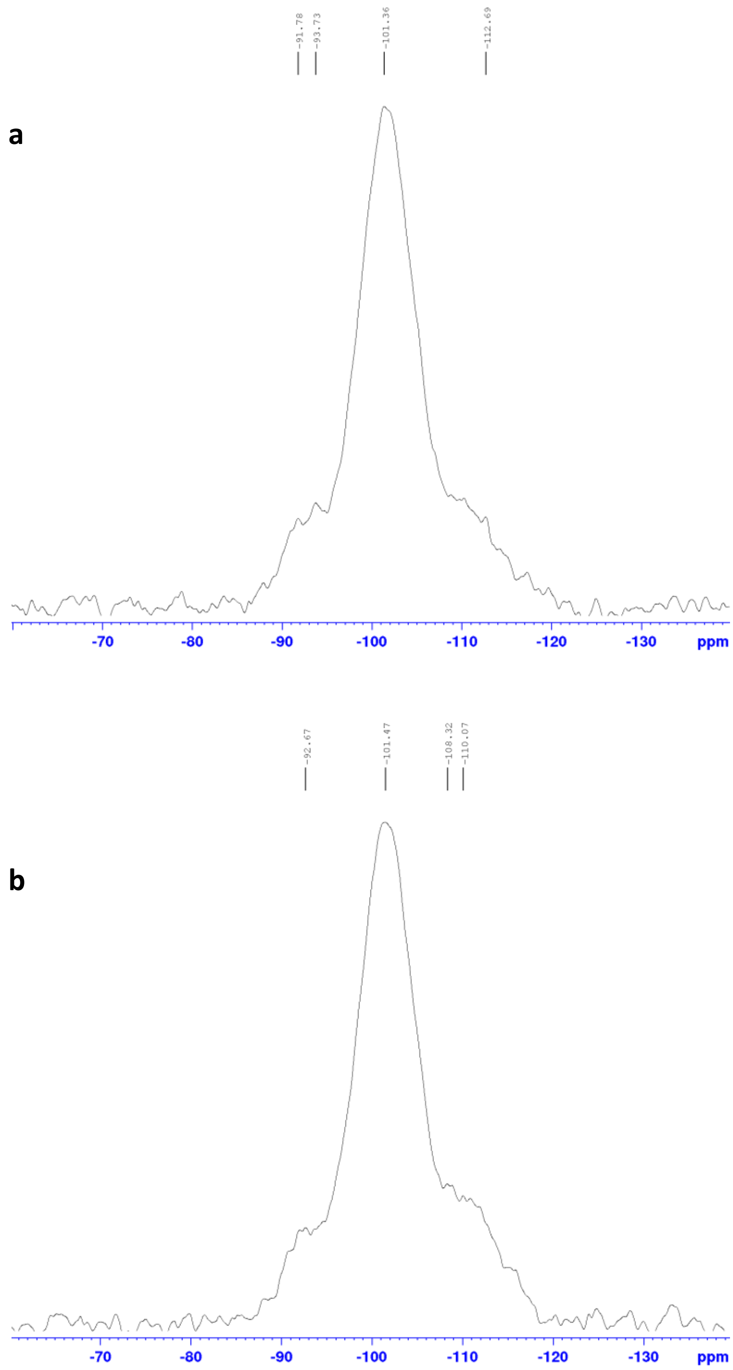

Figure 2.22 Solid-state ^{29}Si NMR for 3rd WSA-MCM-41 (a) and 4th WSA-MCM-4 (b)

In the four NMR spectra shown, silicon types of Q_2, Q_3 and Q_4 were detected. Also, minor small signals around the characteristic peaks of Q_n types, which are probably caused by the shifting of main peak and residues appeared were noted.

2.5 Synthesis of Mesoporous SBA-15 from wheat straw (bottom) ash

In 1998 a new family of mesoporous silica named SBA, with larger pores and thicker walls than the MCM family were synthesized from tetraethyl orthosilicate (TEOS). These materials were synthesized via a micelle template method in an acidic aqueous environment (pH ≈1). The template used for SBA-15 is Pluronic P123, an organic triblock copolymer (polyethylene glycol – polypropylene glycol – polyethylene glycol) which has surfactant properties.[87, 88] The traditional method to produce SBA-15 is to use TEOS as the silicon source, which hydrolyses, condenses, and precipitates as silica with the presence of water by a sol-gel mechanism. In this section, biosilicate extracted from wheat straw ash was considered as an alternative silicon source to produce SBA-15. With the application of biosilicate solution in SBA-15, the total process would be low-cost and environmental friendly.

SBA-15 has the same hexagonal pore structure as MCM-41 and larger pore than MCM-41, which is due to a change in template leading to larger micelles. Mesoporous SBA-15 made from wheat straw biosilicate (WSA-SBA-15) was analysed by N_2 porosimetry, XRD, TEM, SEM and solid-state ^{29}Si NMR.

2.5.1 Porosimetry of SBA-15 from biosilicate solution

The porosimetry data for TEOS-SBA-15 and WSA-SBA-15 is shown in Table 2.12. The surface area of WSA-SBA-15 ranged between 800 m^2 g^{-1} and 960 m^2 g^{-1}. All of the WSA-SBA-15's possessed larger surface area than TEOS-SBA-15. The pore volume and pore diameter between the two types of SBA-15 were similar. Pore volume varied around 0.85 cm^3 g^{-1} and pore diameter was in the range of 4.5 –5.6 nm. According to the porosimetry data only, WSA-SBA-15 was comparable to TEOS-SBA-15 and could be an alternative resource to produce mesoporous SBA-15. N_2 adsorption-desorption isotherms of TEOS-SBA-15 and WSA-SBA-15 are depicted in Figures 2.23-2.27. The adsorption/desorption isotherms showed a significant difference in the porosity between TEOS-SBA-15 and WSA-SBA-15. It is clear that TEOS-SBA-15 sample had a significant sharp steep increase of the isotherm around 0.6 P/P_0 with a hysteresis loop akin to type H4, i.e., narrow mesopores open at both ends[78], similar to mesoporous MCM-41.

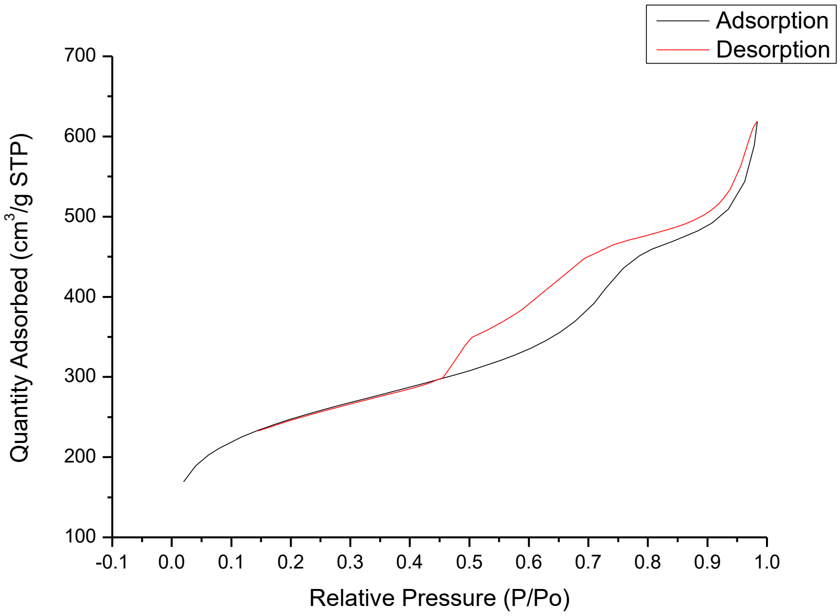

Figure 2.23 N_2 Adsorption Desorption Isotherm for WSA-SBA-41 (biosilicate from 1st extraction)

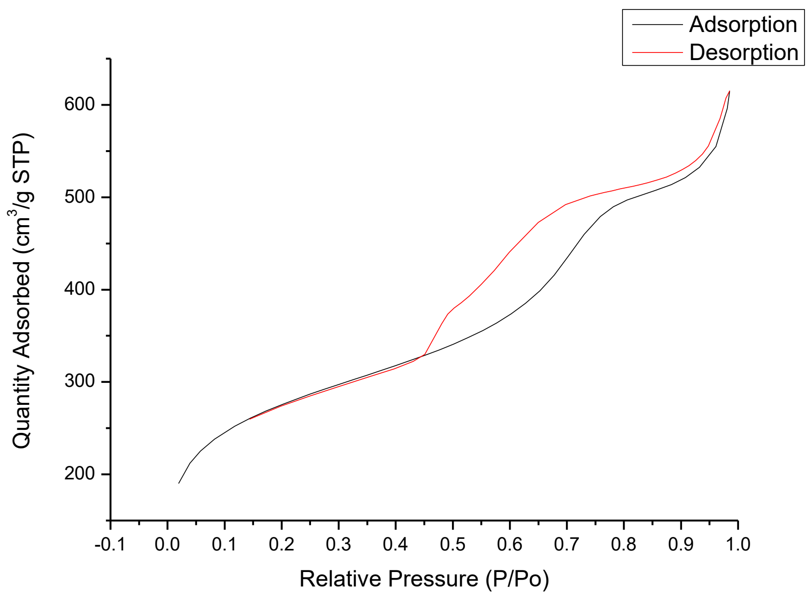

Figure 2.24 N_2 Adsorption Desorption Isotherm for WSA-SBA-41 (biosilicate from 2nd extraction)

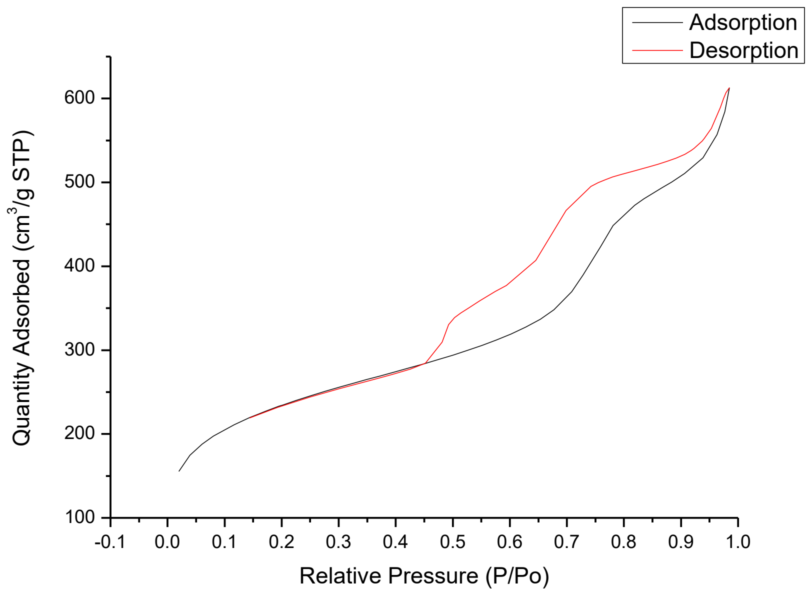

Figure 2.25 N_2 Adsorption Desorption Isotherm for WSA-SBA-41 (biosilicate from 3rd extraction)

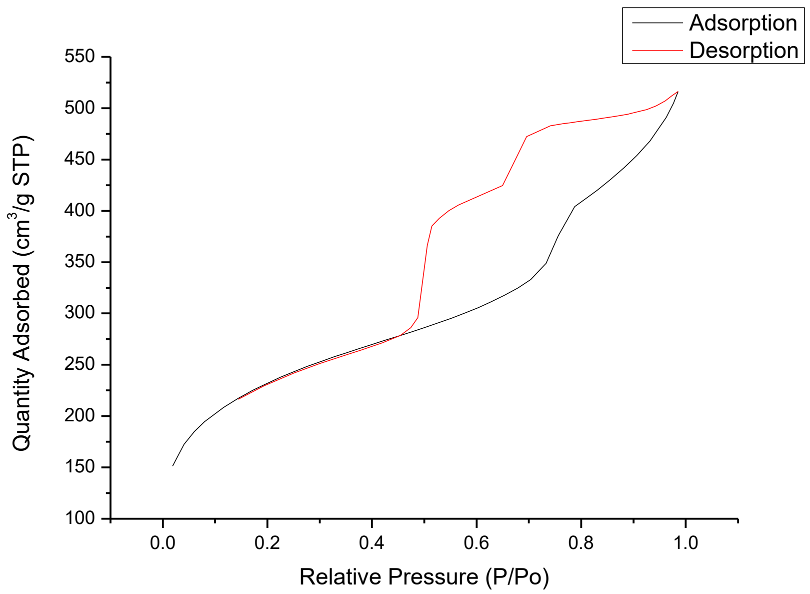

Figure 2.26 N_2 Adsorption Desorption Isotherm for WSA-SBA-41 (biosilicate from 4th extraction)

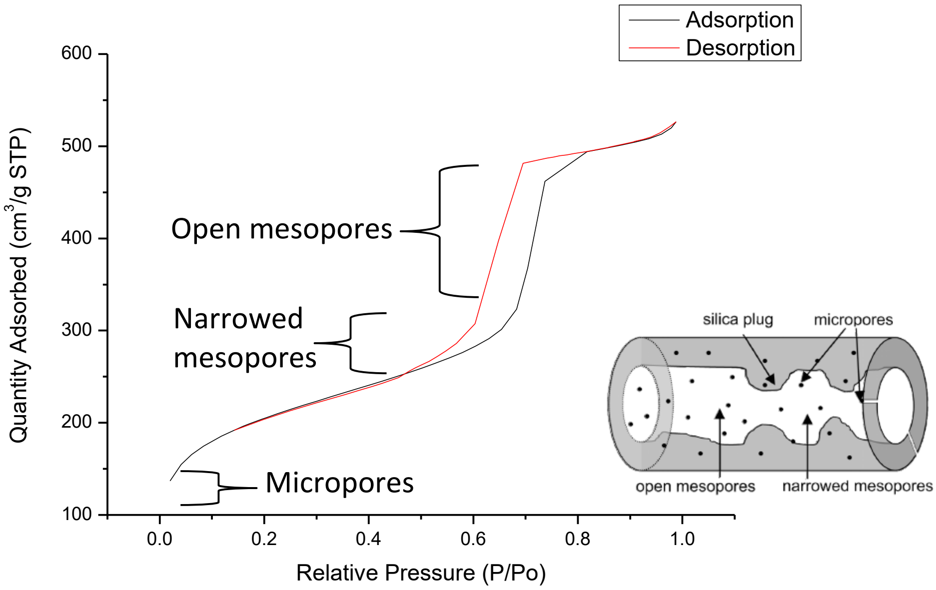

Figure 2.27 Effect of narrowed pores in TEOS-SBA-15 structure on the isotherm shape.

This effect is clearly shown in the pore size distribution of TEOS-SBA-15 and WSA-SBA-15 (Figure 2.27). Initially, the characteristic peaks in the two types of SBA-15 were definitely different. TEOS-SBA-15 had a significant peak around 6 – 7 nm, which indicated much larger pore size and consistent pore. WSA-SBA-15 had two significant peaks at 4 nm and 5 – 7 nm, respectively, which suggested dispersive and small pore size. There was also a sharply defined pore size peak at around 4 nm which is lower than that for TEOS-SBA-15 which is around 5 - 7 nm. This could imply the WSA-SBA-15 materials has thicker pore walls (and thus smaller pores).[12]

Table 2.12 N_2 porosimetry results of TEOS-SBA-15 and WSA-SBA-15

		BET Surface Area ($m^2\,g^{-1}$)	BJH Pore Volume ($cm^3\,g^{-1}$)	Average Pore Diameter (nm)
SBA-15	1st	863	0.85	5.65
	2nd	960	0.82	5.12
	3rd	824	0.88	5.51
	4th	817	0.74	4.50
	TEOS	700	0.80	4.47

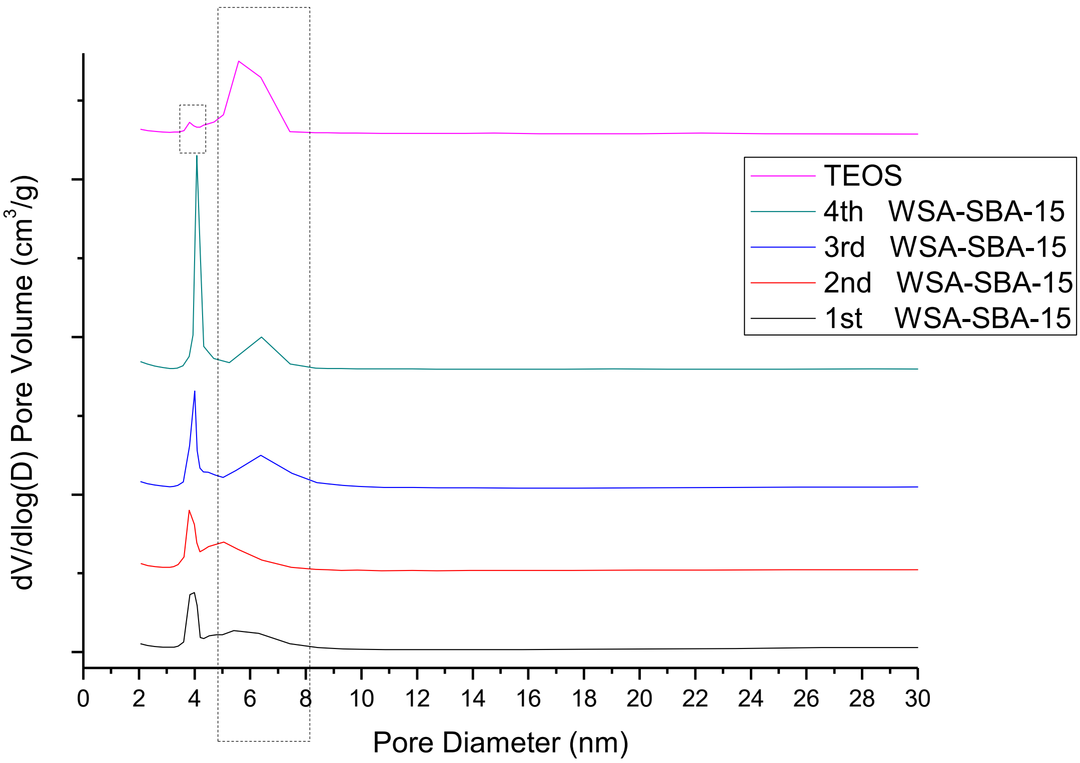

Figure 2.28 BJH desorption pore size distribution of TEOS-SBA-15 and WSA-SBA-15

2.5.2 X-Ray diffraction analysis (XRD)

Low angle XRD patterns of WSA-SBA-15 and TEOS-SBA-15 are shown in Figure 4.28. Typical SBA-15 should have a characteristic peak at 1° (2Θ). However, WSA-SBA-15 did not have any distinct peaks in this region. The crystallized and ordered structure could not be presented clearly in WSA-SBA-15 samples.

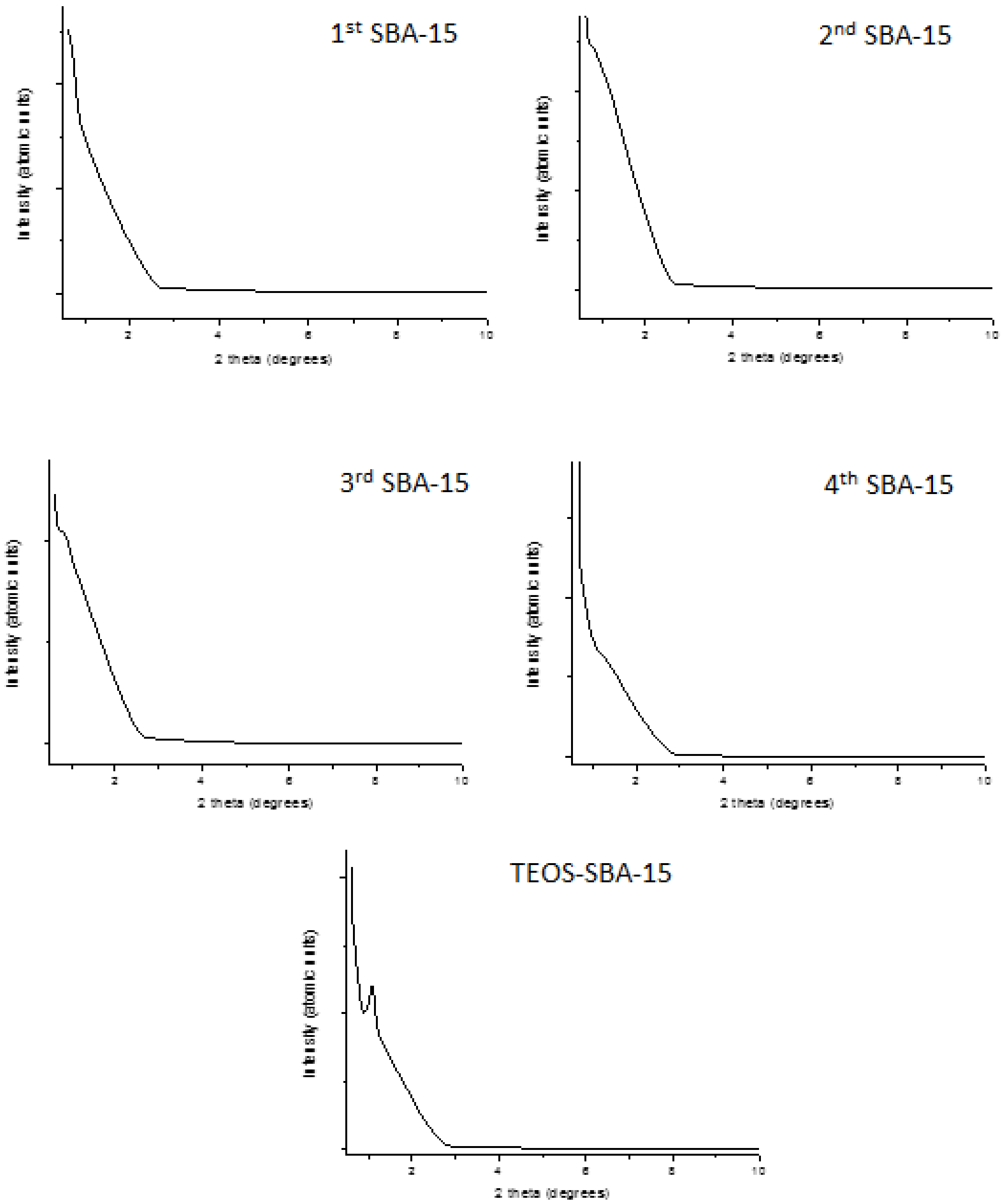

Figure 2.29 XRD analysis of SBA-15 synthesized with biosilicate solution and TEOS (wheat straw bottom ash)

2.5.3 Transmission electron microscopy (TEM) and scanning electron microscope (SEM)

TEM images of WSA-SBA-15 materials are shown in Figure 2.30 and Figure 2.31. The uniform pore and structure are clearly observed for TEOS-SBA-15 and WSA-SBA-15. But it was clear that the structure of TEOS-SBA-15 had strongly organized structure and pore size commensurate with its N_2 porosimetry and XRD results. 1st, 2nd and 3rd WSA-SBA-15 samples also possessed a fair degree of ordered structure and pore size but intermingled with disordered and random areas. TEM of the 4th WSA-SBA-15 sample was similar with TEOS-SBA-15. The two materials have significant ordered arrangement of pore and structure. The hexagonal arrays also could be found in the materials shown in Figure 2.31 b and 2.31 d.

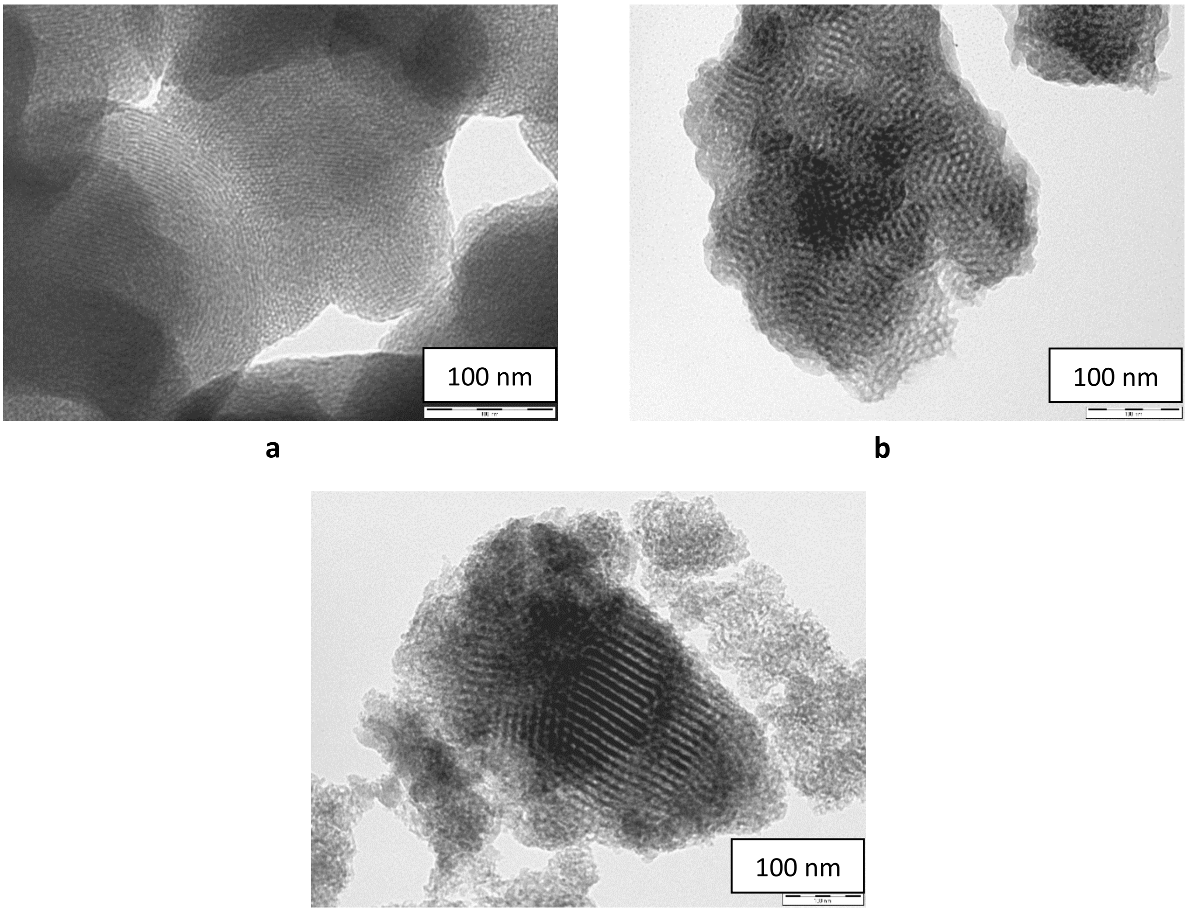

a b

c

Figure 2.30 TEM images of WSA-SBA-15. a—1st WSA-SBA-15 from 3M KOH extraction (large particles); b—2nd WSA-SBA-15 from 3M KOH extraction (powder); c—3rd WSA-SABA-15 from 5M KOH extraction (powder)

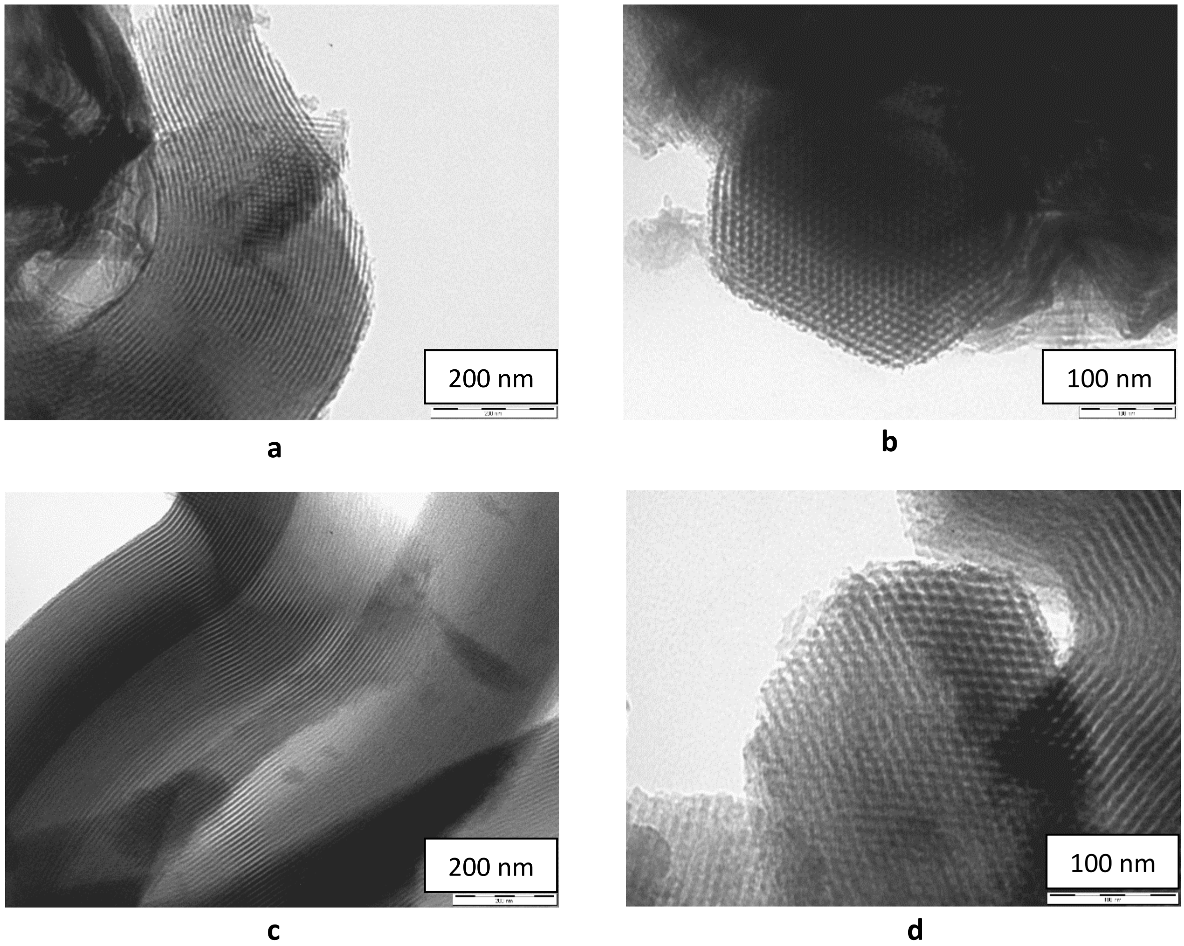

Figure 2.31 TEM images of WSA-SBA-15. a—4th WSA-SBA-15 from 3M KOH extraction (large particles); b—4th WSA-SBA-15 from 3M KOH extraction (large particles); c—TEOS-SBA-15; d—TEOS-SBA-15

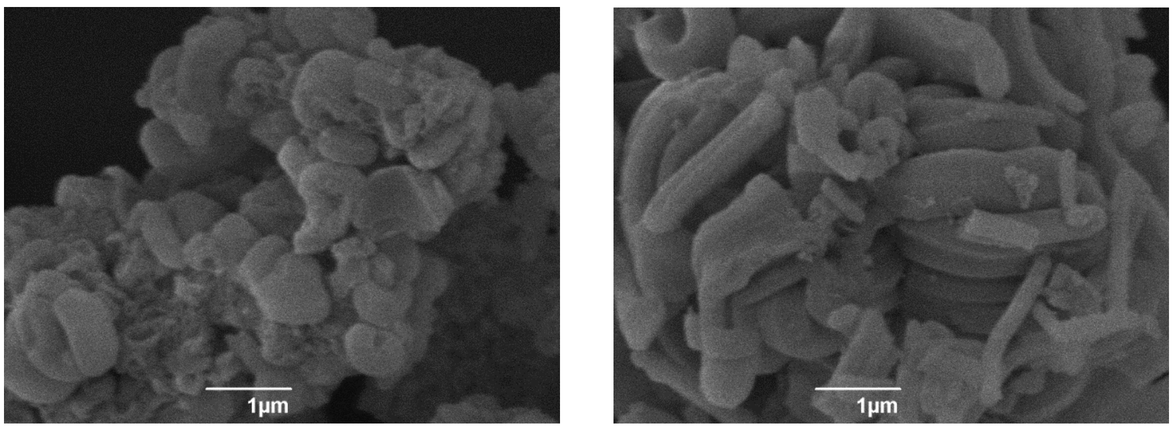

Figure 2.32 SEM analysis of SBA-15, 4th WSA-SBA-15 on the left and TEOS-SBA-15 on the right

SEM images of the 4th WSA-SBA-15 and TEOS-SBA-15 shown in Figure 2.32 visualise the tube structure.

2.5.4 Solid-state nuclear magnetic resonance (Solid-State NMR)

CP-MAS NMR of ^{29}Si was used to prove the presence of Si and different types of Q_n in mesoporous SBA-15. The three major types of connections in mesoporous silica were same to MCM-41, which include siloxane bridges $(SiO)_4Si$ (also named Q_4, resonance around -110 ppm), single silanol $(SiO_3)SiOH$ (Q_3, resonance around -100 ppm) and geminal silanol $(SiO_2)Si(OH)_2$ (Q_2, resonance around -90 ppm).

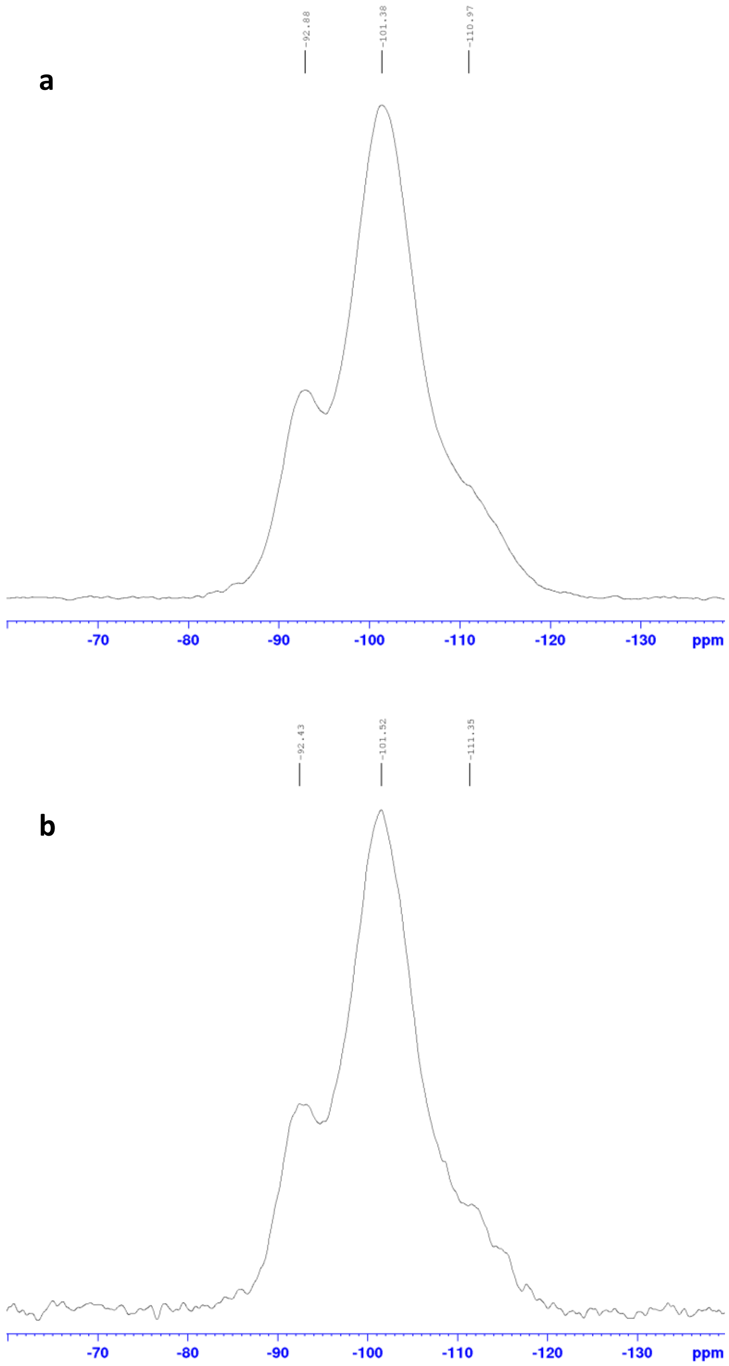

Figure 2.33 Solid-state ^{29}Si NMR for 1st WSA-SBA-15 (a) and 2nd WSA-SAB-15 (b)

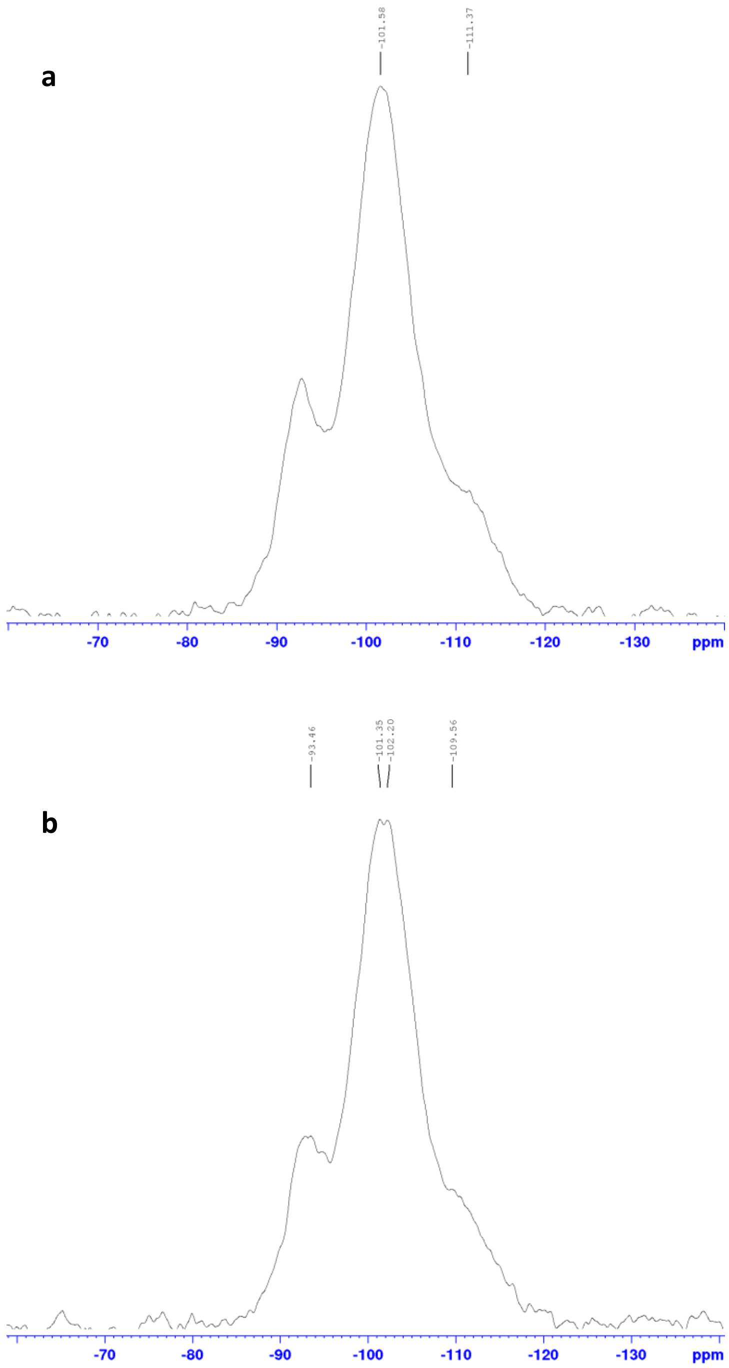

Figure 2.34 Solid-state ^{29}Si NMR for 3rd WSA-SBA-15 (a) and 4th WSA-SAB-15 (b)

It is clear that all the mesoporous silica had the similar result from solid-state ^{29}Si NMR analysis. The Q_2, Q_3 and Q_4 types of silicon were all similar with the results in literature. Even the comparison between WSA-SBA-15 and TEOS-SBA-15, there was no significant difference in the materials.

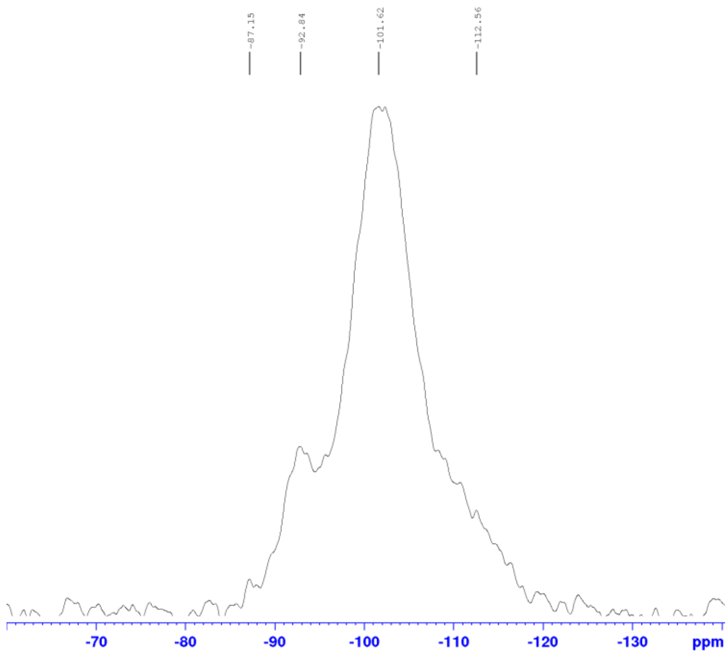

Figure 2.35 Solid-state ^{29}Si NMR for TEOS-SBA-15

2.5.5 The effect of aged time to WSA-SBA-15

The effect of aging of 4th WSA-SBA-15 on pore structure was investigated. The N_2 porosimetry data is shown in Table 2.13.

Significant surface area was still present after aging of 4th WSA-SBA-15 after 1 week and 2 weeks aged. In fact, the 4th WSA-SBA-15 sample aged either for 20 h or 2 weeks have similar porosimetry data. However, samples aged for 1 week showed a large increase in surface area and pore size suggesting pore growth. Interestingly, as the results show the pores do not continue growing but revert back to a *stable* form.

Table 2.13 N_2 porosimetry results of long time aged WSA-SBA-15

Aged Time		BET Surface Area ($m^2 g^{-1}$)	Pore Volume ($cm^3 g^{-1}$)	Average Pore Diameter (nm)
4th WSA-SBA-15	20 h	817	0.74	4.5
	1 week	961	1.52	7.8
	2 weeks	795	0.90	5.4

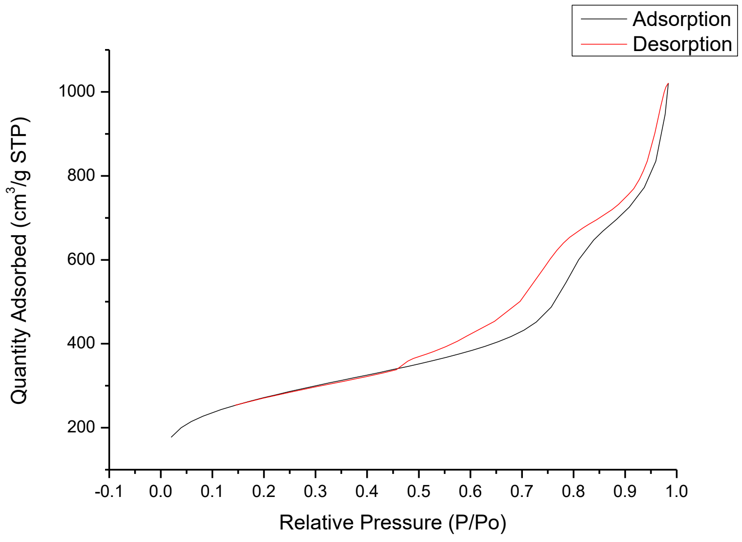

Figure 2.36 N_2 Adsorption /Desorption Isotherm for 4th WSA-MCM-41 aged in 1 week

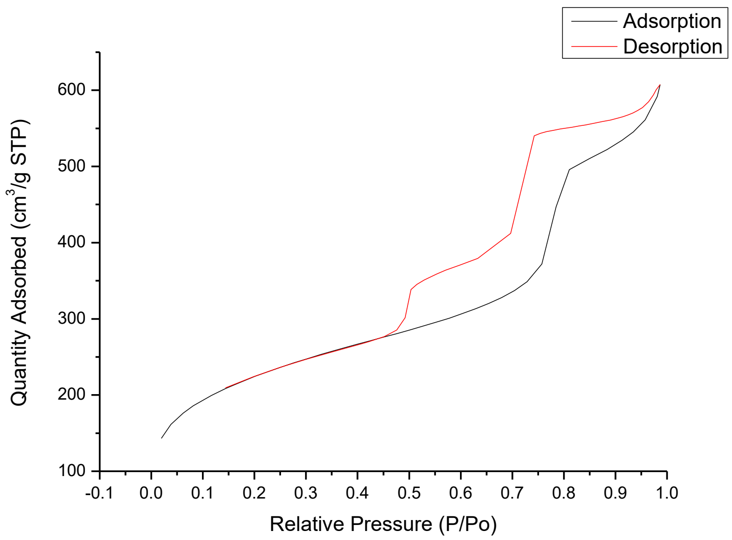

Figure 2.37 N_2 Adsorption /Desorption Isotherm for 4th WSA-MCM-41 aged in 2 weeks

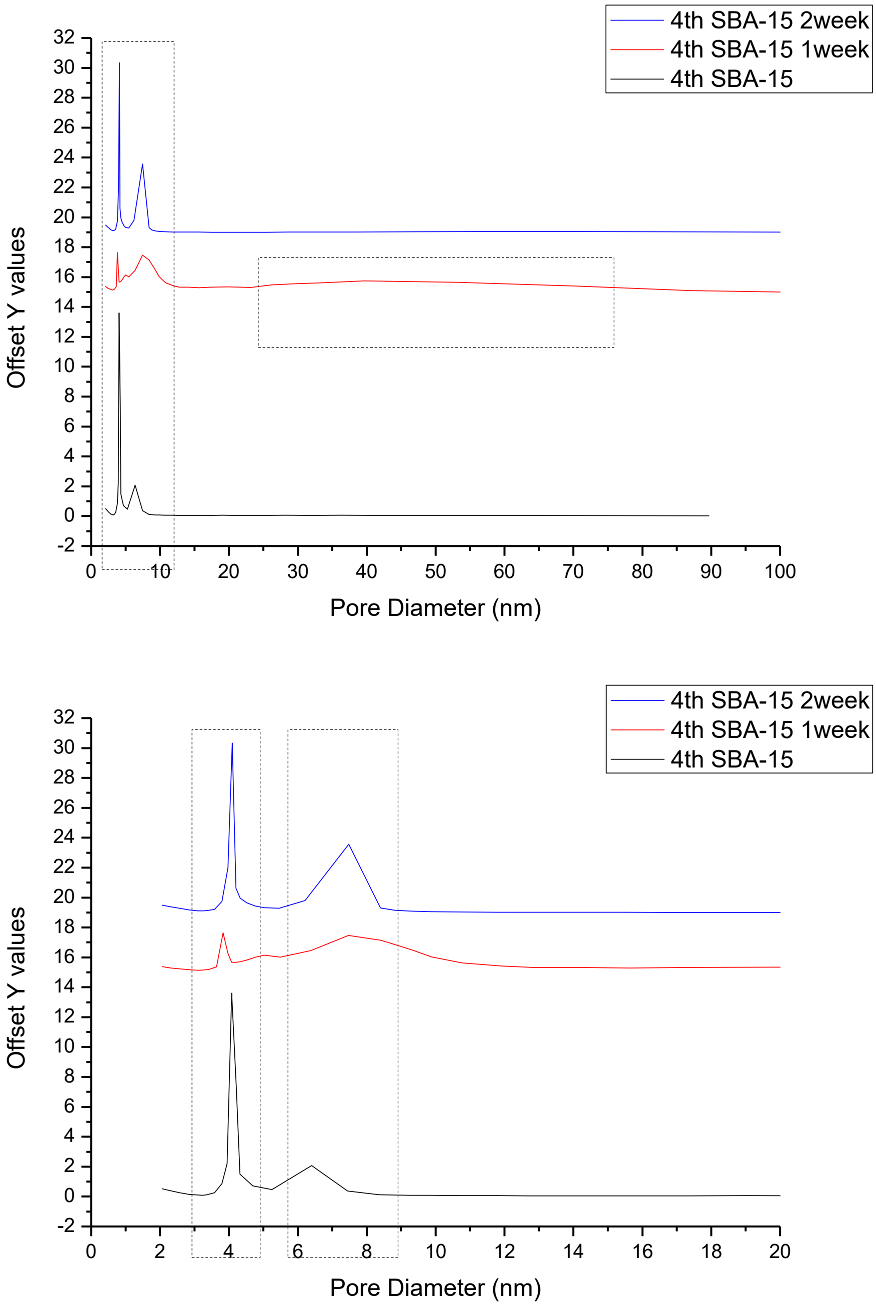

Figure 2.38 BJH adsorption pore size distribution for 4th WSA-SBA-15 in different aged time

The WSA-SBA-15 samples were also aged and their isotherms are shown in Figure 4.37, Figure 4.38, and Figure 4.39. Different aging time did not improve the N_2 porosimetry properties of WSA-SBA-15. There were still several steep increase in isotherm and similar with other kinds of WSA-SBA-15 samples. Pore size expanded after 1 week aged process. The pore diameter started to spread in a wide range, which was between 3 nm and 60 nm. But the dispersion of pore size did not continue increase by longer aged time (2 weeks).

After 2 weeks aging, the pore size of 4th WAS-SBA-15 came close to the 20 h aged samples. The porosimetry values became stable after 2 weeks aged, which the results close the original samples.

TEM figures of long aged samples are shown in Figure 2.39 and Figure 2.40. Hexagonal ordered pores were clearly found in the TEM figures. But the pore structures and orders were partly spread. The ordered structures were only found in short range.

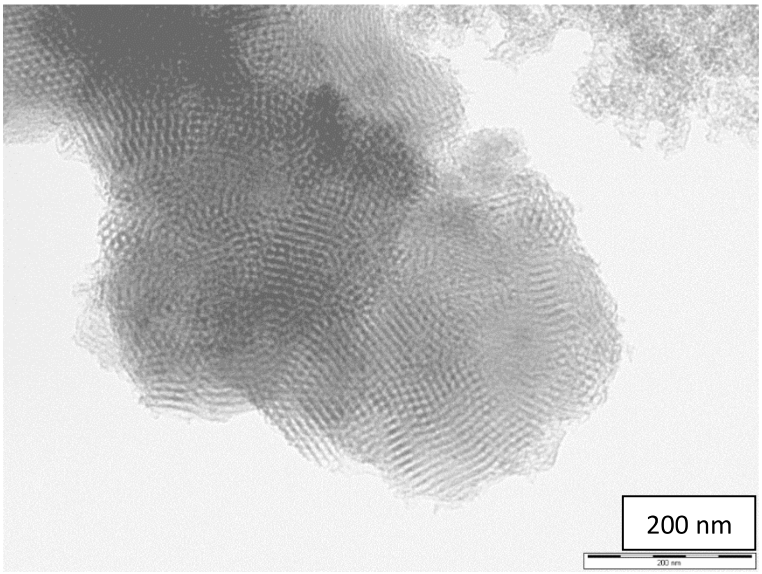

Figure 2.39 TEM image of 4th WSA-SAB-15 for 1 week aging

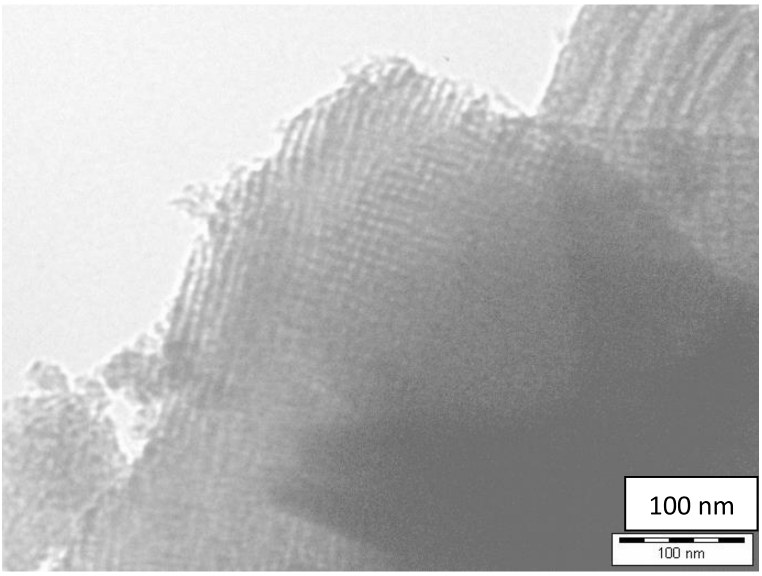

Figure 2.40 TEM image of 4th WSA-SAB-15 for 2 weeks aging

2.6 Conclusion

The first part of this Chapter was to optimize the conditions of the silicate extraction from miscanthus (bottom) ash to produce various biosilicate solutions for binder using; and wheat straw ash for synthesis of mesoporous materials.

Initially, the extraction time, the volume of alkali solution and the concentration of potassium hydroxide were carried out. It was found that the extraction time had limited influence on the properties of biosilicate solutions. Samples after 24 h, 18 h, 12 h and 6 h extraction presented similar silicate concentration. But the mass ratio between K_2O and SiO_2 were different in each samples, especially the highest mass ration in 18 h extraction. Two different concentrations (5 M and 3 M) of potassium hydroxide were used in this part. 5 M KOH extraction gave much more concentrated biosilicate solutions than 3 M KOH extraction. But 3 M KOH extraction had higher mass ratio of K_2O: SiO_2, in which 5 M samples had a ratio around 1: 1.10 and 3 M samples had a ratio around 1: 1.37. The ratio of K_2O: SiO_2 is an important property of biosilicate solutions as higher ratio samples had better performance as binder in bioboards. For different volumes of potassium hydroxide solution in the extraction, it suggested the ideal mass ratio between KOH solutions and miscanthus (bottom) ash was 3: 1. Although the ratio of K_2O: SiO_2 increased as the volume of 3 M KOH solution decreased, less biosilicate solutions were extracted from miscanthus (bottom) ash as the ash powder would adsorb the solutions and the diffusion of solution decreased. IR correlation was introduced to analyse the silicon concentration in biosilicate solutions. The silicon and silicate concentration could be calculated by measuring of the integral of the silicate band (1200-650 cm^{-1}) or by using the maximum intensity in the silicate peak. The results from IR correlation and titration were similar and had the similar tendency.

Bio-MCM-41 materials had been successfully synthesised using biosilicate solutions extracted from wheat straw (bottom) ash in this Chapter. These materials were analysed by appropriate analytical approaches such as N_2 porosimetry, XRD, TEM and solid-state ^{29}Si NMR. Bio-MCM-41 had a comparable property to commercial MCM-41 and other kinds of MCM-41 in literature[93-95] in porosimetry. In contrast to the MCM-41 found in literature which had a surface area around 847 – 1180 m^2g^{-1},[93-95] bio-MCM-41 did have certain large surface area which had a range between 1000 m^2g^{-1} and 1600 m^2g^{-1}.

Bio-MCM-41 also had larger pore volume than other MCM-41 materials. XRD, TEM and solid-state ^{29}Si NMR all verified bio-MCM-41 was a typical MCM-41 materials with significant ordered arrangement of pore, structure and the hexagonal arrays.

In the synthesis of mesoporous bio-SBA-15, a standard SBA-15 was synthesised from a neutral silica source named TEOS. The template Pluronic acid was dissolved in HCl which led to a neutral pH environment for investing porosity within silica structure. Unlike the neutral silica source, biosilicate solution was a kind of alkali solutions. The neutralization happened as the biosilicate solution was mixed with template and other chemicals. So not all of the bio-SBA-15 had the typical features of SBA-15 materials. The isotherm lines of bio-SBA-15 were quite different with TEOS-SBA-15. And it was difficult to find out the characteristic peaks of SBA-15 materials in bio-SBA-15's XRD spectra. It was the same situation in the TEM figures except 4th WSA-SBA-15. 4th WSA-SBA-15 performed quite clear ordered arrangement of pore, structure and the hexagonal arrays. But solid-state ^{29}Si NMR of bio-SBA-15 still performed the typical features of SBA-15 materials. Different kinds of Q_n Si were clearly found in these spectra. As the aging time increased, the surface area did not have a significant difference. But the pore size and the range of pore volume expanded under one week aging. There had been different kinds of pore size appeared under this condition. After two weeks aging, the properties 4th WSA-SBA-15 became similar with virgin 4th WSA-SBA-15

Chapter 3: Composite Bioboards

3.1 Introduction

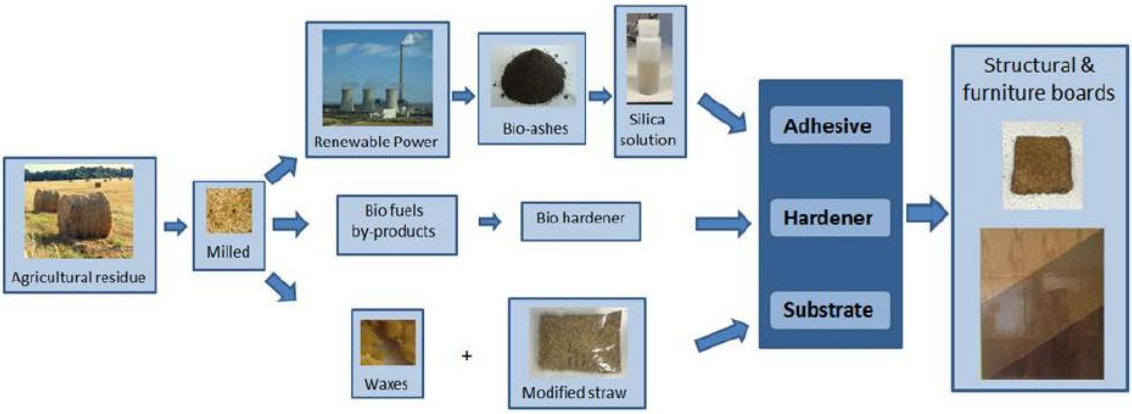

Figure 3.1 The objective of the bioboard process

Figure 3.1 gave an example of the typical procedure of bioboards process. Renewable resources including biomass, ash residues or other waste from food supply chain were reused and recycled to produce bio-composites named bioboards in this project. The bioboards produced in this project were expected to be the alternative replacements of P3 standard boards (shown in Table 3.1) which were usually used as kitchen cabinet doors or cupboards, carcases and worktops.[23, 96] The P3 standard was classified by EN 312 which specifies the requirements for flat-pressed or calendar-pressed unfaced particleboards.[97] In comparison to the conventional board process (Figure 1.6), bioboards was also produced by a hot-press process but with different binder, additives and raw materials. Typically, urea, formaldehyde, isocyanate adhesives or melamine modified urea formaldehyde[98] were utilized as the binder and additives in P3 standard boards. However, formaldehyde had been identified as a 'probable carcinogen'[45] by IARC and also harmful to eye[46]. So the low-toxic silicate solutions expected to avoid any potential risk to human health were used in bioboards process. Also boards became more fire resistant as the existence of silicate.

Table 3.1 Values for P3 standard boards according to EN 312:2003 Particleboards. Specifications[23]

Parameter	Value
Internal Bond Strength (N/mm^2)	0.45
Thickness swelling (%)	14
Bending strength (N/mm^2)	15
Modulus of elasticity in bending (N/mm^2)	2050

3.2 Wheat Straw Boards with commercial silicate solutions

A variety of wheat straw boards were produced with a procedure developed by Dr Mario de Bruyn (shown in Figure 3.2). Wheat straw was milled and sieved to the same size fractions (1 cm – 2 cm). Then these particles were dewaxed by ethanol Soxhlet extraction. The dewaxed process could improve the contact and adhesion between silicate solutions and wheat straw particles by the removal of hydrophobic wax layer on the surface of wheat straw. The wheat straw particles were then mixed thoroughly with silicate solutions and other additives. Later, the mixed materials were pressed to boards by hot-press. The details of this procedure were introduced in Chapter 5.9.

Pieces of 5 cm X 5 cm were cut from the crude bioboards to test the internal bond strength (shown in Figure 3.3) which refers to the strength of the bonding of those separate fibrous layers in boards. Bioboards (5 cm X 5 cm) were stick to two metal plates and tested on an Instron analyser at a pull rate of 10 mm/min. The schematic test was shown in Figure 3.4. And the testing results and other physical properties were shown in Tables 3.1 and 3.2.

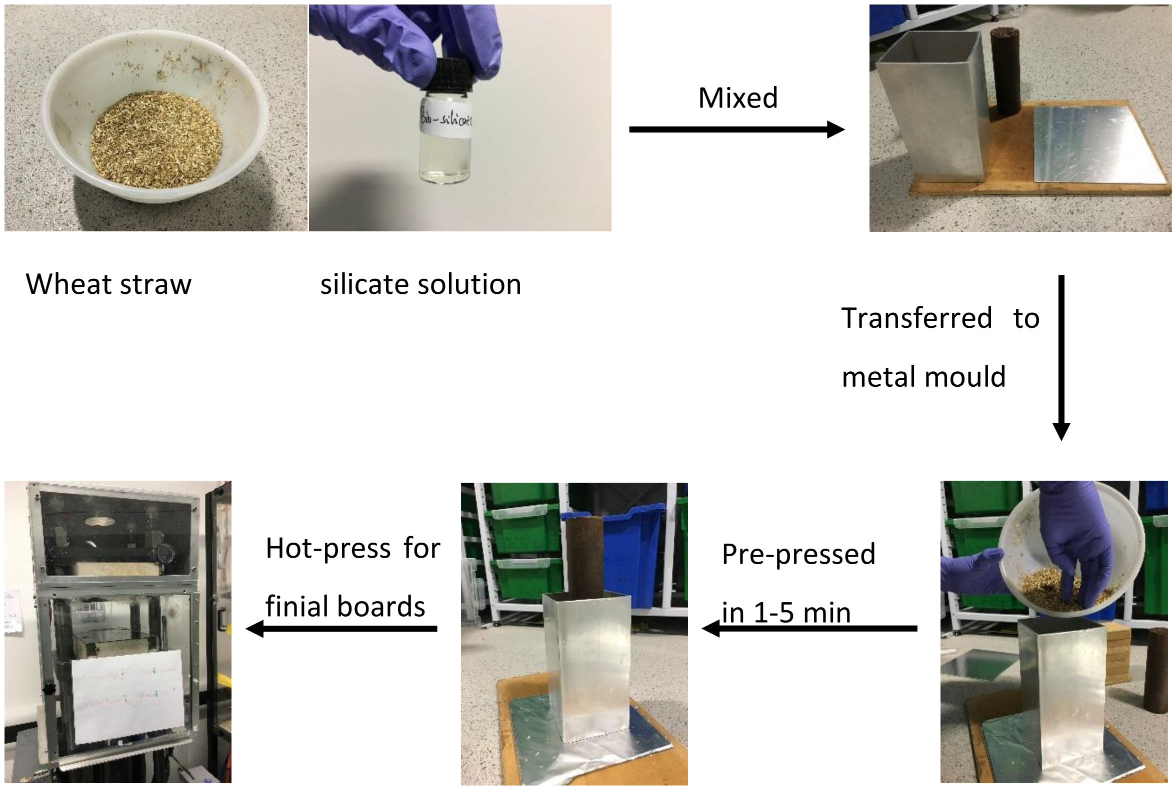

Figure 3.2 The procedure of producing bioboards in lab-scale

Figure 3.3 Finial bioboards cutting for 5 cm X 5cm pieces

Boards without other additives performed an unstable internal bond strength (IBS) when the boards were repeated with the same conditions (shown in Table 3.2). For example, standard samples with K120 solution had two significantly different internal bond strengths (IBS) in repeat experiments. This situation also appeared in other biosilicate and sodium silicate boards. The first series of bioboards were kept for about 1 month before testing whilst the second series of bioboards were all tested in one week after hot-press which could be the most possible reason for the different IBS. Bioboards with commercial K120 as binder had weak resistance to water. It suggested that different moisture content probably influenced the IBS of bioboards. But there also might be other chemical or physical changes of the bioboards with different storage time.

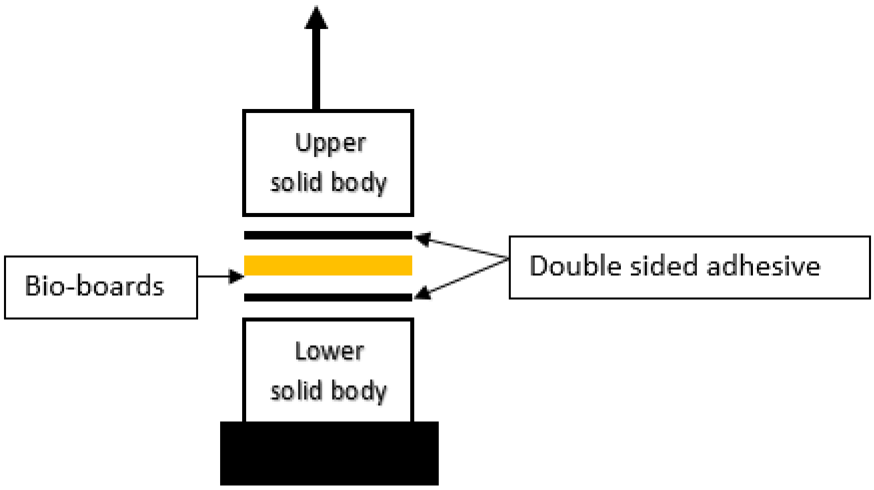

Figure 3.4 Schematic graph of internal bond strength test

For an average comparison of IBS, standard samples with K120 solution gave higher IBS than other series of standard samples. This result was determined by the different ratio of silicon and potassium in the binder. According to the MSDS of K120, the silicon content was more than 20% of total mass. The biosilicate made in this study was only 10% weight of total solution. Also, the biosilicate solution had much more potassium and less silicon than K120 solution. As the silicate solution was the binder in bioboards, much more silicon would give better mechanical properties. Also, the pH of K120 and biosilicate was quite different. The pH of K120 was around 7 whereas the pH of biosilicate was close to 14. It had been reported that high pH had a negative influence on silicate cure, reducing the strength of cured silicate solution. Thus, whey protein which was also from food supply chain waste could be denatured under the action of heat. And it could decrease the pH of the silicate solutions and initiate silicate polymerisation.

The two series of sodium silicate boards (N-04 & N-04’) had similar IBS with potassium silicate samples (N-02, N-02’, N-03 and N-03’). The Na-Si (sigma) samples (N-05 & N-05’) are supposed to have the equal IBS with K120 samples (N-01 & N-01’), but in fact, sodium silicate solution did not give acceptable IBS, even with higher ratio of silicon.

Table 3.2 Sample details of boards with additives

Sample Name	Sample Detail (210^0C for 8min)				Board Width (mm)	Board thickness (mm)	Density (g/cm^3)	Maximum Load (N)	Internal Bond Strength (N/mm^2)
	De-waxed Wheat Straw (g)	Silicate Solution (g)	Protein (0.9g in 2.7g water)	Other Additives (g)					
StarB02	40.64	K120 12.06	Y	Starch (5.25)	50.5	9.5	0.84	1371.5	0.54
N-07	41.16	K120 12.08	Y	H7 Starch (5.16)	50.4	9.6	0.81	1285.9	0.51
BB-Oil01	41.06	K120 12.97	N	Bio-Oil (0.51)	50.6	10.8	0.64	188.3	0.07
BB-Oil02	41.36	K-Si[1] 12.80	N	Bio-Oil (0.52)	50.6	10.8	0.67	355.4	0.14

Table 3.3 Samples details of wheat straw bioboards

Sample Name	Sample Detail (210^{0}C for 8min)				Board Width (mm)	Board thickness (mm)	Density (g/cm^3)	Maximum Load (N)	Internal Bond Strength (N/mm^2)
	De-waxed WS (g)	Silicate Solution (g)	Protein (0.9g in 2.7g water)	Other Additives (g)					
N-01	41.05	K120 12.02	Y	N	51.0	10.4	0.69	388.0	0.15
N-01'	41.07	K120 12.02	Y	N	50.5	10.1	0.66	833.5	0.33
N-02	41.12	K-Si[1] 12.29	Y	N	51.0	10.2	0.72	622.4	0.24
N-02'	41.11	K-Si[1] 12.09	Y	N	50.4	10.1	0.65	422.6	0.17
N-03	41.00	K-Si[2] 12.21	Y	N	50.5	9.9	0.72	622.1	0.24
N-03'	41.01	K-Si[2] 12.02	Y	N	50.4	10.2	0.58	376.6	0.15
N-04	41.60	Na-Si[1] 12.78	Y	N	50.9	10.2	0.67	526.9	0.20
N-04'	41.13	Na-Si[1] 12.10	Y	N	50.6	10.0	0.64	510.2	0.20
N-05	41.61	Na-Si(Sigma) 12.70	Y	N	51.0	10.4	0.71	343.8	0.13
N-05'	41.05	Na-Si(Sigma) 12.11	Y	N	50.6	10.2	0.63	488.7	0.19
N-06	41.44	Calcium Silicate 6	Y	N	50.7	10.7	0.62	NO	NO

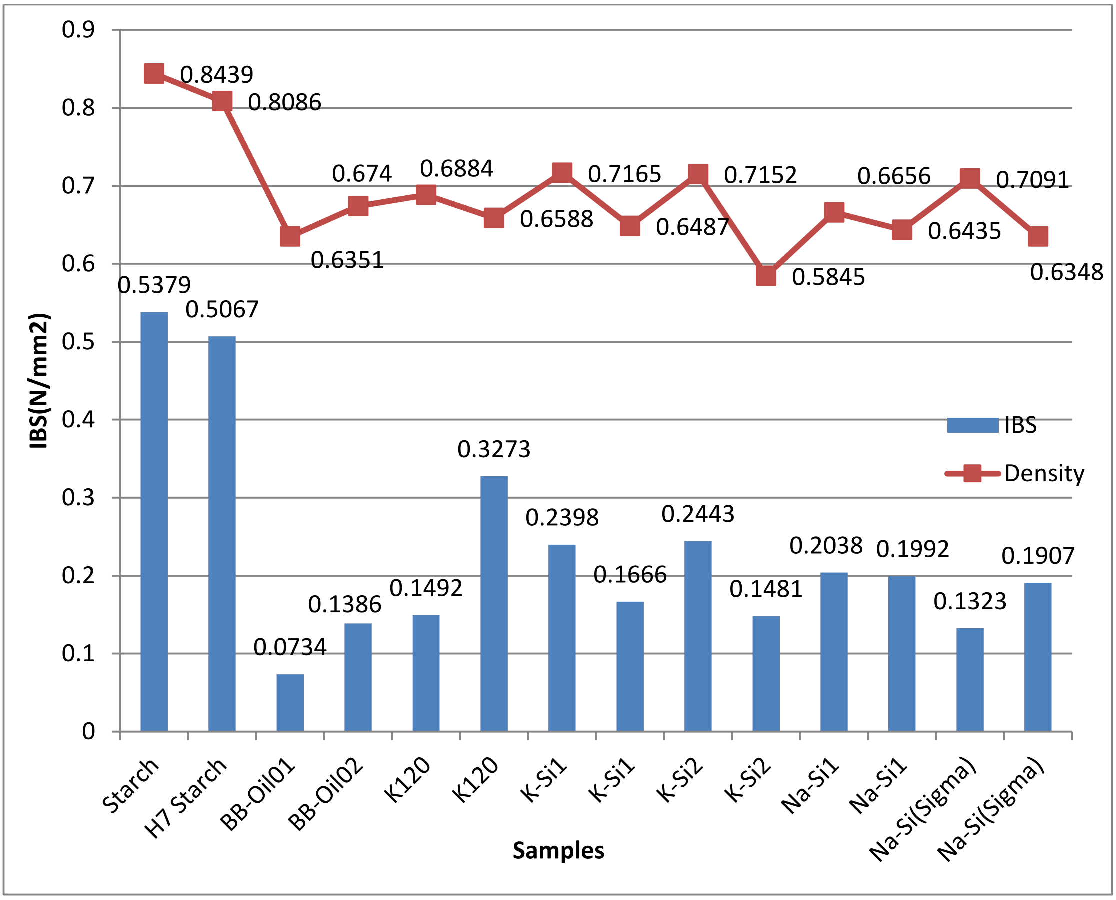

Figure 3.5 Internal bond strength of wheat straw boards

Bioboards with bio-oil (from MW paper) as additives had the worst IBS of all samples tested. As the chemical components of bio-oil are very complicated, it is hard to determine the exact reason for such poor mechanical properties.

Also, starch was utilized as additive in bioboard process. The IBS of starch bioboards were much higher than any other samples. And the two starch samples had similar results. It suggested that the properties of bioboards could be much more stable with starch additives. Starch-silicate binder also had been investigated as combined binder for corrugated paper.[99] It was reported that starch-silicate binder had better effect than the two single binders in corrugated paper.[99] But the mechanism of starch-silicate starch in bioboards should to be investigated in future work. In addition, the high IBS of starch bioboards is probably caused by much higher density than other samples.

3.3 Wheat straw boards with biosilicate solutions

At first, bioboards with commercial silicate solution (K120) were made as standard and comparison samples. The physical properties were showed in Table 3.3. With the similar densities around 0.65 g cm^{-3}, the internal bond strength shifted in the range of 0.17-0.25 Nmm^{-2}. As the density of the bioboard increased, the internal bond strength was also slightly increased. With an internal bond strength of 0.17-0.25 Nmm^{-2}, these compared samples performed acceptable hardness and physical properties. Also, the aim of the bioboards project was to investigate the feasibility of biosilicate solution as the binder in bioboards. So if the boards with biosilicate solution have the similar internal bond strength with commercial silicate solution, there will be a potential application of the biosilicate solution.

Table 3.4 The properties of bioboards using commercial silicate solutions (K120)

Binder	Width (mm)	Length (mm)	Density (g/cm^3)	Maximum load (N)	Internal bond strength (N/mm^2)
K120	49.9	49.8	0.647	454.8	0.18
	49.9	50.0	0.685	614.0	0.25
	49.9	50.0	0.640	422.4	0.17
	49.9	49.8	0.647	532.8	0.21

For all the bioboards made in this condition (50 mm x 50 mm), the density was similar as with commercial silica solution and the highest internal bond strength was obtained biosilicate was obtained using 208 ml of 3M-aqueous KOH solution. The internal bond strength for this bioboard was 0.24 N mm^{-2} and similar to the best internal bond strength obtained with K120 solution. For other the 3 M- and 5 M-aqueous KOH samples, internal bond strength of around 0.16-0.17 N mm^{-2} was achieved. This level of internal bond strength was still comparable with standard samples thus biosilicate is a viable alternative to commercial K120.

Table 3.5 The properties of bioboards using biosilicate solutions extracted by different volume 3 M KOH solution for 18 hours

Binder	Width (mm)	Length (mm)	Density (g/cm^3)	Maximum load (N)	Internal bond strength (N/mm^2)
3 M KOH—100 ml	50.0	50.0	0.641	240.9	0.10
3 M KOH—125 ml	49.8	50.0	0.616	155.1	0.06
3 M KOH—208 ml	50.0	50.0	0.711	589.7	0.24
3 M KOH—290 ml	50.1	49.9	0.647	319.3	0.13
3 M KOH—370 ml	50.0	50.2	0.634	194.4	0.08
3 M KOH—400 ml	50.1	50.3	0.597	148.3	0.06

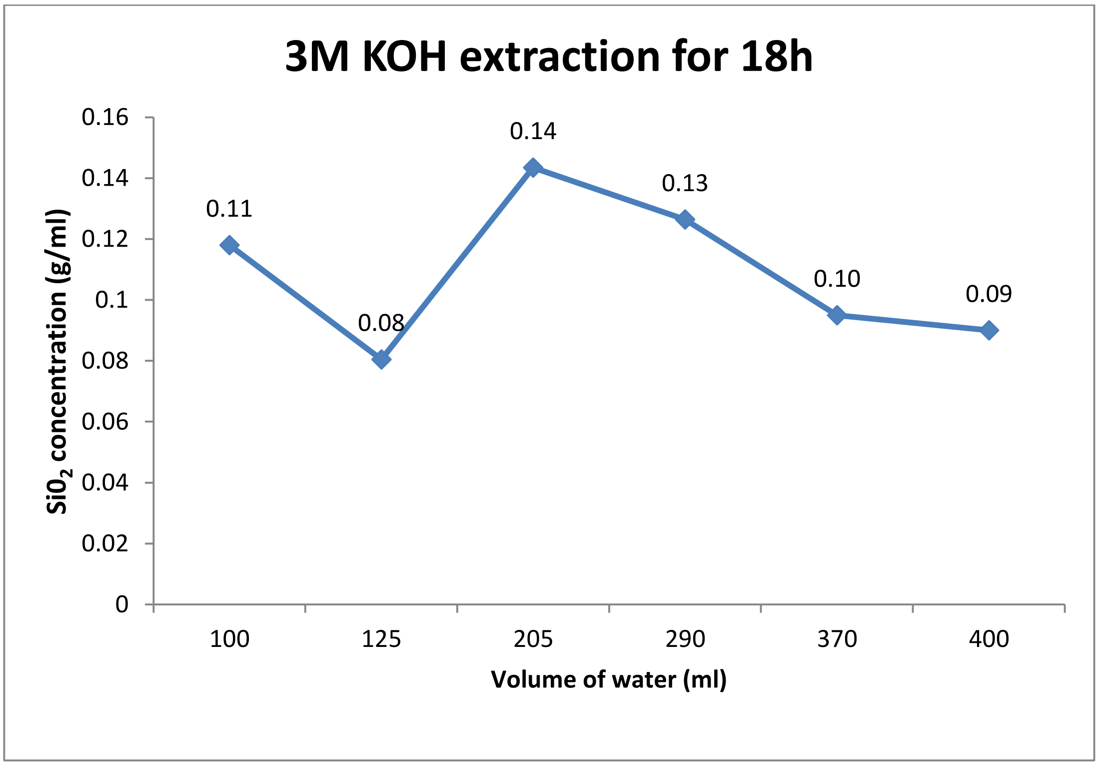

Figure 3.6 SiO_2 concentration in different volume of 3 M KOH extraction for 18 hours

Table 3.6 The properties of bioboards using biosilicate solutions (75 g ash extracted by 125 ml 5 M KOH solution) in different extracted time

Binder	Width (mm)	Length (mm)	Density (g/cm^3)	Maximum load (N)	Internal bond strength (N/mm^2)
5 M KOH—6 h	50.0	49.9	0.639	429.1	0.17
5 M KOH—12 h	50.0	50.0	0.643	427.6	0.17
5 M KOH—18 h	50.2	49.7	0.611	317.9	0.13
5 M KOH—24 h	49.9	49.8	0.652	470.3	0.19

Table 3.7 The properties of bioboards using biosilicate solutions (75 g ash extracted by 208 ml 3 M KOH solution) in different extracted time

Binder	Width (mm)	Length (mm)	Density (g/cm^3)	Maximum load (N)	Internal bond strength (N/mm^2)
3 M KOH—6 h	49.9	49.7	0.692	396.8	0.16
3 M KOH—12 h	49.8	50.0	0.693	298.8	0.12
3 M KOH—18 h	50.0	50.0	0.711	589.7	0.24
3 M KOH—24 h	49.9	49.9	0.655	392.5	0.16

Another set of bioboards was formed. In this series of experiments, de-waxed wheat straw was combined with 12 g of silica solutions to be made into bioboards. The density and the internal bond strength were calculated in Table 3.5. In this case study, both the density and internal bond strength had similar values, but the internal bond strength (IBS) were much worse than other bioboards, which might be cause by less concentrated silicate used in these samples.

Table 3.8 The properties of bioboards using biosilicate solutions extracted by 208 ml 3 M KOH solution in different extracted time

Binder	Width (mm)	Length (mm)	Density (g/cm^3)	Maximum load (N)	Internal bond strength (N/mm^2)
3 M KOH—6 h	49.9	50.0	0.616	262.9	0.11
3 M KOH—12 h	49.8	49.9	0.637	251.2	0.10
3 M KOH—18 h	49.9	50.1	0.602	194.5	0.08
3 M KOH—24 h	50.0	49.9	0.590	271.7	0.11

3.4 Wheat Straw and Pea Pod composite bioboards

Pea pods are by-products from the food industry, which can be used as a potential source of functional components. For the chemical components in pea pod, dietary fibre is the major compound (Table 3.8). Pea pods have great amount of non-soluble dietary fibre than soluble dietary fibre. Non-soluble dietary fibre represents 93% of total dietary fibre in pea pods. Dietary fibre contains non-starch polysaccharides such as arabinoxylans, cellulose, and many other components, such as resistant starch, resistant dextrin, inulin, lignin, wax, chitin, pectin and oligosaccharide.[100] Total low molecular weight chemicals and protein take a large amount of pea pods. The most common sugars in low molecular weight carbohydrates are glucose and sucrose. In addition, the considerable amounts of protein and starch have the potential applications for binder.[100]

Table 3.9 Proximate composition and low molecular weight carbohydrates of pea pod (g/100 g dry matter)[100]

Chemical Component in Pea Pod	
Protein	10.8±0.3
Fat	1.3±0.2
Low Molecular Weight Carbohydrates	22.7±0.2
Sucrose	7.9±0.3
Glucose	11.9±0.6
Galactose	0.8±0.1
Arabinose	0.9±0.2
Fructose	1.2±0.1
Starch	3.7±0.1
Dietary Fibre	58.6±1.2
Non-soluble DF	54.4±1.6
Soluble DF	4.2±0.6
Ash	6.6±.5

Inorganic components only take about 6.6% of pea pods.[100] For the group of inorganics, iron and potassium are the major minerals in pea pods (Table 3.9). Calcium also shows considerable amount in macro-elements. The amounts of sodium, magnesium, zinc and manganese have similar lower level in pea pods. Copper has the lowest amounts than other major minerals.

Table 3.10 Elemental analysis of pea pod (g/100 g dry matter)[100]

Elements in Pea Pod	
Potassium	1.03
Sodium	0.14
Calcium	0.77
Magnesium	0.21
Iron	1.20
Copper	0.06
Manganese	0.27
Zinc	0.16

In this part, de-waxed wheat straw and pea pod waste were the raw materials for bioboards. Pea pod waste was just milled for different size without any chemical pre-treatment. The details of bioboards with different mass ratio (wheat straw:Pea pod waste) shown in Table 3.11, Table 3.12 and Table 3.13. Three kinds of pea pod waste were added into bioboards with the ratio of 90%, 80%, 70% and 60%. The densities of these samples were still between 0.6 g/cm^3 and 0.7 g/cm^3.

In Figure 3.4, the red line represented the maximum IBS of K120 boards. Based on the data shown, the IBS of pea pod waste boards had similar or even higher results than compared with K120 boards under the ratio of 90% and 80%. However, as the ratio of pea pod waste increased, the IBS decreased. This result was apparent for 500 µm-250 µm pea pod boards. For larger particle size of pea pod waste (>500 µm), the downward tendency was very weak. This suggested that pea pod waste (>500 µm) could be a alternative material of wheat straw board. Thus, bioboards comprising two waste agricultural feedstocks could be made providing an alternative to ploughing back in to soil or left festering on the land.

As small particles of pea pod had even larger suface area than others, these particles required much more binder to trap them. The bioboards with pea pod waste had a minimum limited amount of the usage of K120 for binder diffusion. Also, pea pod waste used in this project still contained certain wax and many other kinds of chemical components. The wax could decrease the mechanical properties of wheat straw boards. However, pea pod waste was also rich in protein which would increase the adhesion effort of K120.

Table 3.11 Details of pea pod waste (500µm-250µm) based bioboards

Sample Name	Sample Detail (210^{0}C for 8min)					Board Width (mm)	Board thickness (mm)	Density (g/cm^3)	Max Load (N)	IBS (N/mm^2)
	De-waxed WS (g) (1mm-2mm)	Pea Pod Waste (g) (500µm-250µm)	K120 (g)	Protein (0.9g in 2.7g water)	Additives (g)					
N-P1	90% 36.90	10% 4.10	12.12	Y	N	50.5	10.0	0.71	791.9	0.31
N-P2	80% 32.80	20% 8.20	12.11	Y	N	50.6	10.1	0.66	718.1	0.28
N-P3	70% 28.77	30% 12.31	12.11	Y	N	50.1	10.2	0.69	452.9	0.18
N-P4	60% 24.61	40% 16.44	12.00	Y	N	50.1	10.3	0.69	468.4	0.19

Table 3.12 Details of pea pod waste (1mm-500µm) based bioboards

Sample Name	Sample Detail (210^{0}C for 8min)					Board Width (mm)	Board thickness (mm)	Density (g/cm^3)	Max Load (N)	IBS (N/mm^2)
	De-waxed WS (g) (1mm-2mm)	Pea Pod Waste (g) （1mm-500µm)	Silicate Solution (g)	Protein (0.9g in 2.7g water)	Additives (g)					
N-P12	80% 32.82	20% 8.23	12.02	Y	N	50.2	10.2	0.65	806.7	0.32
N-P13	70% 28.73	30% 12.24	12.06	Y	N	50.1	10.3	0.64	703.9	0.28
N-P14	60% 24.62	40% 16.44	12.30	Y	N	50.1	10.3	0.67	799.0	0.32

Table 3.13 Details of pea pod waste (1mm-2mm) based bioboards

Sample Name	Sample Detail (210^0C for 8min)					Board Width (mm)	Board thickness (mm)	Density (g/cm^3)	Max Load (N)	IBS (N/mm^2)
	De-waxed WS (g) (1mm-2mm)	Pea Pod Waste (g)	Silicate Solution (g)	Protein (0.9g in 2.7g water)	Additives (g)					
N-P21	90% 36.90	10% 4.13	12.03	Y	N	50.1	10.3	0.63	855.3	0.34
N-P22	80% 32.83	20% 8.25	12.07	Y	N	50.1	10.5	0.62	821.0	0.33
N-P23	70% 28.73	30% 12.33	12.03	Y	N	50.1	10.6	0.60	662.1	0.26
N-P24	60% 24.64	40% 16.43	12.02	Y	N	50.2	10.4	0.63	735.5	0.29

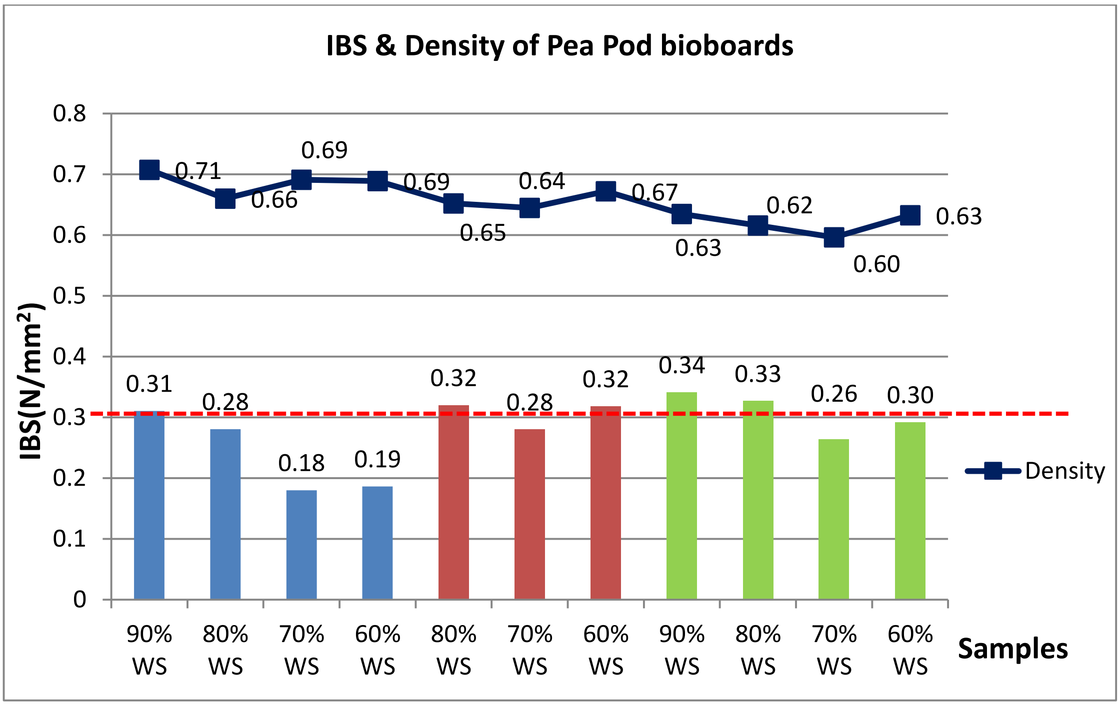

Figure 3.7 IBS of pea pod based bioboards (The red dash line indicated the IBS of 100% WS bioboards which was around 0.31 N/mm²)

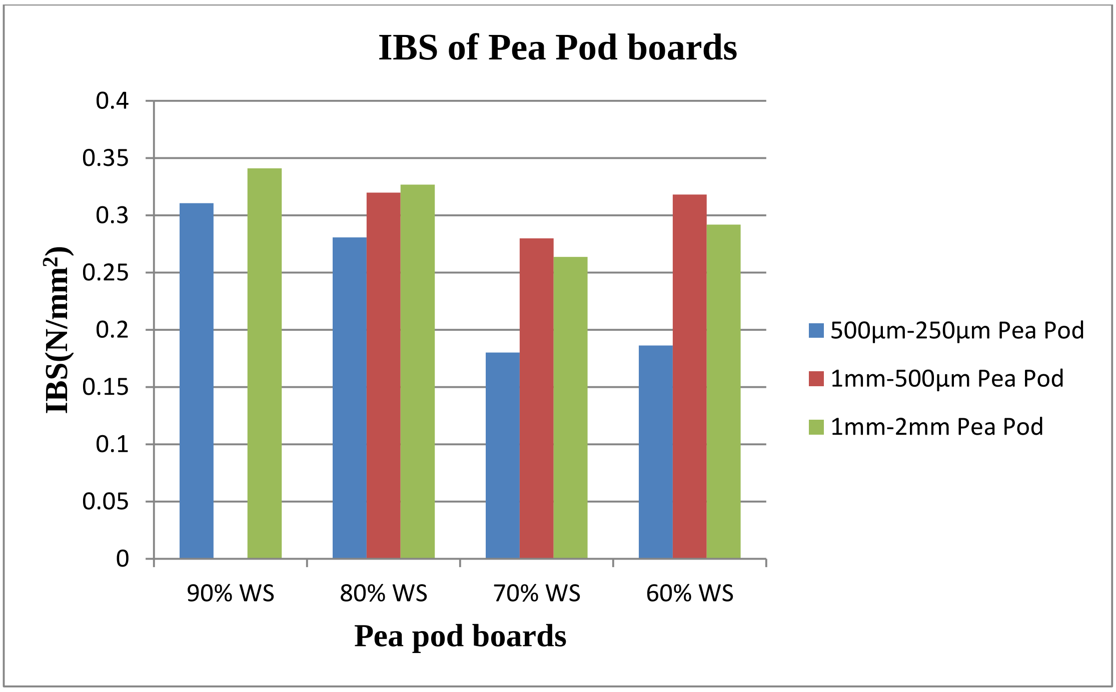

Figure 3.8 IBS of different ratio of pea pod waste

3.5 Lab-scale de-inking residue (DIR) Boards

De-inking residue (DIR) is a by-product from the process of recycling of waste paper, which contains 50% of wet sludge type of material and 50% dry solids content.[101] The dry solids in DIR consist of organics including short fibres or fines, coatings, fillers, ink particles, extractive substances and deinking additives, and inorganic parts including china clay and chalk.[102, 103] The amount or ratio of organic and inorganic contents depend on the resource of waste paper, such as newspaper, magazine, cardboard and so on, and the procedure to produce DIR, such as straight dry and separate dry.[101, 103] Also, the amount of organic content can be adjusted for any further applications.

Moreover, DIR potentially is a high value waste material produced in a large amount each year with abundant fibre content. For example, the Confederation of European Paper Industries (CEPI) has reported that the production of paper and board was 91.1 million tonnes in Europe in 2014, and the consumption of paper and board was 77.1 million tonnes in Europe in 2014.[101] In the production and recycling process, approximately 2.3 million tonnes of de-inking residue are produced per year, which is still rise with time.[101] Also, DIR is rich of fibre content which could be the resource of fibre to produce chemicals, or even bio-composites related to other fibre based products, such as fibreboards and chipboards.

3.5.1 DIR boards cured in the oven

DIR boards were cured in the oven to investigate the feasibility of de-inked paper residue (DIR) as major raw material for bioboards. At first, control samples were made between DIR and distilled water to confirm the function of silicate solution. Table 3.14 showed the results for the control samples. All the control samples failed, i.e., broke under light manual strain.

Table 3.14 DIR Control sample data.

Sample Details				Structure	Manual Test
DIR (g)	K120 (g)	Distilled Water (g)	Procedure		
41.01	No	12.21	4 (160°C—4h)	F	F
41.15	No	24.40	4 (160°C—4h)	F	F
41.02	No	41.11	4 (200°C—1h)	F	F

Thereafter, silicate solution was added to DIR boards as a binder. Formulations of DIR (41 g), K120 (12-24 g) and distilled water (12-24 g) failed give boards on any noticeable structural integrity. It was found that the DIR would adsorb water and silicate solution immediately but after a few minutes mixing, the mixture formed heterogeneous paste-like pieces. After several hours of oven heating, very weak and brittle boards that crumbled were obtained. The silicate solution appeared to be incompatible with DIR thus better mixing was needed. In fact, the amount of distilled water used played an indispensable role in board manufacture.

Table 3.15 Initial test for DIR boards

Sample Details				Structure	Manual Test
DIR (g)	K120 (g)	Distilled Water (g)	Procedure		
41.01	12.05	No	4 (160°C—4h)	F	F
41.12	24.30	No	4 (160°C—4h)	F	F
41.21	12.25	12.27	4 (160°C—4h)	F	F
41.20	12.18	24.31	4 (160°C—4h)	F	F
41.21	12.18	24.10+1g protein	4 (160°C—4h)	F	F
41.09	24.11	12.21	4 (160°C—4h)	F	F
41.15	24.20	24.02	4 (160°C—4h)	F	F

Finally, with the equal ratio (1:1) between the DIR and distilled water, the physical properties of boards had a significant change with different ratio of K120. According to the results in Table 3.15, all the samples with >38.7% water content had strong structure. This level of water content allowed the silicate solution to effectively wet the DIR thus promoting strong adhesion. The resulting data also revealed that the samples with higher ratio of K120 gave qualitatively stronger boards. The samples with 6 g of K120 were easily broken by manual test whilst those 12 g and 24 g of K120 failed to break.

In addition, low temperature (80^{o}C) and high temperature (200^{o}C) were both feasible in DIR board process. Samples under different temperature had different appearance. Boards cured in higher temperature (200^{o}C) had brown and dark surface. Boards cured in lower temperature (80^{o}C) produced a lighter colour. However, it was hard to identify the significant differences with different temperature.

Table 3.16 DIR-boards cure in the oven of 80^{o}C

Sample No.	**Sample Details**				**Structure**	**Manual Test**
	DIR (g)	**K120 (g)**	**Distilled Water (g)**	**Procedure**		
1	41.10	6.03	41.12	4 (80^{o}C—18h)	P	++
2	41.22	6.12	41.27	4 (80^{o}C—18h)	P	++
3	41.01	12.23	41.27	4 (80^{o}C—18h)	P	+++
4	41.11	12.23	41.23	4 (80^{o}C—18h)	P	+++
5	41.07	24.21	41.21	4 (80^{o}C—18h)	P	+++
6	41.09	24.02	41.02	4 (80^{o}C—18h)	P	+++

Table 3.17 DIR-boards cure in the oven of 200°C

Sample No.	Sample Details				Structure	Manual Test
	DIR (g)	K120 (g)	Distilled Water (g)	Procedure		
7	41.36	6.34	41.26	4 (200°C—1h)	P	++
8	41.15	6.07	41.20	4 (200°C—1h)	P	++
9	41.08	12.03	41.13	4 (200°C—1h)	P	+++
10	41.20	12.57	41.29	4 (200°C—1h)	P	+++
11	41.17	24.02	41.08	4 (200°C—1h)	P	+++
12	41.11	24.20	41.07	4 (200°C—1h)	P	+++

Note: No= no water added; P=Pass, the sample can form a board; F=False, the sample can't form a board; "+"means the board can easily be broken by manual test; "++"means the board are hard to be broken by manual test; "+++"means the board can't be broken by manual test.

3.5.2 Hot-press DIR boards

In this part, bioboards process was introduced to producing DIR boards which were expected to have strong structure. Three different procedures (Procedure 1, 2 and 3) were formulated which described in Chapter 6.15. According the initial study of oven dried board, the ratio between DIR powder and water was fixed to 1:1. Due to the high moisture content (43.6%) in the mixture, samples needed longer time to cure than other kinds of bioboards.

Table 3.18 Sample details from procedure 1

Sample No.	Sample Details				Structure	Manual Test
	DIR (g)	K120 (g)	Distilled Water (g)	Procedure		
DIR-H01	41.20	12.00	41.06	1 (160°C—8min)	F	F
DIR180-01	41.02	12.28	41.00	1 (180°C—20min)	P	+
DIR180-03	41.30	24.22	41.03	1 (180°C—20min)	P	+
DIR200-03	41.28	12.15	41.20	1 (200°C—10min)	P	+
DIR200-01	41.12	12.02	41.26	1 (200°C—20min)	P	++

According to the results shown in Table 3.18, Table 3.19 and Table 3.20, the hot-press samples could form structural boards under the conditions of 160°C-200°C and 10 min-20 min. In addition, the pressing time was decreased with pre-heating in the hot-press machine. As higher temperature was needed with shorter pressing time and lower temperature needed longer pressing time, there should be some kind of relationship between temperature and pressing time. For example, DIR boards could be made with the conditions of 160°C-20 min. In addition, DIR boards could be made with the conditions of 200°C-10min. Figure 3.9 shown the potential relationship between temperature and pressing time. The conditions (temperature and pressing time) above this potential line were the available area for making hard or structural DIR boards; otherwise the samples will fail.

From the manual test, DIR boards under 180°C-200°C had better physical properties than other samples. Moreover, pre-heating in the hot-press machine increased the hardness of boards. For example, DIR180-01 and DIR180-03 were easily broken in manual test. However, DIR180-02 performed better in manual test. It was found that 200°C-20min was the best conditions for DIR boards. In addition, higher ratio of K120 solution did not give any significant promotion on the physical properties.

Table 3.19 Sample details from procedure 2

Sample Name	Sample Details				Structure	Manual Test
	DIR (g)	K120 (g)	Distilled Water (g)	Procedure		
DIR-H02	41.12	12.24	41.21	2 (160°C—10min)	F	F
DIR-H03	41.20	12.05	41.20	2 (160°C—16min)	P	+
DIR-H04	41.15	12.23	41.13	2 (160°C—20min)	P	+
DIR180-02	41.02	12.10	41.25	2 (180°C—20min)	P	++
DIR200-02	41.17	12.14	41.31	2 (200°C—20min)	P	++

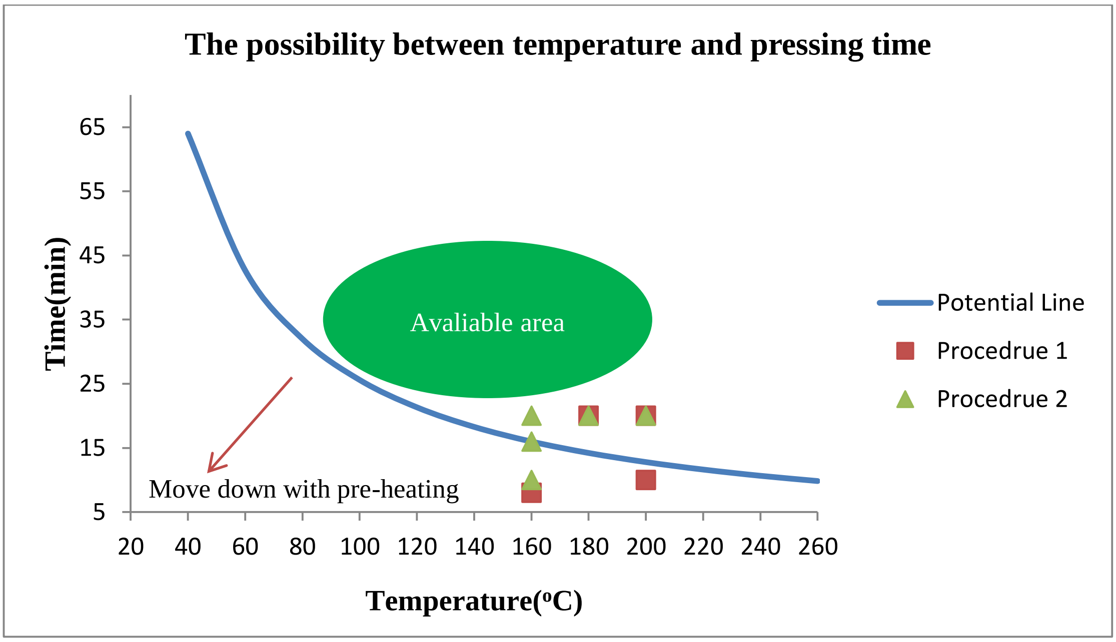

Figure 3.9 The assumption of DIR boards with different temperature and pressing time

According to the results of procedure 1 (typical bioboards process) and procedure 2 (typical bioboards process with pre-heating), an assumption of the formation of structural DIR boards was given in different temperature and pressing time (shown in Figure 3.6). Structural DIR boards could be produced under high temperature and relatively short period of time, or low temperature and relatively long period of time. For example, DIR boards could be produce under 200^{o}C—10min (DIR200-03) and 160^{o}C—20min (DIR-H04). Possibly, any conditions near the potential line or above the potential line could be the available temperature and pressing time to produce DIR boards. DIR boards produced by relatively high temperature or long period of time possibly had strong structure. It's the available area in Figure 3.9. In procedure 2 and procedure 3, pre-heating was introduced to help the formation of DIR boards. It was found that DIR boards with pre-heating could be produced under relative short period of time or low temperature, such as sample DIR-H03 (160^{o}C—16min) and DIR-H07 (50^{o}C -160^{o}C—10min). It suggested that the potential line would move down with pre-heating. And the DIR boards could be produced under lower temperature or shorter time in hot-press process.

In procedure 3, pre-heating in the oven and hot-press machine was applied before high pressure and high temperature pressing. Table 3.20 gave the details of these DIR boards. It was found that pre-heating in the oven had a positive influence on the physical properties of DIR boards. At first, the sample formed a hard board with 160^{o}C-10min pressing. The energy requirements of making a hard board decreased. The potential line in Figure 3.9 probably moved down. Secondly, the hardness of DIR boards increased with procedure 3. For example, DIR-H08 & DIR-H10 had higher manual test results than DIR-H04.

In addition, DIR-H11 had a similar hardness as oven-dried boards. This DIR board could not be broken in the manual test. High concentration of binder (K120) gave better physical properties than other samples.

Table 3.20 Sample details from procedure 3

Sample Name	Sample Details				Structure	Manual Test
	DIR (g)	K120 (g)	Distilled Water (g)	Procedure		
DIR-H07	41.10	12.31	41.01	3 (50°C -160°C—10min)	P	+
DIR-H06	41.04	12.20	41.06	3 (50°C -160°C—20min)	P	++
DIR-H08	41.21	12.07	41.25	3 (50°C -160°C--20min)	P	++
DIR-H09	41.15	12.28	41.16	3 (80°C -160°C—10min)	P	+
DIR-H10	41.00	12.02	41.24	3 (80°C -160°C—20min)	P	++
DIR-H11	41.12	24.02	41.03	3 (80°C -160°C—20min)	P	+++

3.6 Conclusions

The feasibility of bioboards with different waste materials (wheat straw, pea pod waste and DIR), commercial silicate solution (K120) or biosilicate solution and other chemical additives had been investigated in this Chapter. Bioboards also have acceptable physical properties, especially with starch as additives. Bioboards bonded with biosilicate solution had various internal bond strength as the different concentrations of silicate and the ratio of K_2O: SiO_2. It was clear that the binders with low concentration of silicate and low ratio of K_2O: SiO_2 had worse results than other kinds of bioboards. Biosilicate solutions extracted by 208 ml 3 M-aqueous KOH was the best binder ever found.

Pea pod waste also could be an alternative raw material for making boards. Boards with the mixture of de-waxed wheat straw and untreated pea pod waste showed similar IBS with other kinds of DWS boards, especially in low ratio pea pod bioboards.

For other kinds of waste material, DIR mixture with high moisture content (>38.7%) also can form a hard board with oven dry or hot-press. But the high moisture content also brought some issues for hot-press and adhesion.

In order to obtain a structural DIR board, water content needed to higher than 38.7%. With this ratio of water, the DIR powder was made to paste which was easily mixed with K120 solution and other components. However, high moisture content also dilutes the silicate solution which deteriorates adhesion and crosslinking.

Oven dried samples were much better than hot-press samples. The manual test showed that most of oven dried samples could not be broken. In contrast to oven dried samples, hot-press samples were not always cured completely. The surface of hot-press samples would be dried immediately by high temperature and high pressure. But the inside of hot-press samples were still wet as the water was trapped by the cured exterior.

Chapter 4: Novel research on the potential applications of waste cardboard/paper

4.1 Introduction

This chapter discusses the potential applications and properties of cardboard/paper by novel research methods. This includes the utilization of wheat straw powder in cardboard manufacture and the use of low power microwave (MW) processing of cardboard/paper to elicit a *sticky surface*.

4.1.1 Paper Background

Paper is a common material mainly used for writing, printing, drawing or packaging and so on. Paper is made by pressing wet fibres or pulp together. After pressing the wet fibre in designed moulds, the crude paper sheets are dried for usage. Typically, the major structural component of paper is cellulose, but sometimes lignin also will be present in paper. Also, unlike most of chemical raw materials; the fibres which are used for paper making are not produced by human but bio- synthetic from plant cell. So paper manufacture has little control over fibre shape and chemical composition in the making process except they can use crop selection and strategies for growth and harvesting.[17] It suggested that the content of different cellulose group, lignin, resins and organic extractives will all influence the paper-making process and finial products. Even if some raw materials have similar chemical compositions, the final products probably have different properties caused by the fibre length or structural alignment. All of these will have a significant influence on the subsequent chemistry of the paper-making process, and also have an influence on the physical and mechanical properties of the paper sheets.

4.1.2 Pulp

Pulp process is the preparation for cellulose-based materials to designed conditions. There are several methods for pulping including both chemical and mechanical approaches.

In order to release cellulose, a chemical pulp process is utilized to separate lignin from fibres. During this process, lignin is dissolved with organic solvents in a tank, so that it can be divided from cellulose fibres. Chemical pulp is widely used in wood resource. There are also some studies about chemical pulp process for wheat straw. For example, acetone and ethanol can be used for pulping wheat straw.[104, 105] Three main chemical approaches[106] are always applied in chemical pulp process: i. Sulfite process; ii. Kraft process, and; iii. Soda pulping. The sulfite process produces pulp by using sulfate to extract lignin from raw materials. The salts used in this pulping process could be SO_3^{2-}, HSO_3^-. The cation could be Na^+, Ca^{2+}, K^+, Mg^{2+} or NH_4^+.[107] The Kraft process can convert wood into wood pulp with a mixture of sodium hydroxide and sodium sulfide.[107] During the Kraft process, most of inorganic chemicals can be recovered or reused. Soda pulping is a chemical process for making pulp from straws, bagasse and woods with sodium hydroxide. In the soda pulping process, anthraquinone can be used as additive to decrease the carbohydrate degradation.[108] In addition, mechanical pulp, thermo mechanical pulp and deinked pulp (recycled pulp) are also widely used in paper industry.[106]

4.1.3 Fibre Pre-treatment

After the biomass has been converted into pulp by any pulping methods, it is ready to be made into paper. The process of making paper from pulp has many steps, each of which has an influence on the properties of final products. Typically, there are three important steps in the treatment of crude pulp before the pulp is delivered to the paper machine.

The first one is the dispersion of the pulp as slurry in water.[17] The second one is refining of the fibres in their mechanical properties to improve or get appropriate physical and mechanical properties for final products.[17] The third one is the chemical additives in the pulp which will impact certain properties of product or improve paper-making process.[17] After the pre-treatment process, pulp is usually diluted and transferred into paper machine for forming the final products.

4.2 Wheat straw powder as additive in cardboard/paper

4.2.1 Tensile Test of Cardboard

This work was performed at the premises of Sonoco-Alcore, Stainland Mill, Halifax, England. A range of cardboard/paper samples were made (shown in Figure 4.1 and Figure 4.2) and their properties were also analysed.

Figure 4.1 Lab-scale cardboard with pulp and wheat straw powder

Figure 4.2 Cardboards sheets after tensile test

In the initial study, the Difference value (D-value) was introduced into the analysis of tensile strength as the pulps from Sonoco-Alcore were different from batch to batch. The tensile test data for samples made is shown in Table 4.1 and Figure 4.3.

With the same ratio of waxed and de-waxed wheat straw in the cardboard/paper sheets, the latter (de-waxed) gave higher tensile force than the former, except at the ratio of 5%. Wheat straw can be easily complemented in to the cardboard/paper process without severely affecting integrity. Inclusion of de-waxed wheat straw at low ratios can increase the tensile strength noticeably thus providing a positive enhancement. This may be due to enhanced hydrogen bonding or simply a physical effect whereby the wheat straw powder acts as filler. However, at higher ratio of wheat straw (30% and 40%), paper strength decreased.

Table 4.1 Tensile tests of different ratio of waxed and de-waxed wheat straw sheets D-value%= (TS (WS sheets)-TS (Blank*))/TS (Blank*); Blank* is the blank that produced by same pulp with wheat straw sheets. TS means Tensile strength

	Ratio of WS	Average Weight (GSM)	Average Tensile Force(N)	D-value	D-value %
Cardboards with de-waxed WS powder (<125µm)	5%	201.8	89.4	-1.2	-2.3
	10%	204.5	67.4	8.9	15.2
	15%	222.5	92.9	2.3	2.5
	20%	207.5	66.2	7.7	13.2
	30%	209.8	63.1	-5.4	-7.9
	40%	203.8	61	-7.5	-10.9
Cardboards with virgin WS powder(<125 µm)	5%	212.3	93.7	3.1	3.4
	10%	213	85.4	2.1	2.5
	15%	199.3	74.5	-16.1	-17.8
	20%	200.8	59.6	1.2	2.1
	30%	194.5	46.6	-11.9	-20.3
	40%	196.9	47.5	-10.9	-18.7

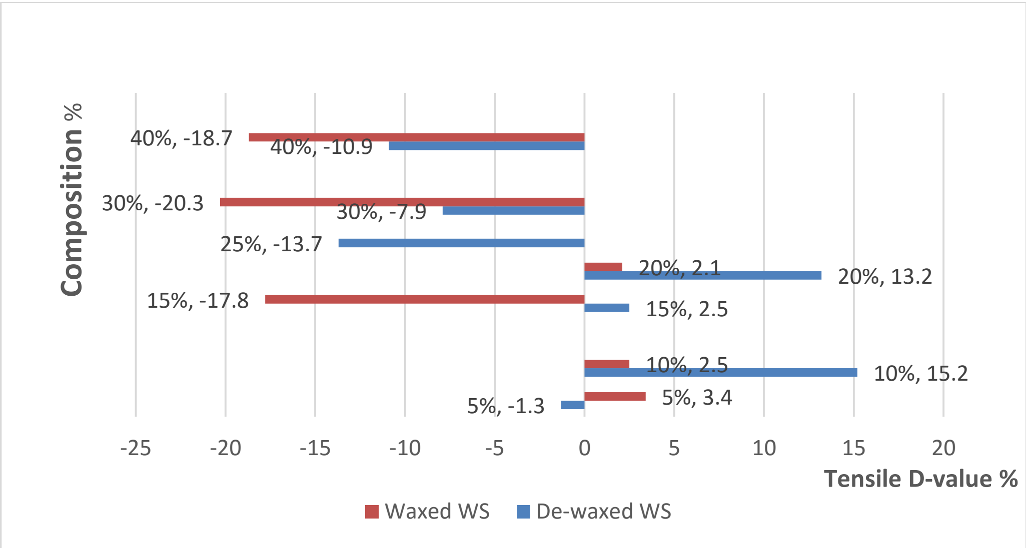

Figure 4.3 Tensile test of wheat straw sheets in the initial study

4.2.2 Tensile Index of Cardboard

Further analysis of the tensile index was conducted. The results of waxed wheat straw sheets (also named WS sheets) are shown in Table 4.2 & Figure 4.4 and for de-waxed WS sheets in Table 4.3 & Figure 4.5.

Table 4.2 Tensile Index of different ratio of waxed wheat straw sheets

Sample name	Mass of paper (g)	Paper weight (GSM)	Tensile Force (N)			Average Tensile Force(N)	Tensile Strength (N/m)	Tensile Index (Nm/g)
Blank	4.02	201	98.7	94.2	101.2	98.03	6535.6	32.5
	4.42	221	108.4	107.4	102	105.93	7062.2	32.0
5% Original	4.48	224	100.5	102.3	89.5	97.43	6495.6	29.0
	4.43	221.5	85.9	88.1	85.6	86.53	5768.9	26.0
10% Original	4.96	248	101.1	98.3	99	99.47	6631.1	26.7
	4.58	229	98.3	92.3	86.7	92.43	6162.2	26.9
15% Original	5.07	253.5	96	83.6	95.9	91.83	6122.2	24.2
	5.16	258	91.8	90.2	88.3	90.10	6006.7	23.3
20% Original	4.17	208.5	78.2	81.0	75.4	78.20	5213.3	25.0
	4.13	206.5	83.8	81.2	68.7	77.90	5193.3	25.1
30% Original	4.74	237	72.4	73.2	69.7	71.77	4784.4	20.2
	4.46	223	70.1	68.5	68.4	69.00	4600.0	20.6

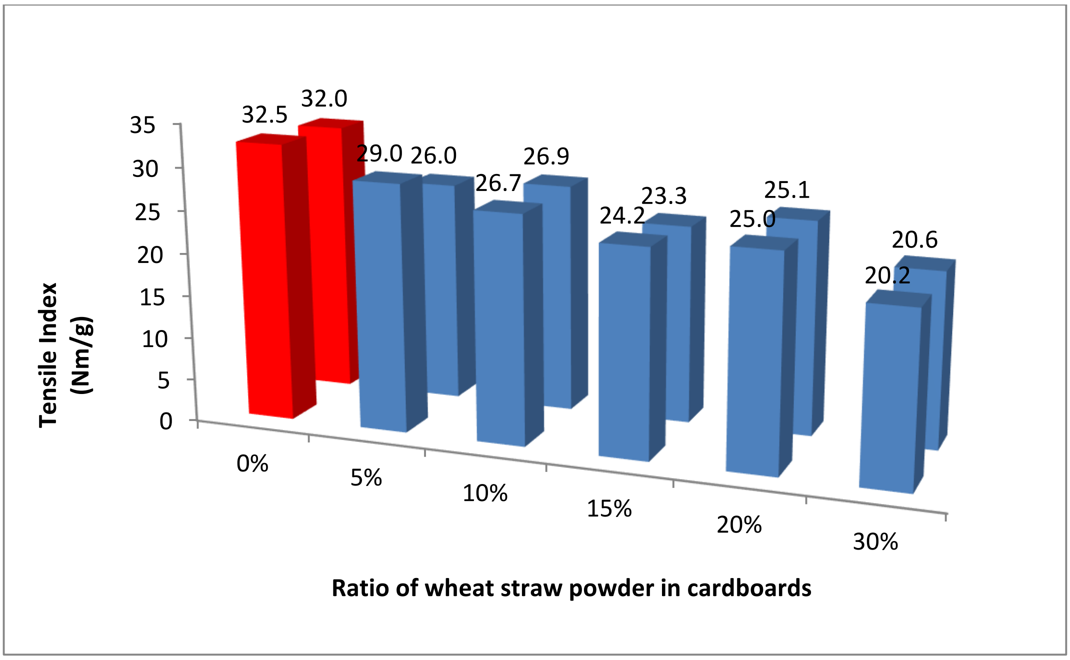

Figure 4.4 Tensile Index of WS Cardboards--wheat straw

Table 4.3 Tensile Index of different ratio of de-waxed wheat straw sheets

Sample name	Mass of paper (g)	Paper weight (GSM)	Tensile Force (N)			Average Tensile Force(N)	Tensile Strength (N/m)	Tensile Index (Nm/g)
Blank	4.02	201	98.7	94.2	101.2	98.03	6535.6	32.5
	4.42	221	108.4	107.4	102	105.93	7062.2	32.0
5% De-waxed	2.81	140.5	73.9	74.2	72.8	73.63	4908.9	34.9
	2.88	144	72.8	63.1	68.3	68.07	4537.8	31.5
10% De-waxed	4.21	210.5	110.8	101.2	113	108.33	7222.2	34.3
	4.23	211.5	109.6	95.9	120.3	108.60	7240.0	34.2
15% De-waxed	3.9	195	90	83.8	91.6	88.47	5897.8	30.2
	4.18	209	83.9	89.4	93.8	89.03	5935.6	28.4
20% De-waxed	4.32	216	88.7	94.5	87.5	90.23	6015.6	27.8
	4.53	226.5	76.6	85.3	72.1	78.00	5200.0	23.0
25% De-waxed	4.55	227.5	82.3	78.1	83.9	81.43	5428.9	23.9
	4.52	226	83.8	85.9	78.5	82.73	5515.6	24.4

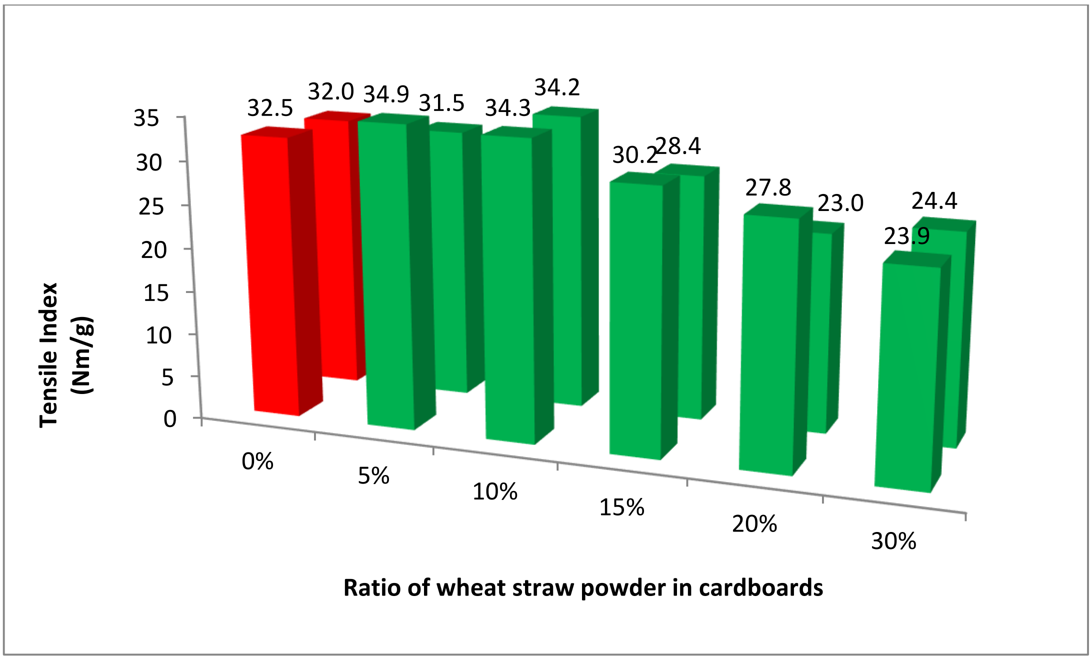

Figure 4.5 Tensile Index of WS Cardboards--De-waxed wheat straw

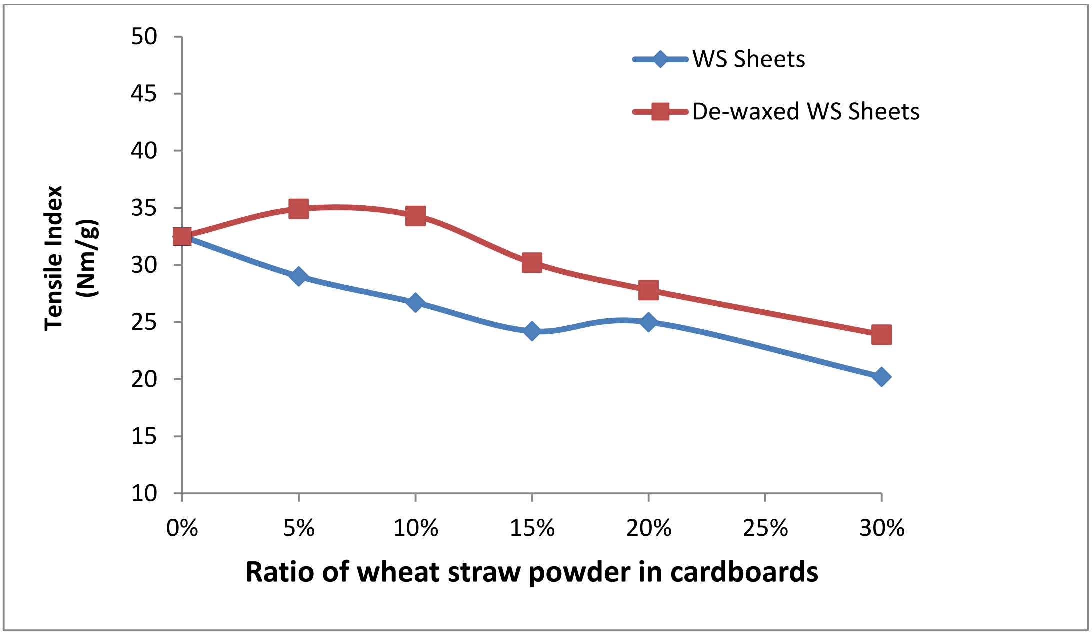

Figure 4.6 Low ratio WS sheets and de-waxed WS sheets

According to these results, original wheat straw (waxed wheat straw) slowly decreased the tensile index of cardboard/paper, and they have a significant decreasing tendency. Although the waxed wheat straw sheets have a lower tensile index than blanks sheets, the differences between the tensile indexes were tiny. For example, 5%, 10% and 15% waxed wheat straw paper sheets had the similar results with blank sheets. The difference value of tensile index between waxed wheat straw sheets and blank sheets was less than

10. Sometimes it was the same or -1. Therefore, the physical and mechanical properties of paper probably did not change significantly after adding waxed wheat straw.

For the de-waxed wheat straw cardboard/paper, the results of tensile index were different from waxed samples and blank samples. All of the de-waxed samples gave higher tensile index than blank sheets (shown in Figure 4.5). The previous results suggested the physical and mechanical properties of paper sheets decreased when the waxed wheat straw is more than 20%. Based on the recent results, parts of the de-waxed WS sheets had relatively higher tensile index than blank sheets, especially the cardboard/paper sheets contained 5%, 10% and 15% de-waxed wheat straw powder. And it was clear that cardboard/paper sheets, which contained high ratio wheat straw powder such as 20%, 30% and 40%, had a significant lower tensile index than all other kinds of paper sheets.

In conclusion, low ratio of de-waxed wheat straw could enhance the tensile strength of paper sheets, which had a higher or similar tensile index (shown in Table 4.3). The high ratio de-waxed wheat straw paper sheets probably had a lower tensile index than blank sheets. The tensile index of waxed wheat straw paper sheets had a lower results as much more waxed wheat straw was added, which suggested that waxed wheat straw had gradually decreased the mechanical or physical properties of cardboard. But the waxed samples had a similar tensile index with blank sheets at the ratio of 5%, 10% and 15%. In these conditions (5%, 10% and 15%), waxed wheat straw sheets should have the similar physical and mechanical properties with blank paper sheets. These results suggested that both waxed and original wheat straw were the alternative additives or replace parts for the paper sheets. Potentially, the wheat straw powder could bring or enhance some specific properties of the paper sheets. This was discussed in Chapter 4.2.3.

Table 4.4 Tensile Index of wheat straw sheet

Sample name	Mass of paper (g)	Paper weight (GSM)	Tensile Force (N)			Average Tensile Force (N)	Tensile Strength (N/m)	Tensile Index (Nm/g)
Blank	3.29	164.5	61.6	53.1	64.6	59.77	3984.4	24.2
	3.45	172.5	59.4	55.6	61.9	58.97	3931.1	22.8
5%	3.58	179	61.6	61.7	60.4	61.23	4082.2	22.8
Original	3.49	174.5	62.9	54.2	57.8	58.30	3886.7	22.3
10%	3.27	163.5	56.4	60.4	59.9	58.90	3926.7	24.0
Original	3.29	164.5	54.5	56.3	55.8	55.53	3702.2	22.5
15%	3.29	164.5	50.3	48.6	48.2	49.03	3268.9	19.9
Original	3.24	162	50.5	46.6	49.9	49.00	3266.7	20.2
20%	3.53	176.5	45.3	41.8	43.7	43.60	2906.7	16.5
Original	3.58	179	51.6	52.3	47.9	50.60	3373.3	18.8
25%	3.25	162.5	45.7	47.4	47.6	46.90	3126.7	19.2
Original	3.87	193.5	57.5	54.3	51.5	54.43	3628.9	18.8
30%	3.39	169.5	46.5	42	46.2	44.90	2993.3	17.7
Original	3.35	167.5	44.1	43.1	41.1	42.77	2851.1	17.0

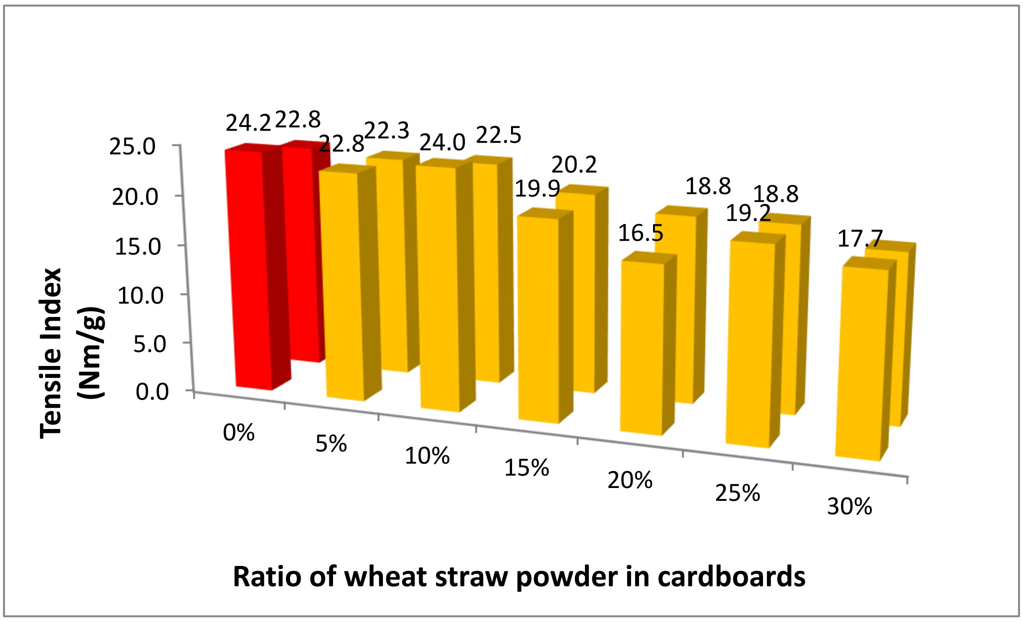

Figure 4.7 Tensile Index of low ratio WS (original) cardboards

4.2.3 Water adsorption capacity

Water adsorption capacity is another important property of cardboard. It shows the resistance of cardboard to water. The test were carried out in room temperature and the results are listed in Table 4.5 and Figure 4.8.

Table 4.5 Water resistance test of wheat straw sheets

	Ratio of additives (%)	Mass of paper (g)	Paper weight (GSM)	Water content (%)
Blank	0	3.54	177.0	1.232
	0	4.44	222.0	1.158
	0	3.80	190.0	1.150
	0	3.88	194.0	1.165
	0	3.63	181.5	1.287
Waxed (<125μm)	10	5.25	262.5	1.208
	20	3.70	185.0	1.278
	30	3.59	179.5	1.217
	40	3.31	165.5	1.063
De-waxed (<125μm)	10	3.68	184.0	1.111
	20	5.80	290.0	1.172
	30	3.39	169.0	1.080
	40	3.96	198.0	1.116

At first, not all the samples could pass this test. Blank sheets without any wheat straw powder were all failed as the water was leaking during the test. For WS sheets and de-waxed WS sheets, the test successfully finished as the sheets with wheat straw powder could hold the water for 10 sec and there was no leaking during the rest. In contrast to blank sheets, samples with wheat straw powder had certain water adsorption/retention capability. The water resistant ability of cardboard was significantly increased by the wheat straw powder as the WS sheets had finished this test. After this test, the water content of the sheets was all increased in the range of 1.1% - 1.3%. Although sheets with wheat straw powder became more hydrophobic, the sheets still adsorbed certain amount of water. Overall, waxed samples and de-waxed samples had a similar water content after the test. Waxed samples could adsorb more water than de-waxed samples in the ratio of 10%, 20% and 30%. It approximately caused by the wax layer on the surface of wheat straw and the wax layer could help trap more water in the samples. In the ratio of 40%, this results was opposite. But the water content of waxed and de-waxed samples had minor differences. This result will be investigated in the future work.

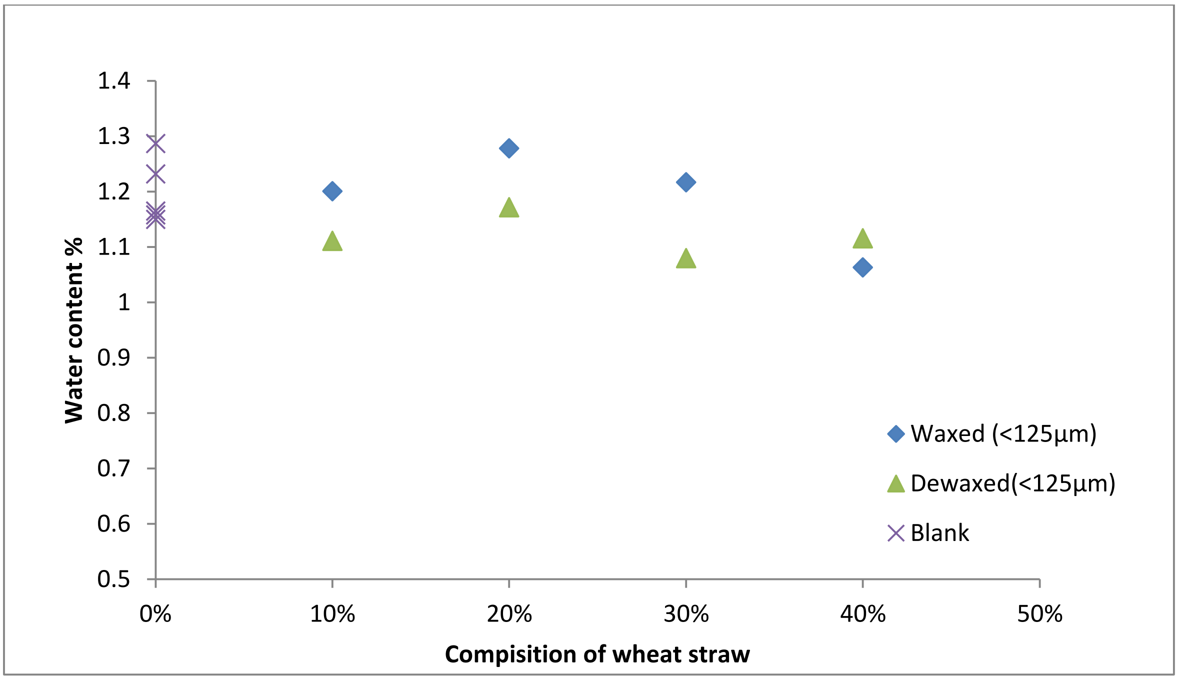

Figure 4.8 Water adsorption capability of paper sheet

4.2.4 FT-IR

FT-IR showed that the chemical components on the surface of cardboards did not vary significantly. Samples with additives and blank sheets all had similar spectra. Cellulose was still the major chemical component. Also, all the tested samples have the characteristic bands for O-H and C-O groups associated with cellulose or cellulosic matter.

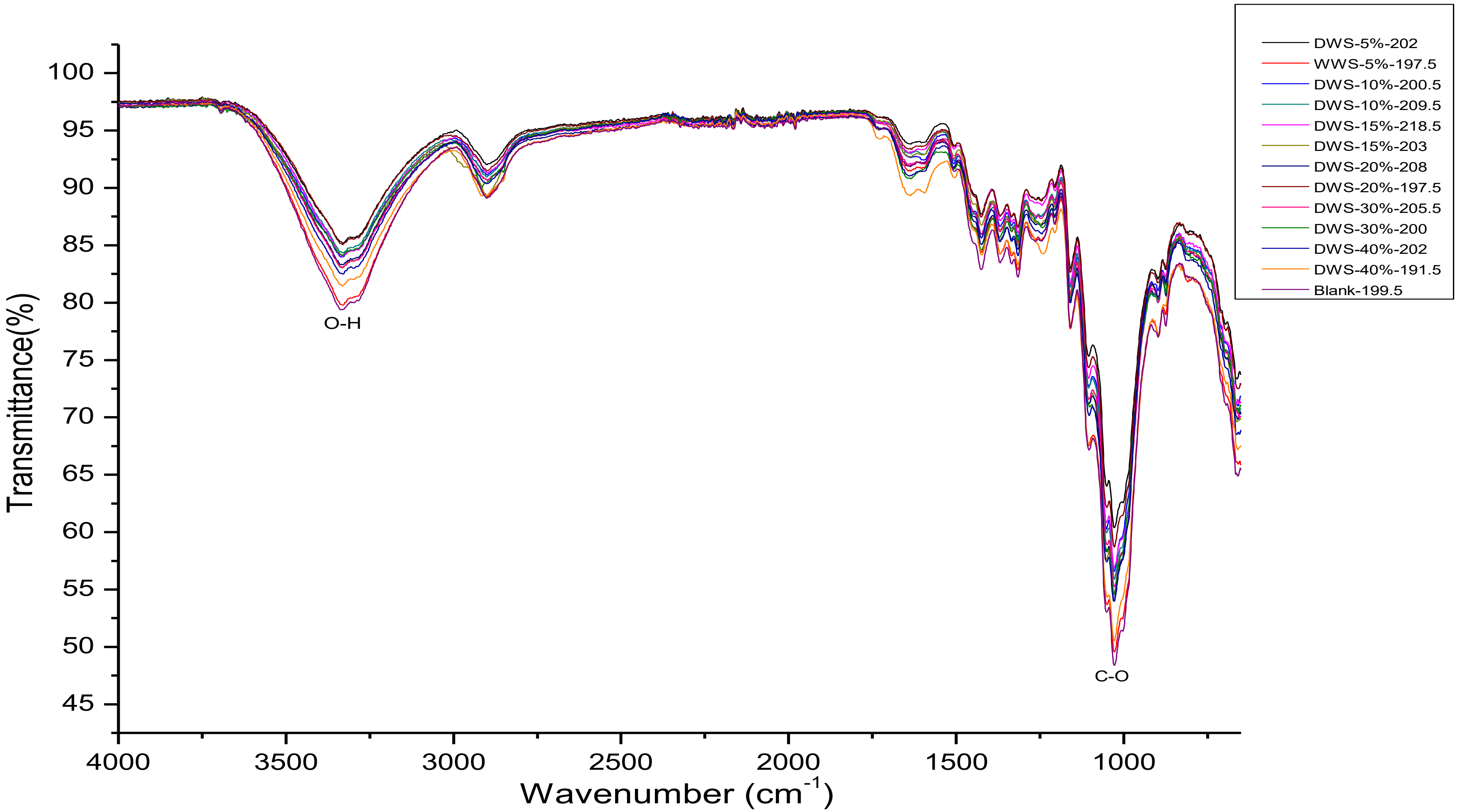

Figure 4.9 FT-IR—back side of sheets

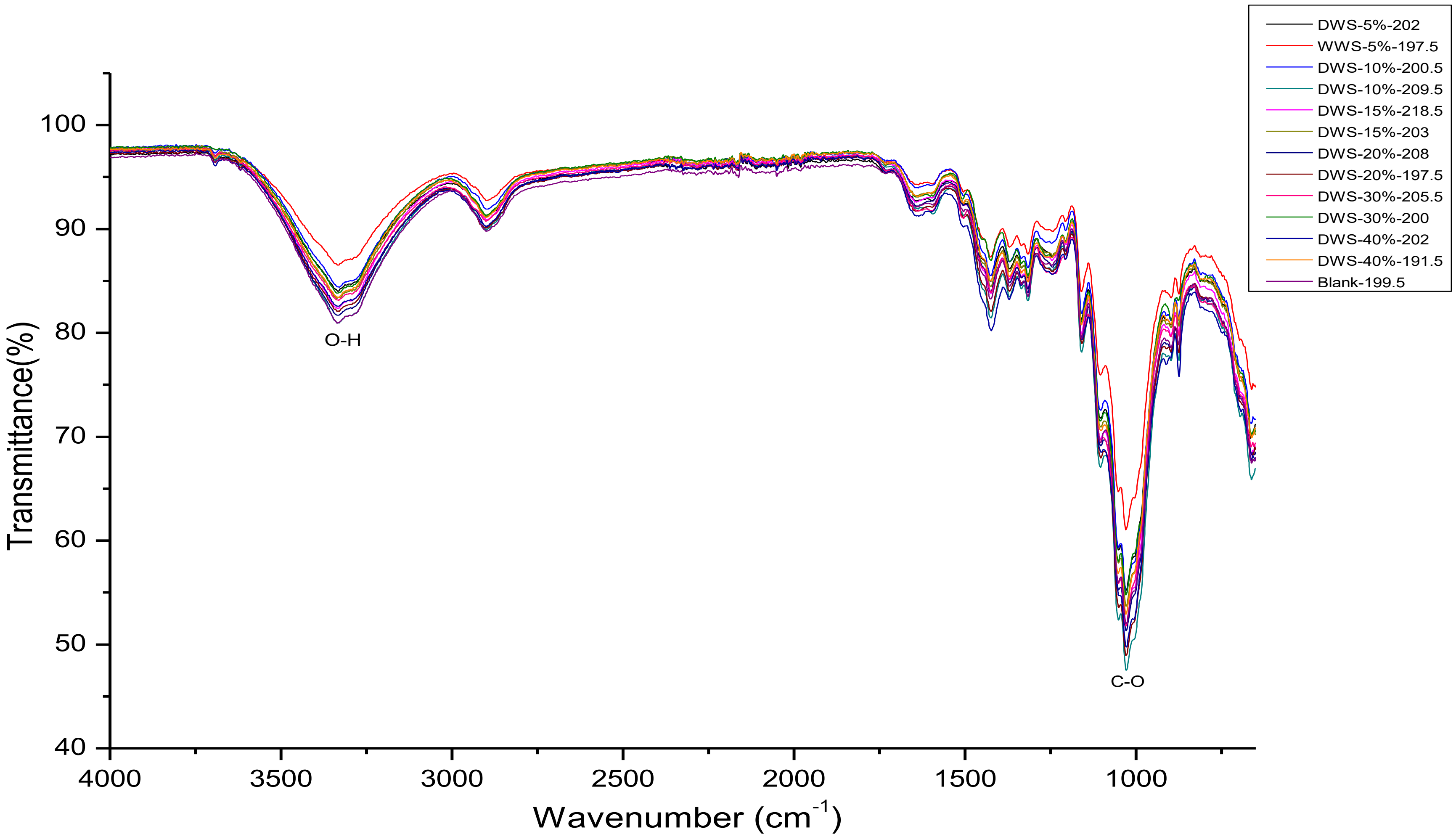

Figure 4.10 FT-IR—front side of sheets

4.3 MW Cardboards

Microwave pyrolysis of paper is well known to elicit sugars, bio-oil and biochar essentially from the breakdown of cellulose.[109] In this short study, waste cardboard was subjected to low temperature microwave pyrolysis to induce partial cellulose breakdown such that the resultant sugars could rise to the surface thus producing a sticky surface, i.e., *in-situ* adhesive production. Thus, two types of waste cardboard were subjected to low-temperature MW processing and their surfaces examined. Two different MW conditions were tested in position 1 and position 2. The results of high-grade cardboards showed in Table 4.6 and Figure 4.11 and the results of low-grade cardboards showed in Table 4.7 and Figure 4.12.

Initial Observations

When subjected to 200 W and 150 W power in position 1, some colourless liquid or aqueous phase was observed near the top of MW tube together with bio-oil in the middle of tube. The initial colour of the cardboard changed from light brown-beige to dark brown signifying considerable charring (See Figure 4.11 and Figure 4.12). In position 2, there was still some colourless liquid observed at the top of tubes. However, the cardboard did not discolour significantly. This was an important result such that the cardboard position was dependent on interaction with MW irradiation, i.e., dependent on position within the tube, either the full face of the cardboard was subjected to irradiation (Position 1) or just one edge/side (position 2). Thus for a softer interaction with MW irradiation, and to avoid charring, Position 2 was a better choice than position 1 for this work.

Table 4.6 MW cardboards of high-grade details in position 1

		High-Grade (a)	High-Grade (b)	High-Grade (c)	High-Grade (d)
MW Power (W)		200	150	200	150
Time (min)		5	5	5	5
Paper Position		1	1	1	1
Weight (g)	**Original**	0.77	0.75	0.75	0.76
	After MW	0.67	0.69	0.59	0.65
	D-Value	-0.10	-0.06	-0.16	-0.11
	D-value%	-12.99	-8.00	-21.33	-14.47
Highest Temperature(^{o}C)		219	178	250	204

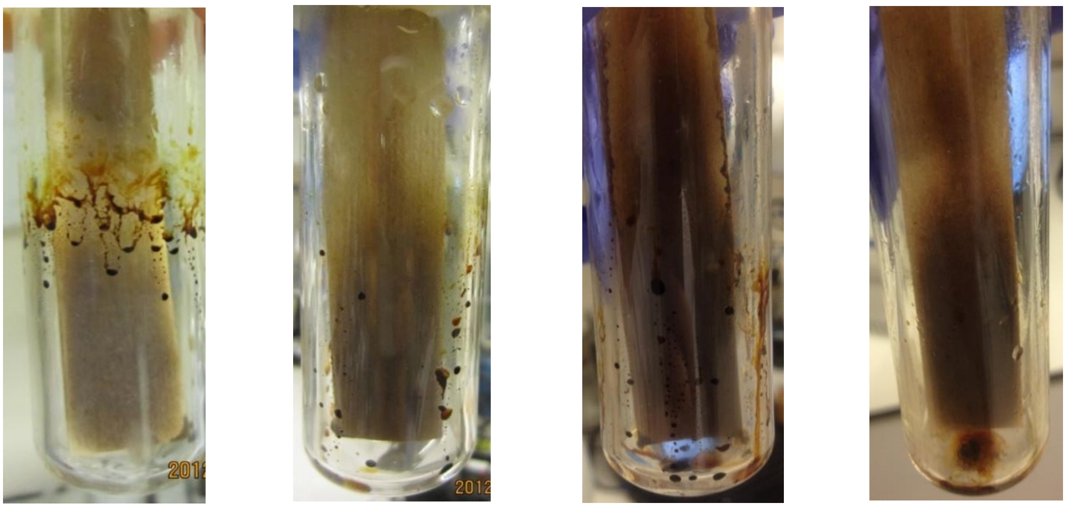

a **b** **c** **d**

Figure 4.11 MW cardboards of high-grade details in position 1

Table 4.7 MW cardboards of low-grade details in position 2

		Low-Grade (a)	Low-Grade (b)	High-Grade (c)	High-Grade (d)
MW Power (W)		200	150	200	150
Time (min)		2	2	2	2
Paper Position		5	5	5	5
Weight (g)	Original	0.76	0.68	0.80	0.77
	After MW	0.74	0.65	0.78	0.72
	D-Value	-0.02	-0.03	-0.02	-0.05
	D-value%	-2.63	-4.41	-2.50	-6.49
Highest Temperature(^{o}C)		195	146	215	160

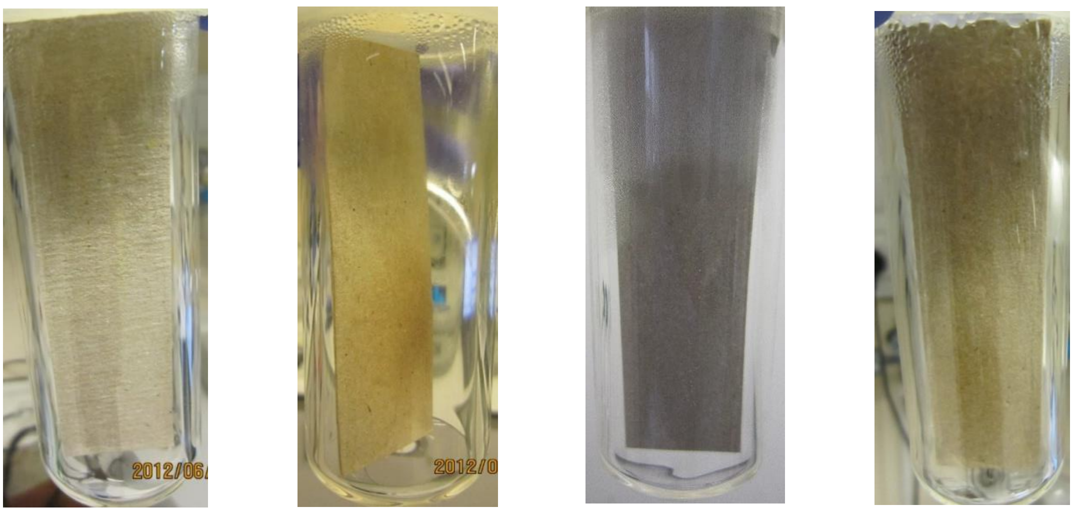

a b c d

Figure 4.12 MW cardboards of low-grade details in position 2

4.3.1 FT-IR of cardboards

FT-IR was used to analyse the surface of cardboard (200 W-5min). For each cardboard, the spectrum was recorded at 11 points across its surface as shown in Figure 4.13.

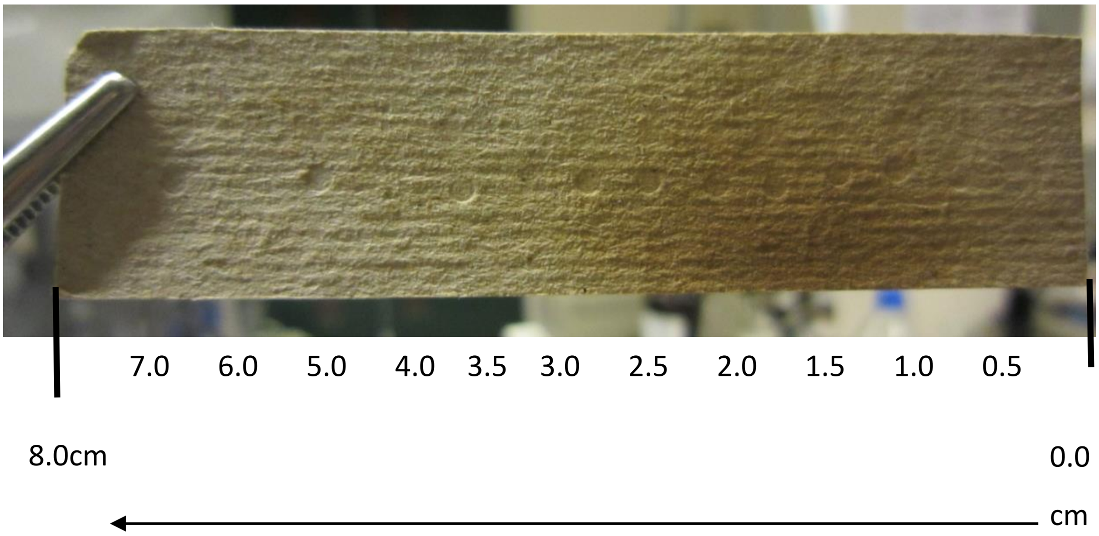

Figure 4.13 Testing points of the cardboard

Spectra were recorded for both surfaces, i.e., front and back, thus 22 in total. Eight typical FT-IR spectra were shown in Figures 4.14 to 4.21. There were no significant differences between the spectra. No change in functional groups for pre- and post-MW cardboard was detected. The characteristic bands for cellulose were noted: O-H group, C-H group, and C-O group. Minor changes in their intensities were observed, mainly the O-H stretch (3500 cm^{-1}) which may be due to dehydration.

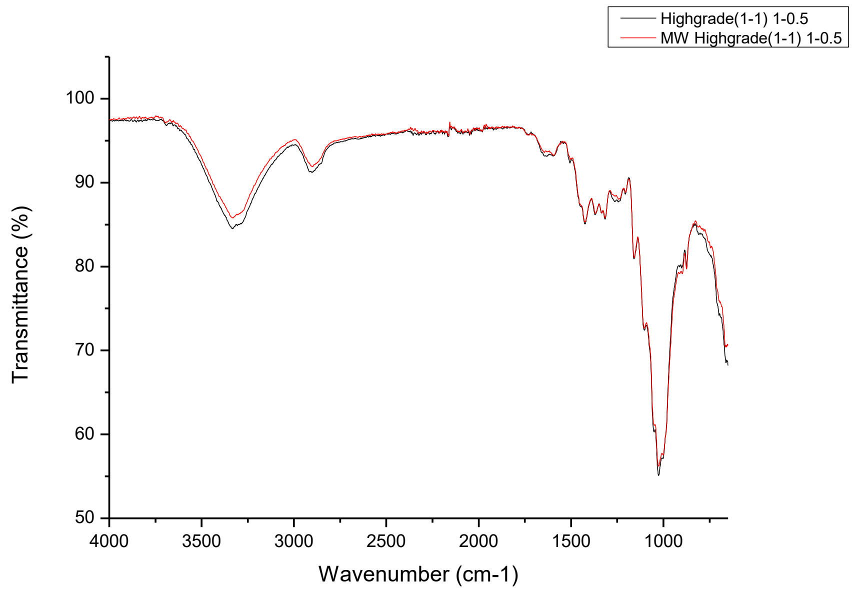

Figure 4.14 Position2: High-grade cardboard with 200W-5min Point: 0.5cm, Side: Front side

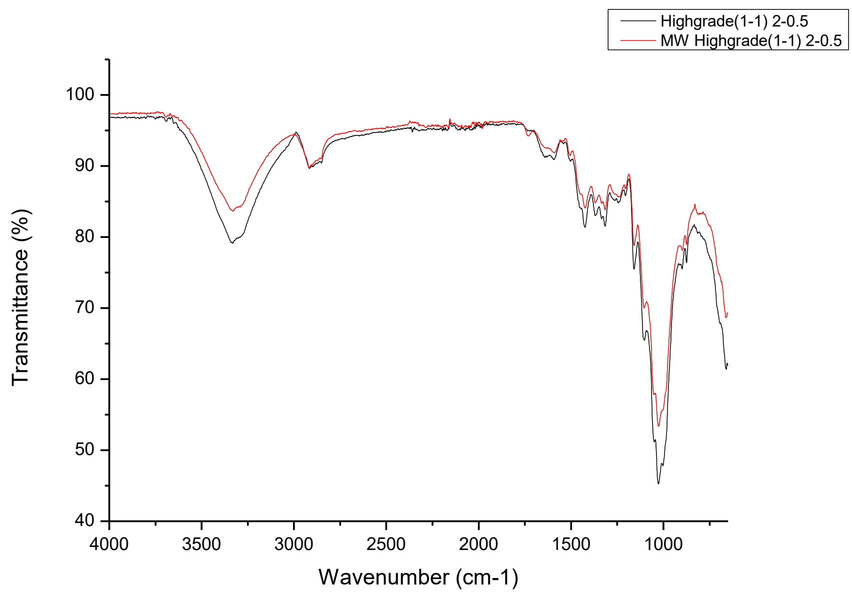

Figure 4.15 Position2: High-grade cardboard with 200W-5min, Point: 0.5cm, Side: Back side

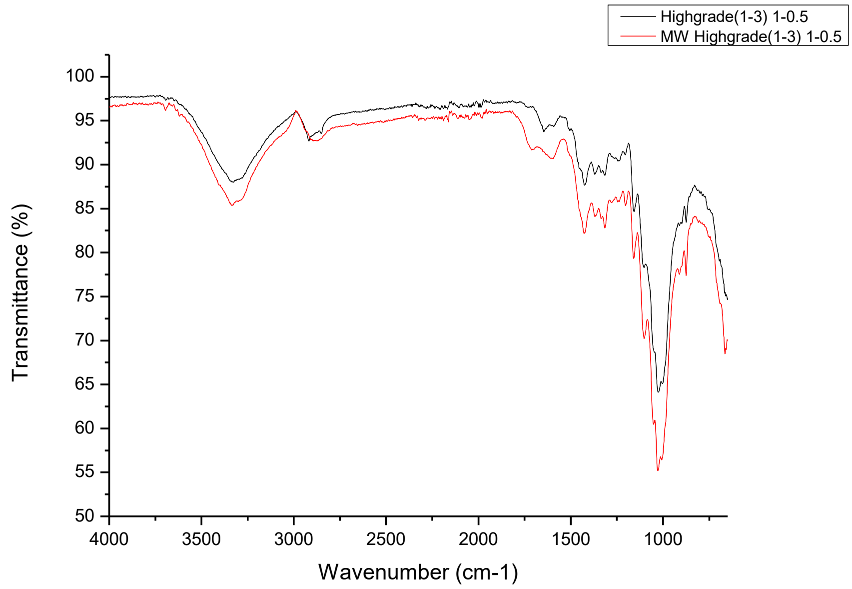

Figure 4.16 Position1: High-grade cardboard with 200W-5min, Point: 0.5cm, Side: Front side

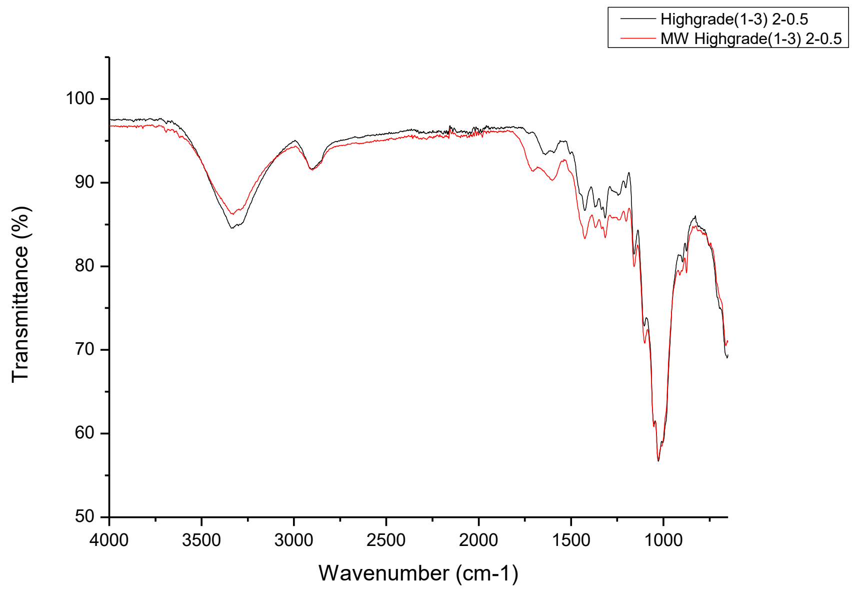

Figure 4.17 Position1: High-grade cardboard with 200W-5min, Point: 0.5cm, Side: Back side

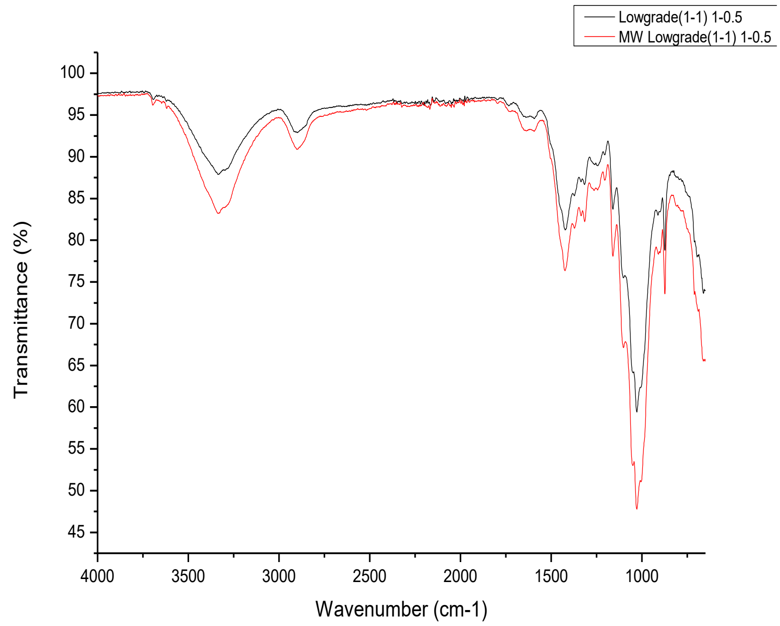

Figure 4.18 Position2: Low-grade cardboard with 200W-5min, Point: 0.5cm, Side: Front side

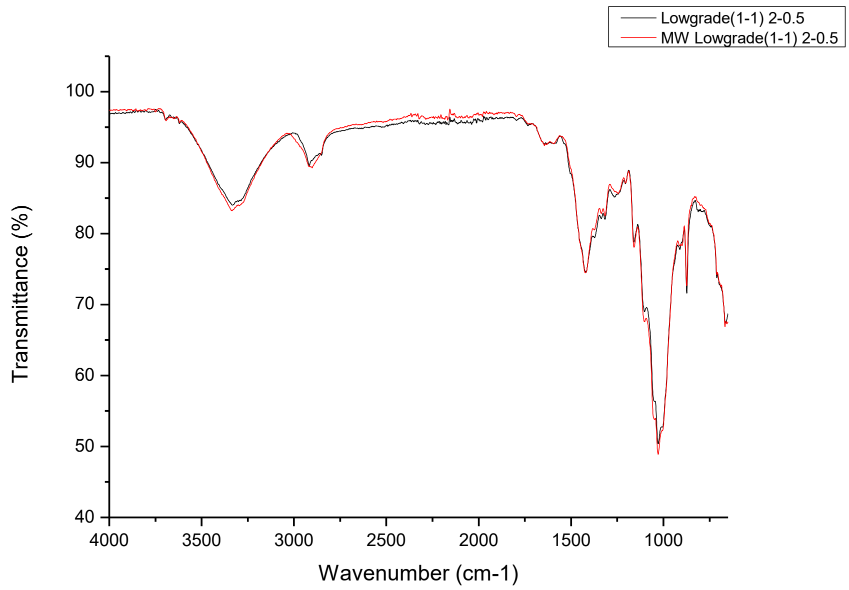

Figure 4.19 Position2: Low-grade cardboard with 200W-5min, Point: 0.5cm, Side: Back side

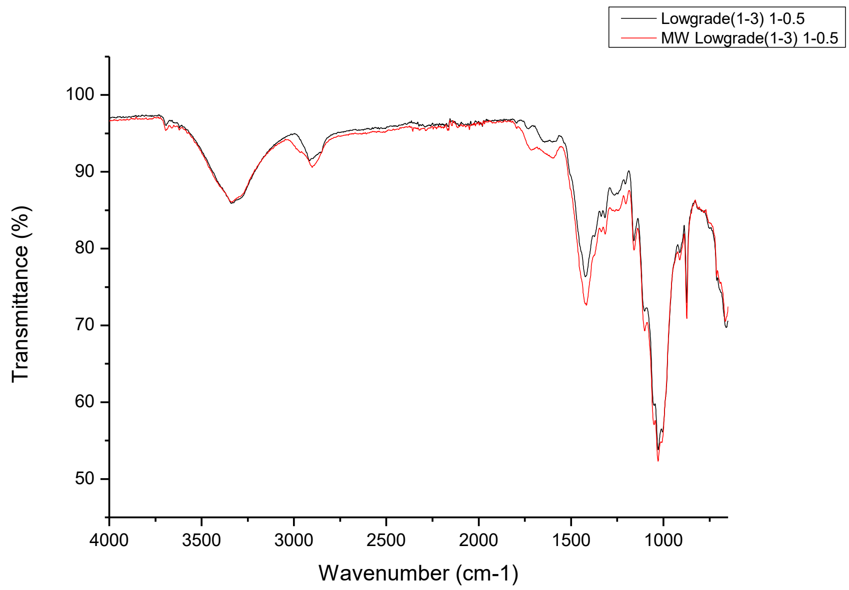

Figure 4.20 Position1: Low-grade cardboard with 200W-5min, Point: 0.5cm, Side: Front side

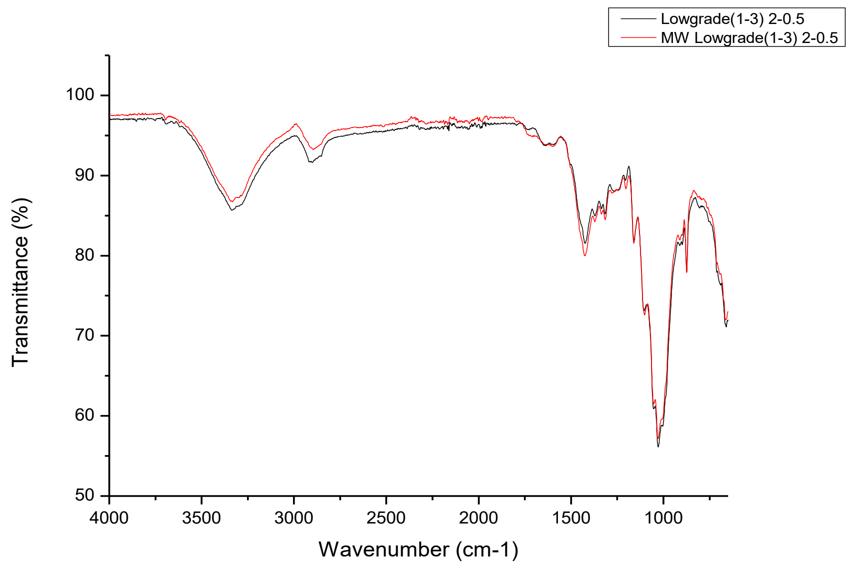

Figure 4.21 Position1: Low-grade cardboard with 200W-5min, Point: 0.5cm, Side: Back side

4.3.2 GC-MS of Oil

The bio-oil from both low-grade and high-grade cardboard subjected to MW irradiation (200 W-5min) in position 1 was analysed by GC-MS (Figure 4.22 and Figure 4.23). Bio-oil both from high-grade cardboard and low-grade cardboard possesses levoglucosan

(1,6-anhydro-β-D-glucopyranose), a known intermediate from the pyrolysis of cellulose. 2-Hydroxymethyl furfural (HMF) was also detected. HMF is a recognised platform molecule.

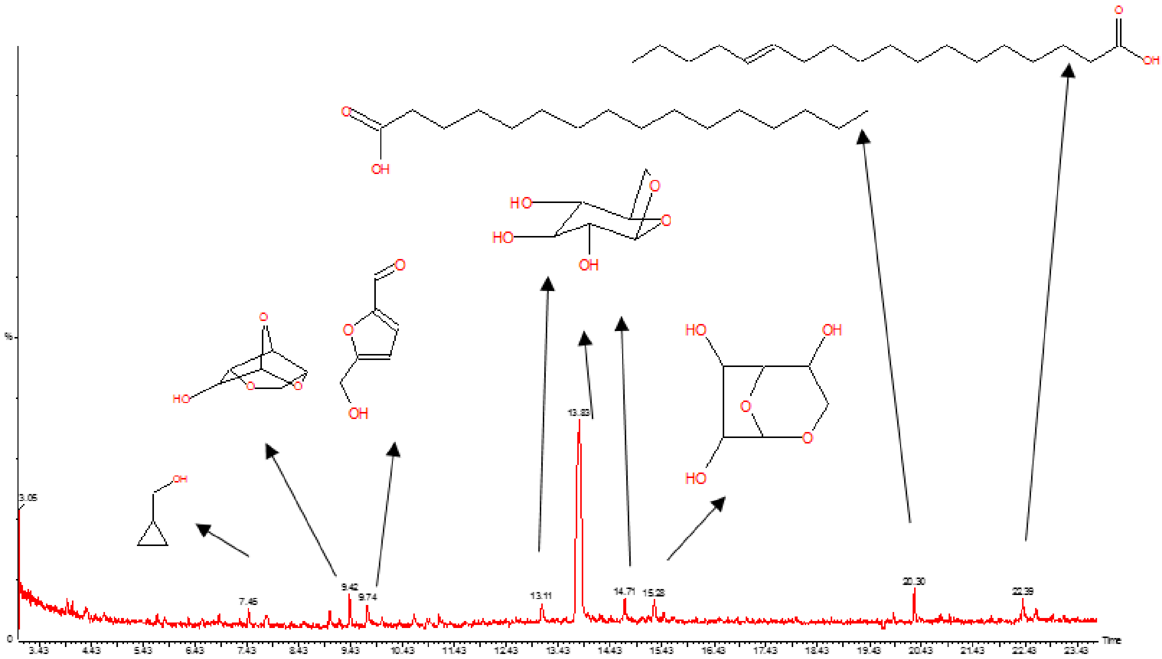

Figure 4.22 GC-MS of oil from MW High-grade cardboard under 200W-5min, Position1

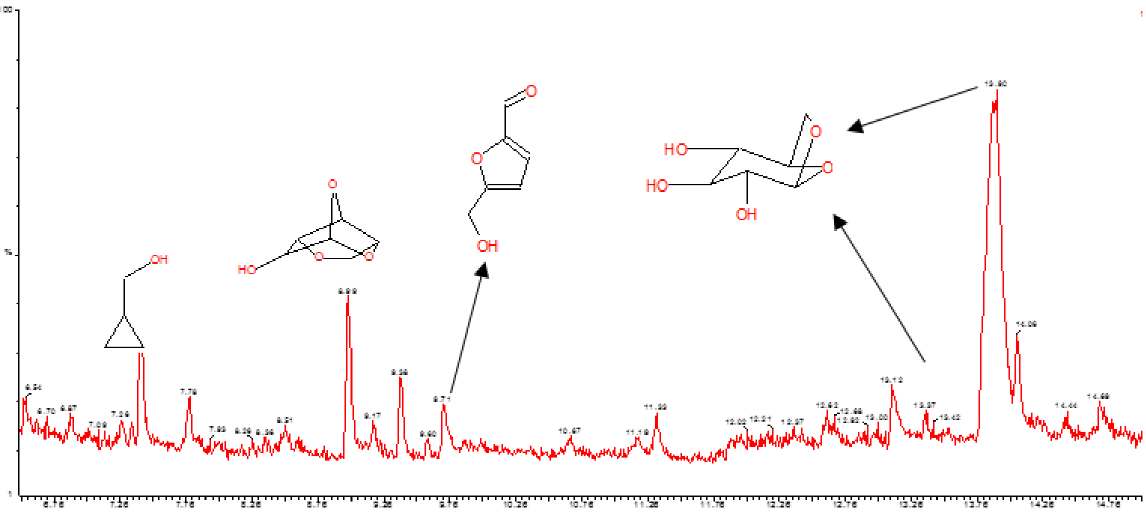

Figure 4.23 GC-MS of oil from MW Low-grade cardboard under 200W-5min, Position1

4.3.3 Low Temperature MW of cardboard in Position 2

As discussed earlier. Position 2 was more prevalent to MW irradiation leading to rapid bio-oil and biochar formation. Thus, MW power was reduced from 200 W to 50 W in 50 W intervals (Table 4.8 and Table 4.9).

Table 4.8 MW high-grade cardboards with different power

		a	b	c	d	e
MW Power (W)		200	150	100	75	50
Time (min)		5	5	5	5	5
Paper Position		1	1	1	1	1
Weight (g)	**Original**	0.75	0.76	0.75	0.79	0.80
	After MW	0.59	0.65	0.69	0.74	0.75
	D-Value	-0.16	-0.11	-0.06	-0.05	-0.05
	D-value%	-21.33%	-14.47%	-8.00%	-6.33%	-6.25%
Highest Temperature (^oC)		250	204	145	117	90

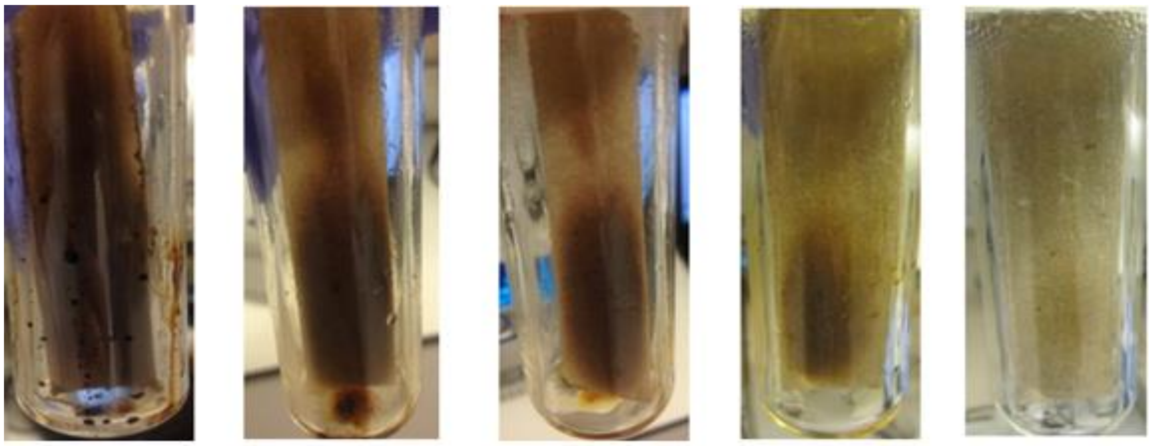

a b c d e

Figure 4.24 MW of high-grade cardboards with different power

Table 4.9 MW low-grade cardboards with different power

		a	b	c	d	e
MW Power (W)		200	150	100	75	50
Time (min)		5	5	5	5	5
Paper Position		1	1	1	1	1
Weight (g)	**Original**	0.77	0.75	0.75	0.70	0.71
	After MW	0.67	0.69	0.72	0.69	0.70
	D-Value	-0.10	-0.06	-0.03	-0.01	-0.01
	D-value%	-12.99%	-8.00%	-4.00%	-1.43%	-1.41%
Highest Temperature (^oC)		219	178	133	118	84

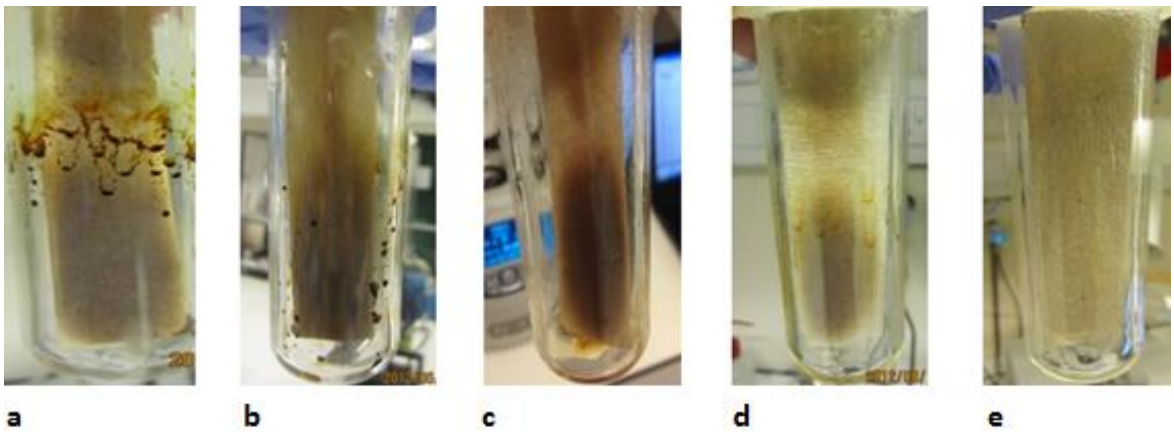

Figure 4.25 MW of low-grade cardboards with different power

As the MW power decreased, the appearance of the cardboard was more acceptable, i.e., significant charring was reduced. For example, MW-50W-5min produced a small amount of colourless liquid at the top of tube, with no sign of bio-oil and/or biochar formation.

FT-IR of cardboards

For each cardboard, 7 points on the cardboards were tested. The front and the back side were analysed by FT-IR and 4 typical FT-IR spectra were shown in Figure 4.26 - 4.29.

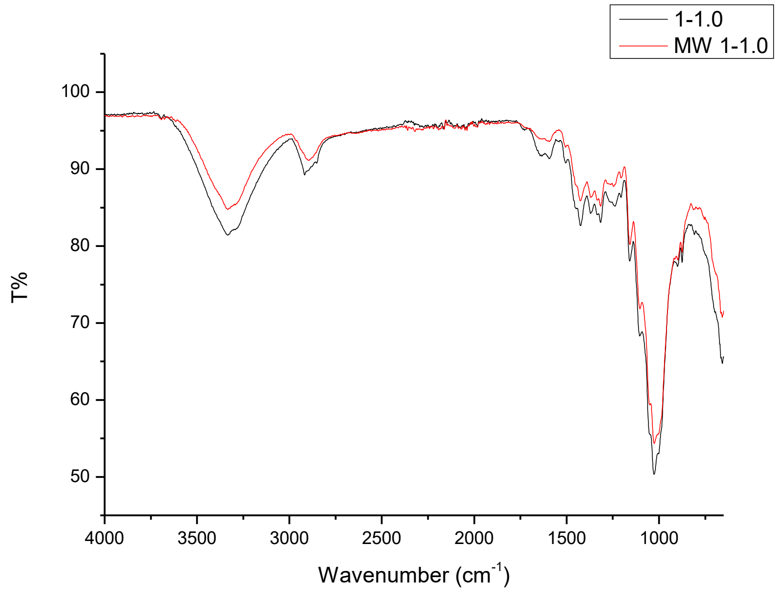

Figure 4.26 Position1: High-grade 50W-5min, Point: 1.0cm, Side: Front side

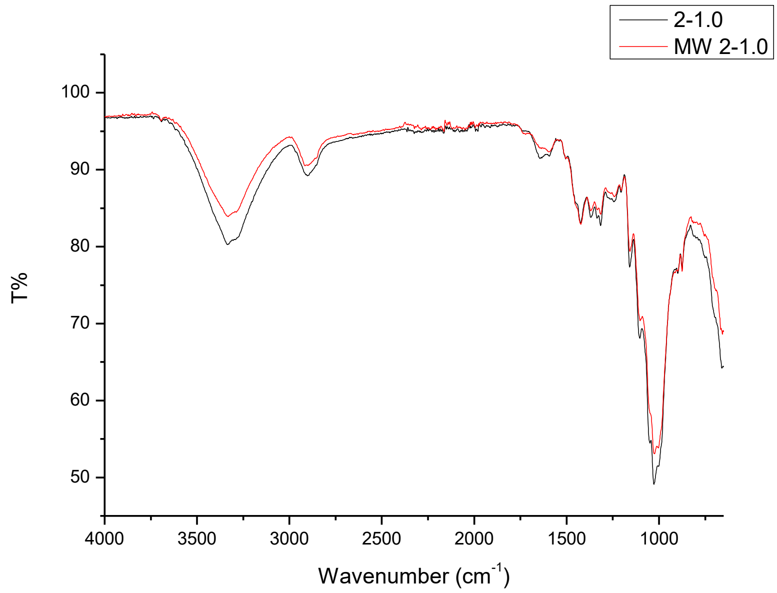

Figure 4.27 Position1: High-grade 50W-5min, Point: 1.0cm, Side: Back side

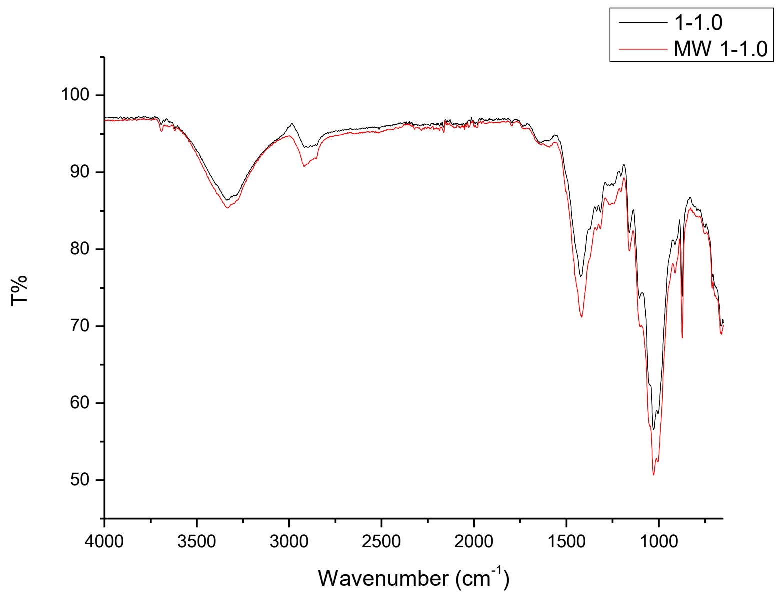

Figure 4.28 Position1: Low-grade 50W-5min, Point: 1.0cm, Side: Front side

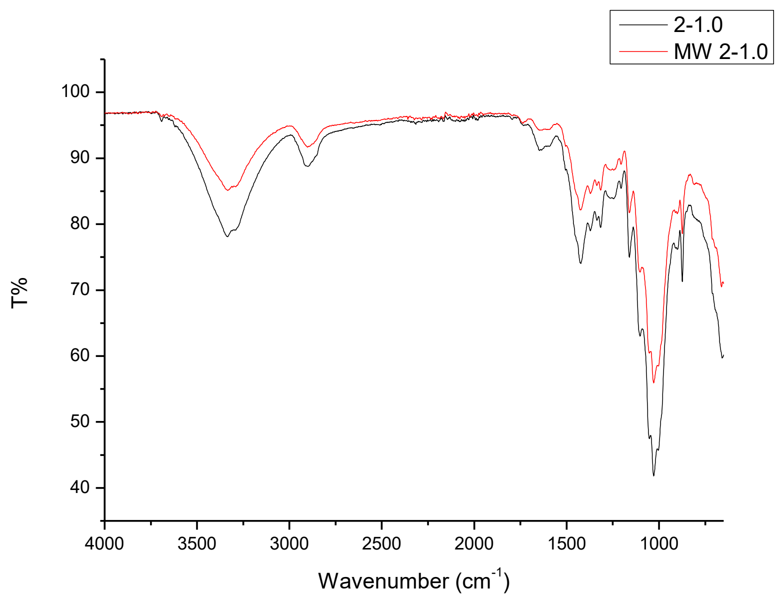

Figure 4.29 Position1: Low-grade 50W-5min, Point: 1.0cm, Side: Back side

Again, the spectra did not reveal any significant differences, except for slight changes in intensity.

4.3.4 Low power MW irradiation: influence of time

With having determined that 50 W power was the most subtle treatment, i.e., least destructive, both high-grade and low-grade cardboard were subjected to different time regimes from 1 min to 8 min. The mass change with respect to time in depicted in Figure 4.30 and Figure 4.31.

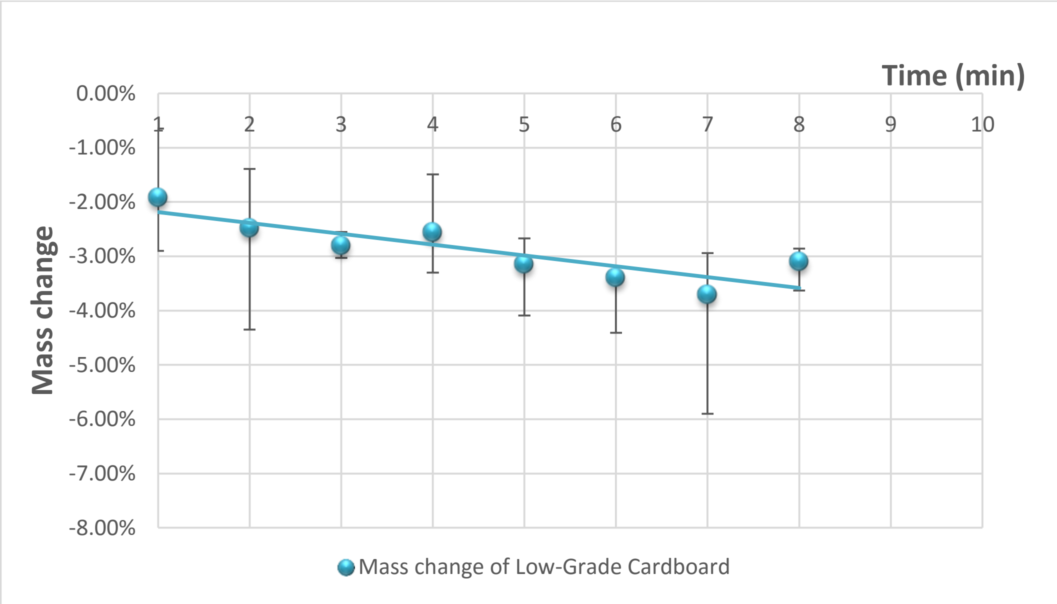

Figure 4.30 Mass change of low-grade cardboard at 50W

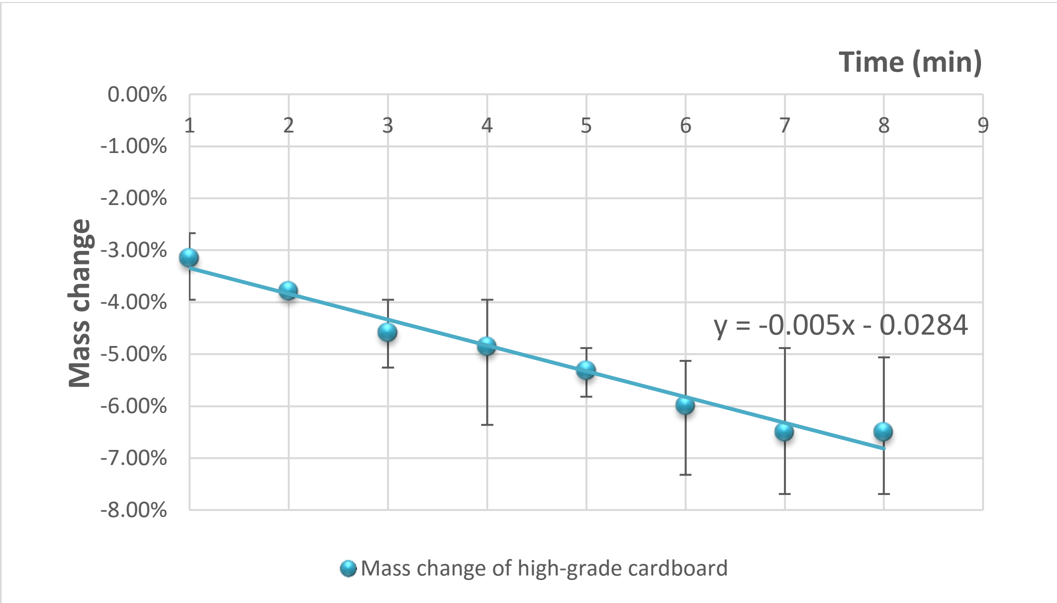

Figure 4.31 Mass change of High-grade cardboard at 50W

According to the average mass change data, high-grade and low-grade have the same tendency as the reaction time is increased, i.e., decreasing mass. The mass loss from high-grade cardboard is much higher than compared to low-grade cardboard but the variation in mass loss is much less. Obviously, high grade paper is manufactured to a more controlled composition than low grade paper.

FT-IR of *aqueous* phase

The FT-IR spectra of the aqueous phase are shown in Figure 4.32 and Figure 4.33. Interestingly, in addition to the expected absorption bands as 3500 cm^{-1} and 1600 cm^{-1} characteristic of water, C-H stretching bands are noted at approximately 3000 cm^{-1}, possibly C-C stretching bands at 1450 cm^{-1} and a fairly strong absorption band at approximately 1100 cm^{-1} might be due C-O stretching vibrations, indicative of carbon containing (organic) compounds probably sugars. However, at the time of this work we did not have access to HPLC but based on the FT-IR data this does warrant further investigation. Sugars might have been selectively elicited from the surface of the cardboard thus producing an *in-situ* adhesive.

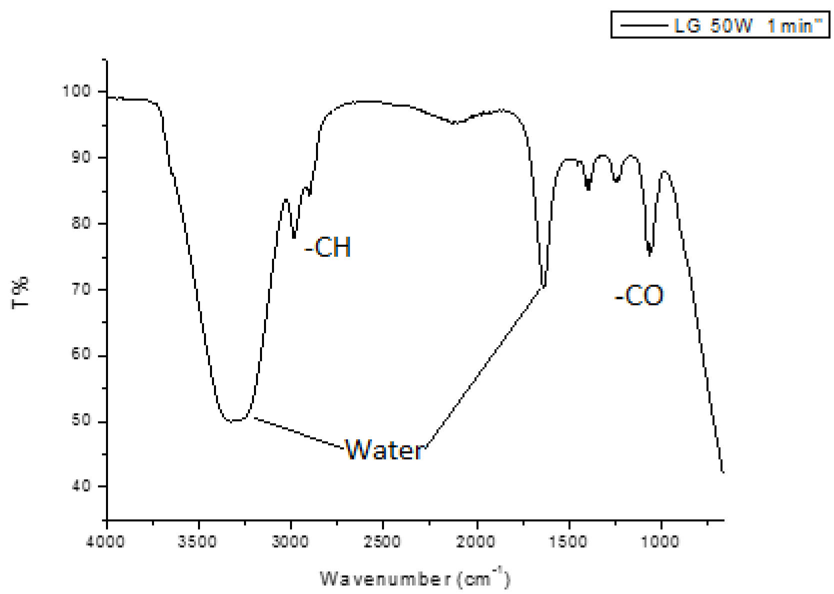

Figure 4.32 FT-IR of aqueous phase: low-grade under 50W-1min, group3

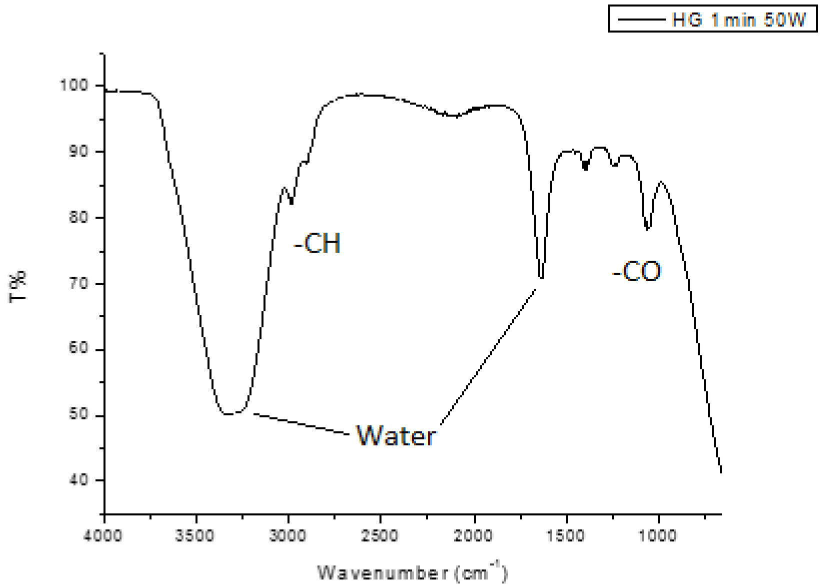

Figure 4.33 FT-IR of aqueous phase: high-grade under 50W-1min, group3

4.3.5 Solid-State NMR of MW cardboards

The surface of cardboard/paper was ground to powder for solid-state ^{13}C NMR analysis. The spectra of three typical high-grade cardboard/papers post MW irradiation are shown in Figure 4.35, Figure 4.36 and Figure 4.37. The NMR spectrum of the virgin cardboard/paper is shown in Figure 4.34. As the cardboard was made from recycling paper, the major chemical component should be cellulose. The solid-state ^{13}C NMR of high-grade cardboard waste also proved this point. Peak around 105.22 ppm was C_1; peaks around 89.17 ppm and 83.00 ppm were C_4; peaks around 75.11 ppm and 72.50 ppm were C_2, C_3 and C_5; peaks around 65.36 ppm and 62.98 ppm were C_6.[110] Also the cardboard/paper waste probably contained other kinds of chemical additives during the fibre pre-treatment process as described in Chapter 4.1.3. So the peaks here were not completely matched with standard cellulose. And in C_6 area, it was typical simple sp3 carbon (C > CH > CH_2 > CH_3). It all suggested that other kinds of organic appeared in high-grade cardboard.

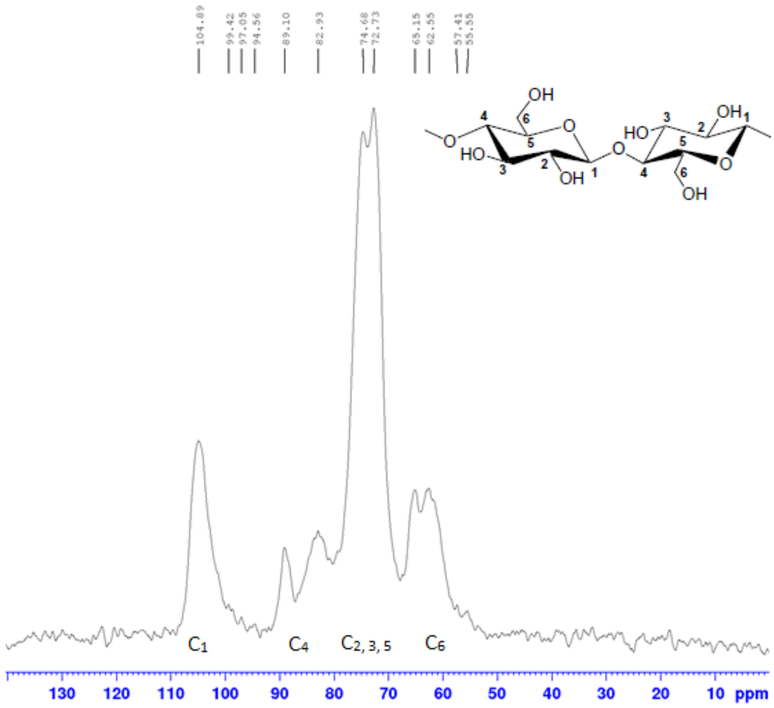

Figure 4.34 Solid-state ^{13}C NMR of virgin high-grade cardboard

High-grade cardboard after MW in 50 W for 1-5 min showed different spectra compared to virgin cardboard. It was clear that the spectra of MW cardboards had less noising peaks than virgin samples. The relative intensity of peaks between 72 ppm and 74 ppm were gradually changed. The C_2, C_3 and C_5 had been influenced by low temperature MW, which the –OH group connected. Also, simple sp^3 carbon area was clearly changed. The carbon groups that was different with C_6 group were appeared. It was supposed to be low molecule weight chemicals as the total spectrum did not change too much. All of these differences indicated that the high-grade cardboard released some low molecule weight chemicals which expected to be sugars on their surface after MW. And the main chain of cellulose did not change too much. The MW cardboards should be similar with virgin cardboards but sticky as the chemical components been released. High-grade cardboard after MW in 100 W for 5 min had some significant differences to virgin samples. This cardboard were burnt from the appearance and changed to dark colour. Char and bio-oil were produced on the surface of cardboard. Then the NMR spectrum changed a lot on the main peaks, which might have alcohols or ethers or esters around the area of 72-75 ppm; and different CH_n groups around 60 ppm.

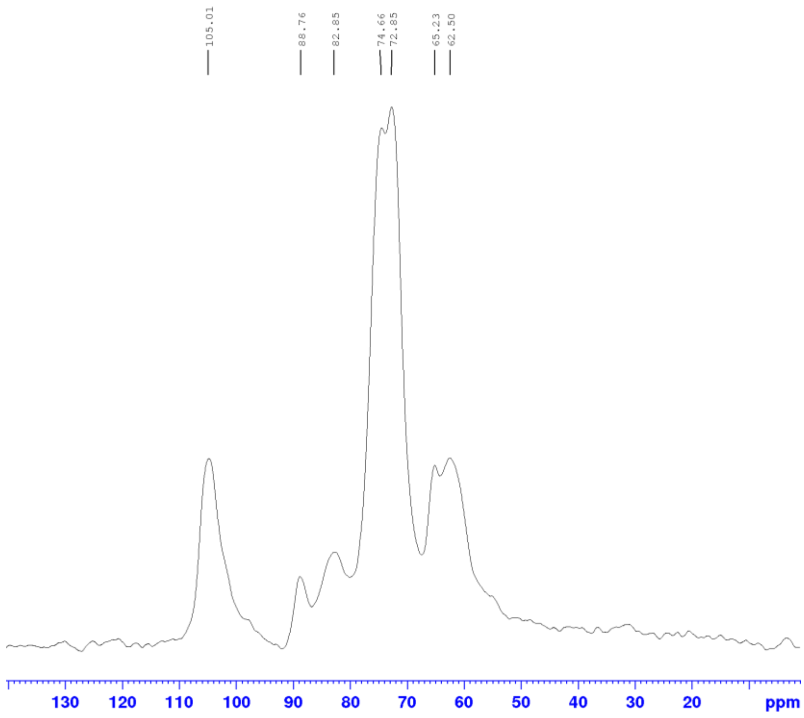

Figure 4.35 Solid-state ^{13}C NMR of MW high-grade cardboard under 50 W for 1min (Position 1)

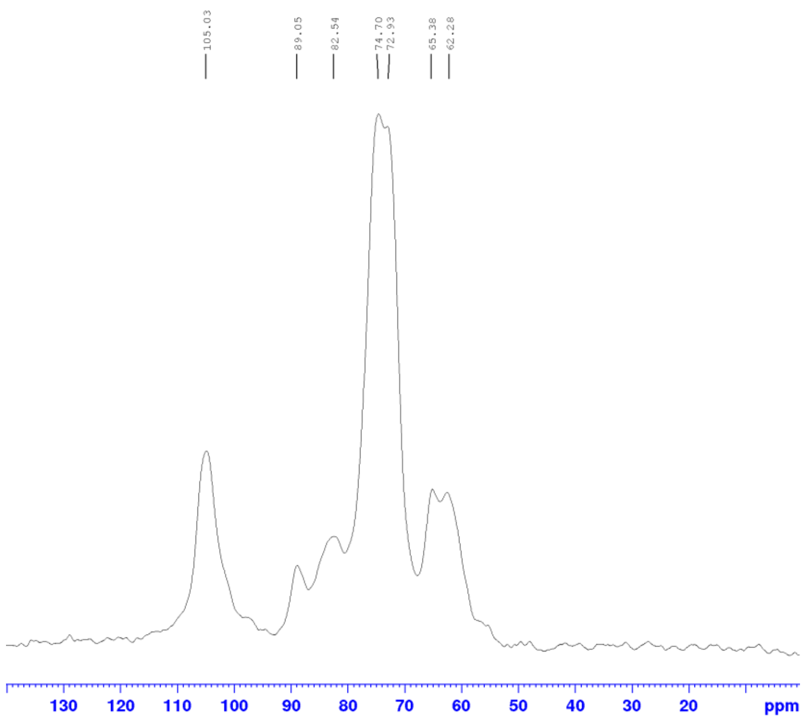

Figure 4.36 Solid-state ^{13}C NMR of MW high-grade cardboard under 50 W for 5min

(Position 1)

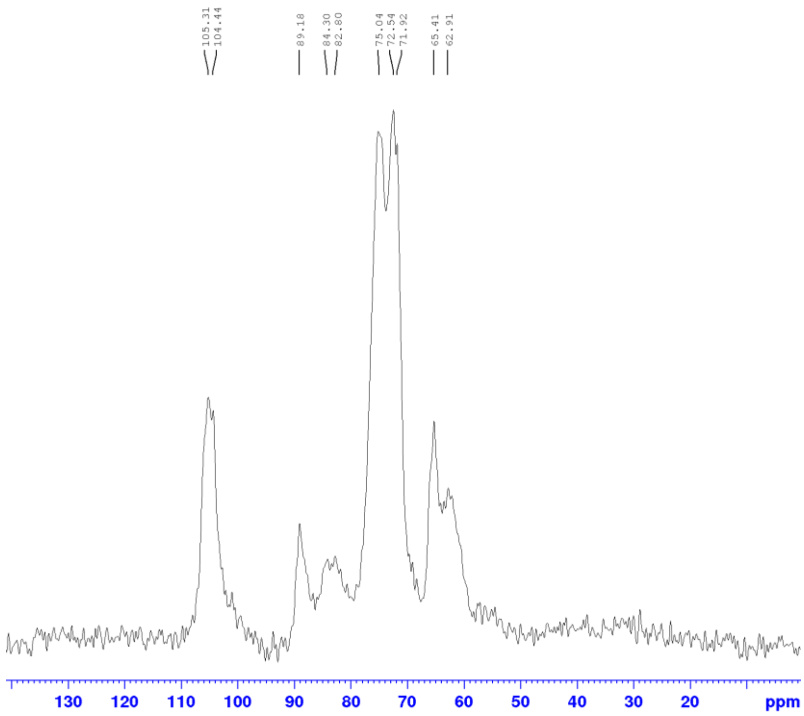

Figure 4.37 Solid-state ^{13}C NMR of MW high-grade cardboard under 100 W for 5min (Position 1)

The surface of cardboard/paper were ground to powder for solid-state ^{13}C NMR analysis. The spectra of three typical high-grade cardboard samples post MW irradiation are shown in Figure 4.39, Figure 4.40 and Figure 4. 41 and virgin cardboard in Figure 4.38. The resource of low-grade cardboard was also recycling paper and cardboard, but different kinds of waste paper or cardboard with high-grade. The solid-state ^{13}C NMR of low-grade cardboard had the similar peak with high-grade cardboard, which mainly was cellulose. But they were recycled from different kinds of waste paper source. Slightly different NMR spectrum appeared. These three types of MW low-grade cardboards: 50 W for 1 min, 50 W for 5 min and 100 W for 5 min had the similar with high-grade cardboard (50W). The major peaks slightly changed as low molecular weight chemicals were produced under MW. It also identified that the surface of cardboards became sticky as these chemicals on the surface.

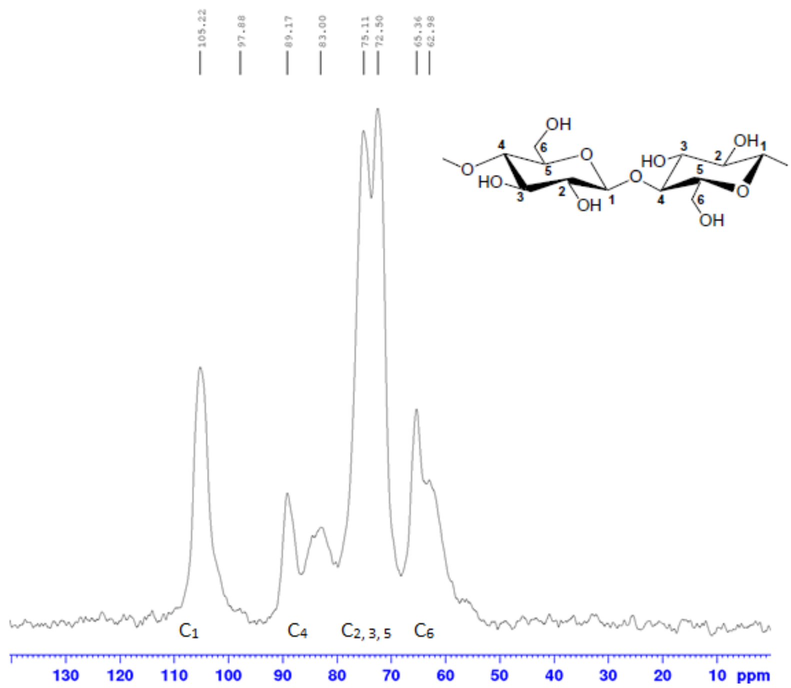

Figure 4.38 Solid-state ^{13}C NMR of virgin low-grade cardboard

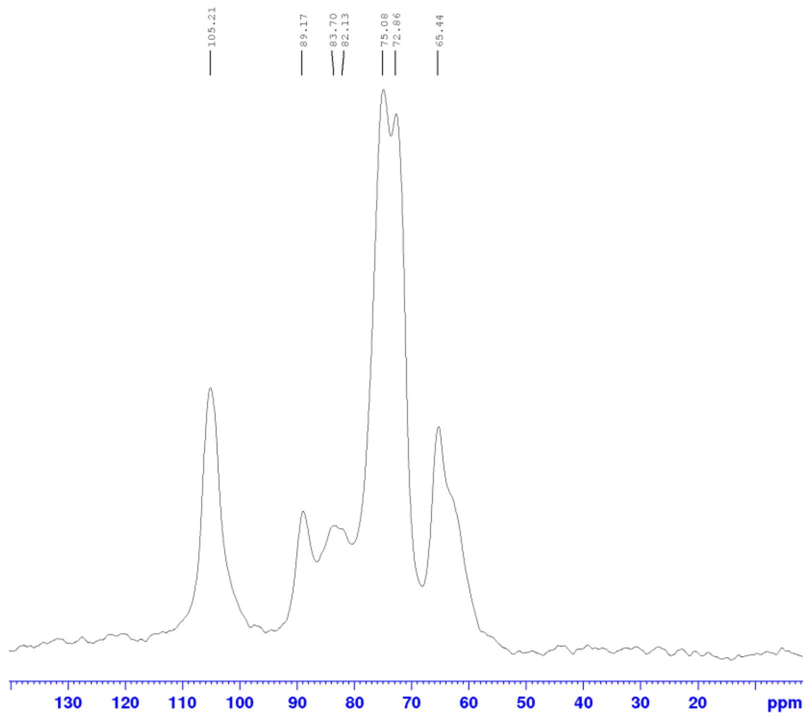

Figure 4.39 Solid-state ^{13}C NMR of MW low-grade cardboard under 50 W for 1min (Position 1)

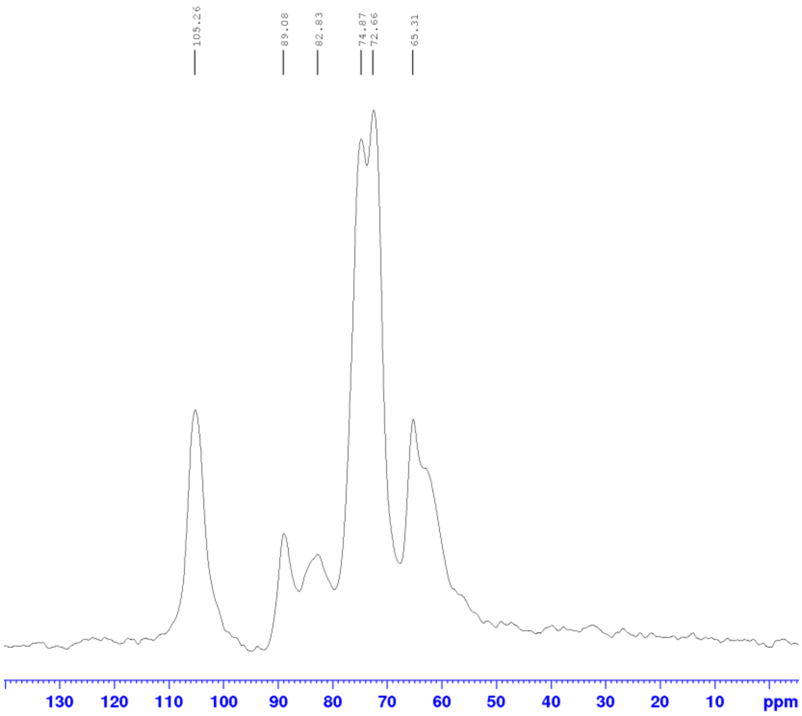

Figure 4.40 Solid-state ^{13}C NMR of MW low-grade cardboard under 50 W for 5min (Position 1)

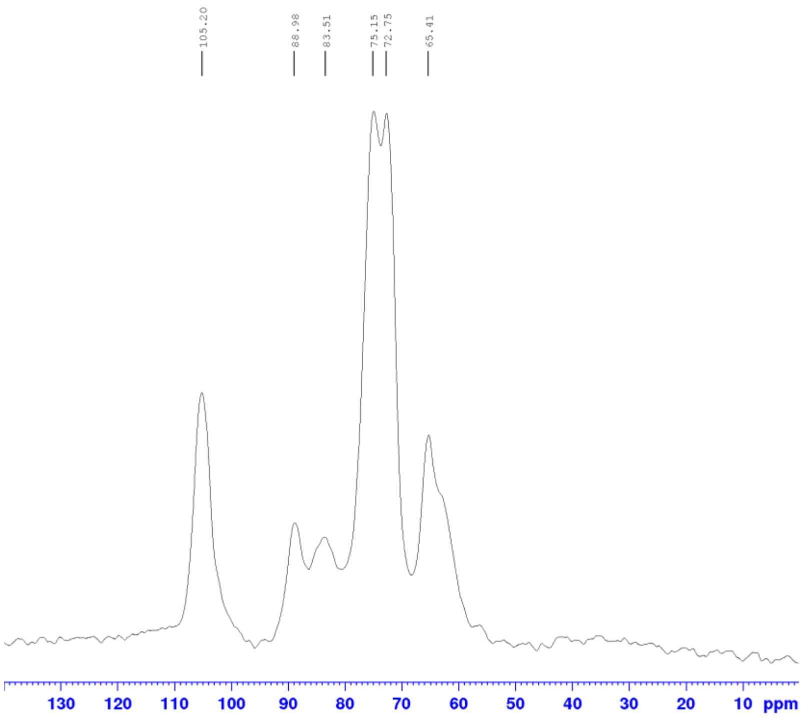

Figure 4.41 Solid-state ^{13}C NMR of MW low-grade cardboard under 100 W for 5min (Position 1)

4.4 Conclusion

Wheat straw as an alternative additive has positive influence on the properties of cardboard/paper. Low ratio WS cardboard and de-waxed WS cardboard such as 5% and 10% have the similar mechanical properties with virgin cardboard. Low ratio de-waxed WS cardboards perform better mechanical properties than normal cardboards. But this difference is not significant. In addition, cardboards with WS and de-waxed WS have strong water resistance.

MW cardboards with different positions have a significant difference. The direction of MW will influence the efficiency of pyrolysis in the process. Cardboards will be *burnt* if the MW power is higher than 50 W in 5 min but yield bio-oil rich in levoglucosan and an aqueous phase. Surface analysis by FT-IR of cardboard provided minimal evidence of any change. The FT-IR of original cardboards and MW cardboards are the same. However, the FT-IR of the aqueous phase does show evidence of organic matter.

Solid-state ^{13}C NMR had verified the existence of low molecular weight chemicals or sugar on the surface of cardboards as the different spectra between virgin samples and MW samples. But it was still hard to calculate the contents and identify the components released on the surface of cardboards after MW.

Chapter 5:

Materials and Methodology

5.1 Wheat straw cardboards

Wheat straw was used from a batch within the Green Chemistry Centre of Excellence. Milled straw (< 125 µm) was supplied by Dr J Dodson. Both original and de-waxed wheat straws were utilized in this study. The de-waxed wheat straws used in this study were produced with the following steps: after hot extraction for 4 h with ethanol the wheat straws were then dried at room temperature. Waste paper fibres and pulp was provided by Sonoco-Alcore, Stainland Mill, Halifax.

The process of making paper sheets was shown in Figure 5.1 and Figure 5.2. At first, pulp and wheat straw powder were mixed together in a high speed blender (shown in Figure 5.1). After the preparation of the raw materials, the mixture was transfer into a cylindrical mould with litres of water. The mixture and water were then diffused thoroughly in the metal mould. The water was gradually removed from the mould and the wet paper sheet was left on the metal plate. Two pieces of absorbent paper and a smooth metal dish were put on the wet paper sheet and extra water was removed by pressing with a copper roller. Later, the crude paper sheet was fixed in a frisket and dried for 10 min with the temperature of 105^{o}C.

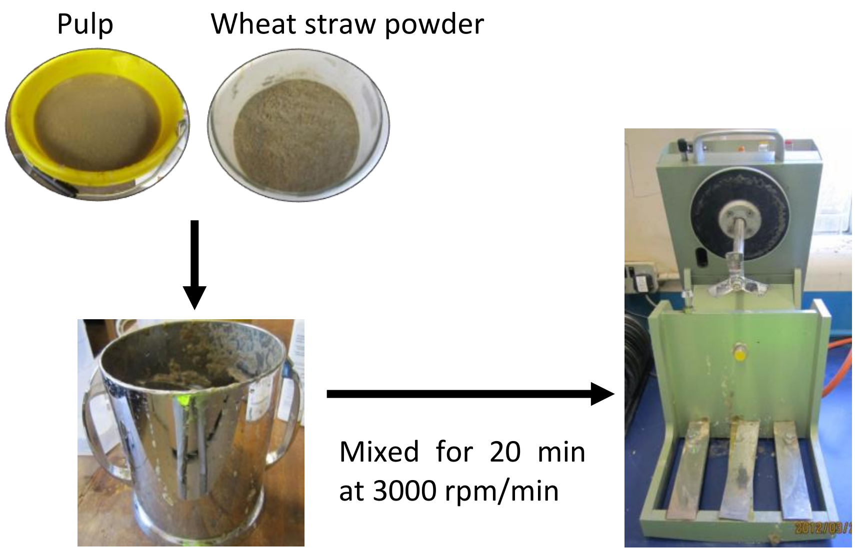

Figure 5.1 Preparation for wheat straw paper sheets

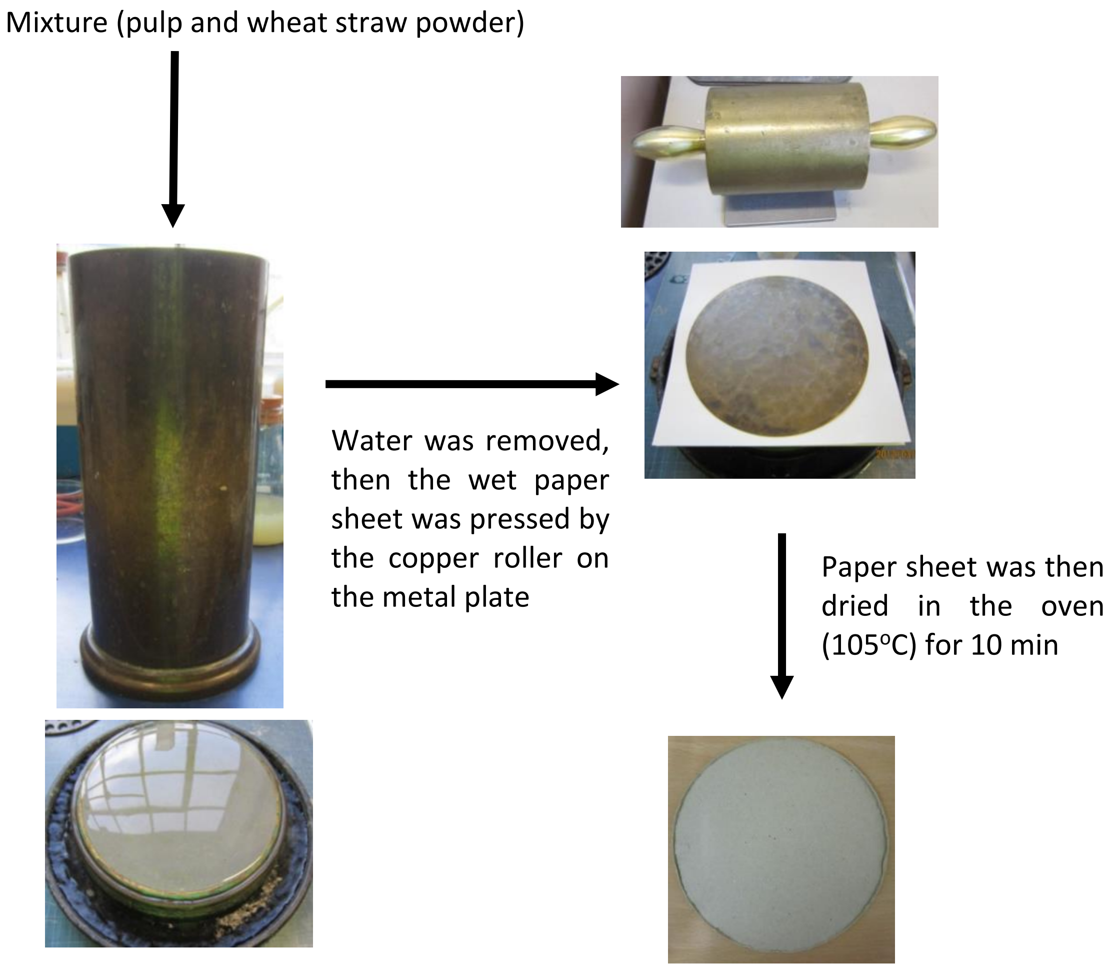

Figure 5.2 The procedure of making wheat straw paper sheets

Three samples were made for each type. One sample was prepared for water resistance test and other two samples were cut for tensile test. All samples were designed at same weight of 200 GSM (grams per square metre).

5.2 <u>Water adsorption capacity of cardboard</u>

The cardboard was fixed in the middle of the testing machine. And 100ml water was pulled into the system. The cardboard was took and weighted after 10 sec. The testing system was shown in Figure 5.3.

Figure 5.3 Water adsorption capacity test for cardboards

5.3 Silicate extraction form Ely Bottom ash—miscanthus

Ground bottom ash (35 g) was added to an aqueous potassium hydroxide solution of the required concentration (3M or 5M) and volume (100-400 ml), made up in a volumetric flask using distilled water. The mixture was heated in a Teflon round bottom flask with stirring under reflux for the appropriate time. Once the reaction was completed and allowed to cool, the mixture was separated by centrifuging for 30 min at 3000 rpm. The clear solution was decanted and stored in a sealed propylene bottle for further analysis.

$$SiO_2 + 2KOH \xrightarrow[180^{o}C\ -200^{o}C]{24h} K_2SiO_3 + H_2O$$

5.4 Silicate extraction form Ely Bottom ash—wheat straw

Potassium silicate was extracted from power station bottom ash (powder). This reaction was carried out at a temperature in the range 180^{o}C -200^{o}C for 24 h reflux in a Teflon round bottom flask. A starting mixture with a mass composition of 3 Ash: 1.4 KOH: 5 H_2O was prepared for extraction. For example, 3 g wheat straw ash powder (3 g) was mixed with potassium hydroxide (1.4 g) and distilled water (5 ml) contained in the Teflon flask and heated under reflux with rapid stirring for 24 h. When the extraction finished, the samples were left to cool to room temperature. Then the mixture was separated by centrifuging (3000-3500 rpm) for 30 minutes. The supernatant was decanted and stored in a sealed propylene sample bottle for further analysis.

5.5 <u>Soxhlet extraction of wheat straw</u>

In order to remove wax from wheat straw, wheat straw particles (1 mm-2 mm) were pre-treated by ethanol soxhlet extraction. For 1L scale, the extraction time was 8 h. For 2.5L scale, the extraction time was 12 h. After ethanol extraction, de-waxed wheat straw was air-dried in a fume cupboard for 24 h.

5.6 <u>MW Cardboards</u>

Cardboards were cut to a desired size (8 cm x 2 cm).

Process: The position of cardboard in the tubes are showed in Figure 5.4 and Figure 5.5.

Figure 5.4 Position 1 of MW cardboards

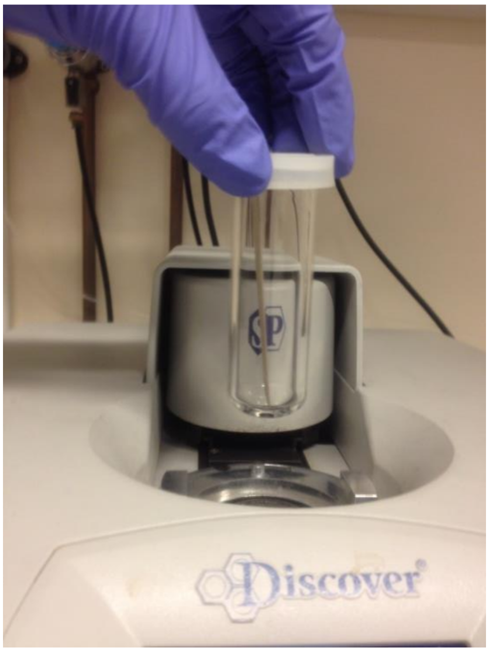

Figure 5.5 Position 2 of MW cardboards

All the experiments were carried out in Discover CEM-MW machine with fixed power and closed vessel model.

A brief procedure is shown in Figure 5.6.

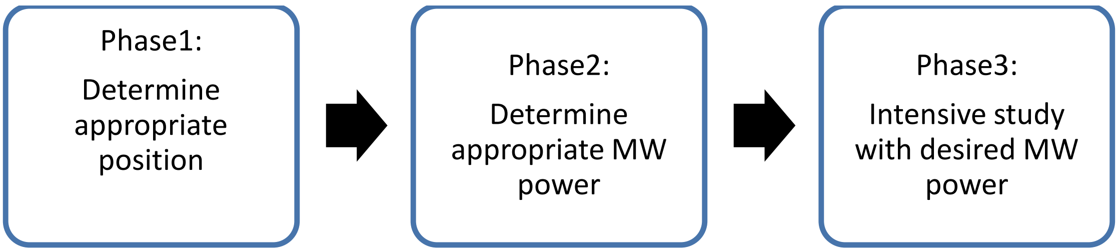

Figure 5.6 Procedure of MW cardboards

5.7 Synthesis of MCM-41 from biomass ash derived alkali silicate solution

Commercial K120 (1.64 ml) was mixed with CTAB (1 g) and H_2O (40 ml) at 85 ˚C. Ethyl acetate (3.1 ml) was added to this mixture with rapid stirring for 10 minutes. The solutions were left cool to room temperature. An aliquot (10 ml) of the reaction mixture was adjusted to pH 10 with either concentrated H_2SO_4 or concentrated NaOH. The solutions were then left to age at room temperature for 24 h. Following this the precipitates were filtered, washed with water and dried for 2 h at 100˚C and calcined at 550˚C for 4 h.

This synthesis was adapted for the biosilicate solution by replacing the K120 (1.64 ml) with the appropriate biosilicate solution. All other elements of the experiments remained the same. In order to have the same amount of silicon with K120, the volume or mass of biosilicate solution should be calculated in concentration.

5.8 Synthesis of SBA-15 using TEOS and biosilicate solution

Commercial Pluronic P123 (4 g) was dissolved water (29.8 ml) and 1M-aqueous HCl (116.5 ml) at 35 ^{o}C with constant stirring. Once the template was completely dissolved (approximately 2 h), tetraethylorthosilicate (TEOS, 9.05 ml) was added to the mixture and the solution left to stir for 20 h at 35 ˚C. The ensuing white solution/precipitate was aged at 80 ˚C (oil bath), for 24 h, without stirring. The resulting mixture was filtered under vacuum, washed with water, dried at room temperature overnight, and calcined at 500 ˚C for 6 hours in air.

This synthesis was adapted for the biosilicate solution by replacing the TEOS (9.05 ml) with certain biosilicate solution. All other elements of the experiments remained the same. In order to have the same amount of silicon with TEOS, the volume or mass of biosilicate solution should be calculated in concentration.

5.9 Titration

The titration of potassium silica solution is carried out in two contiguous steps.[111] In the first titration, the caustic component (K_2O) is determined:

$$K_2O \cdot SiO_2 + 2HCl + H_2O \rightarrow Si(OH)_4 + 2KCl$$

Later with the same sample, a second titration is carried out. An excess of solid sodium fluoride is then introduced, and hydroxide ions released by the reaction and equivalent to the SiO_2 content are then titrated:

$$Si(OH)_4 + 6NaF \rightarrow 4NaOH + Na_2SiF_6$$

$$4NaOH + 4HCl \rightarrow 4H_2O$$

To determine the end point methyl red was used as indicator. It was possible to carry out the titration in a usual glass flask since in quick titration of a solution with pH > 4.4 the glass practically does not dissolve. The determination is carried out in the following way. A volume of 0.5 ml of the potassium silica solution is taken in a glass flask, to which 20 ml of water and a few drops of methyl red are added. Then the alkali is titrated with 0.5M HCl solution until the red colour appears. To the second titration, 2.5 g of sodium fluoride and additionally 4-5 drops of methyl red are added. The alkali formed is titrated with the same 0.5 M HCl solution until the red colour appears.

5.10 Typical board formation procedure

Boards (5 cm x 5 cm) were produced with a procedure developed by Dr Mario de Bruyn. Whey protein (0.9 g) was dissolved in distilled water (2.7 g) and one half of the whey protein solution was added dropwise to the wheat straw before addition of silicate solution. Then silicate solution (12 g) was dropped over the de-waxed wheat straw (41 g) in three aliquots and mixed them completely. After that, another half of protein solution was added into mixture drop wise. Then the mixture was poured into a metal mould and pre-pressed for 1 min--5min. The pre-pressing time depended on the mixture materials. When the crude bioboard was formed, the metal box was removed and another aluminium platen was placed on the top of the crude board. Then the crude board was transferred to the hot-pressing machine. The materials were pressed for 8min with the temperature of 210 °C. In addition, the distance between the two hot plates was around 11.7 mm to make sure the thickness of bioboard was 10 mm after hot press. Finally, bioboard will be cut to 5x5 cm for further analysis.

5.11 Internal bond strength test

Internal bond strength tests of bioboards were carried out at University of York. Tests were carried out on an Instron analyser at a pull rate of 10 mm min^{-1}.

5.12 Tensile strength

Tensile strength tests of cardboard/paper sheets were carried out by Dennis Fell at the company of Sonoco-Alcore in Halifax.

5.13 Formulation of DIR boards

In this study, there were four procedures to produce DIR boards. Procedure 1, Procedure 2 and Procedure 3 were based on hot-press. Procedure 4 was based on oven heating.

Procedure 1:

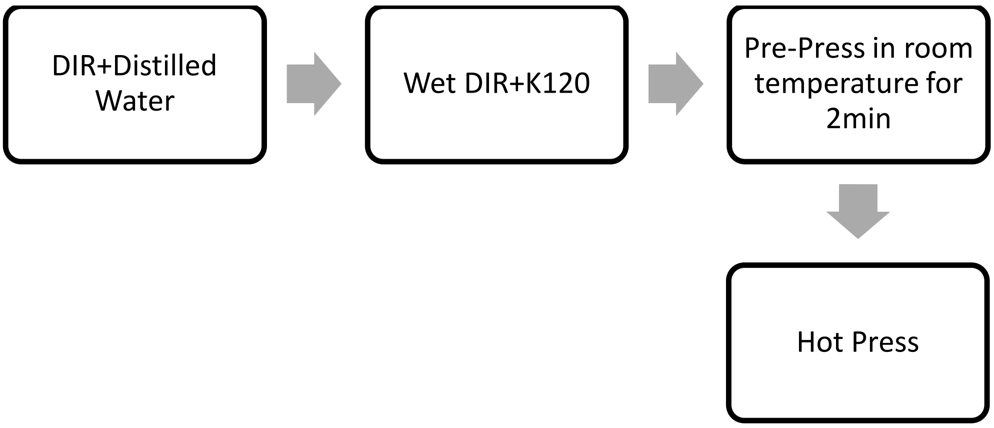

Procedure 2:

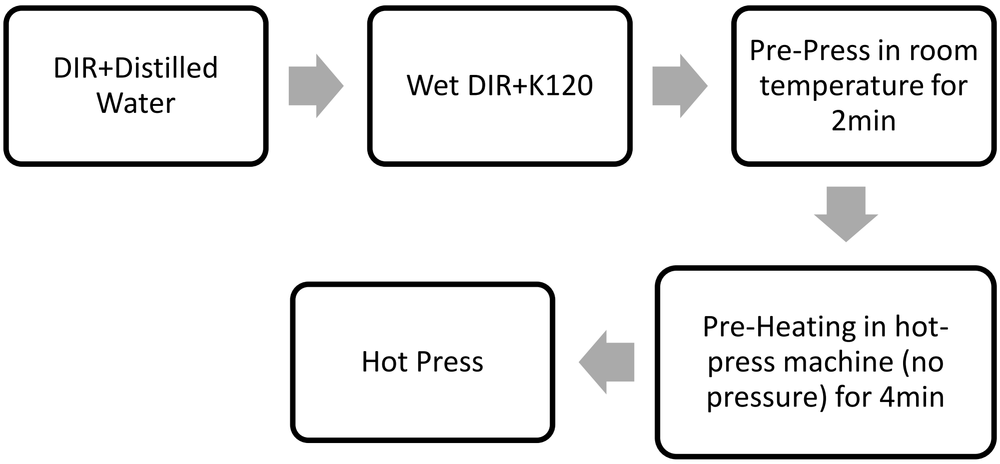

Procedure 3:

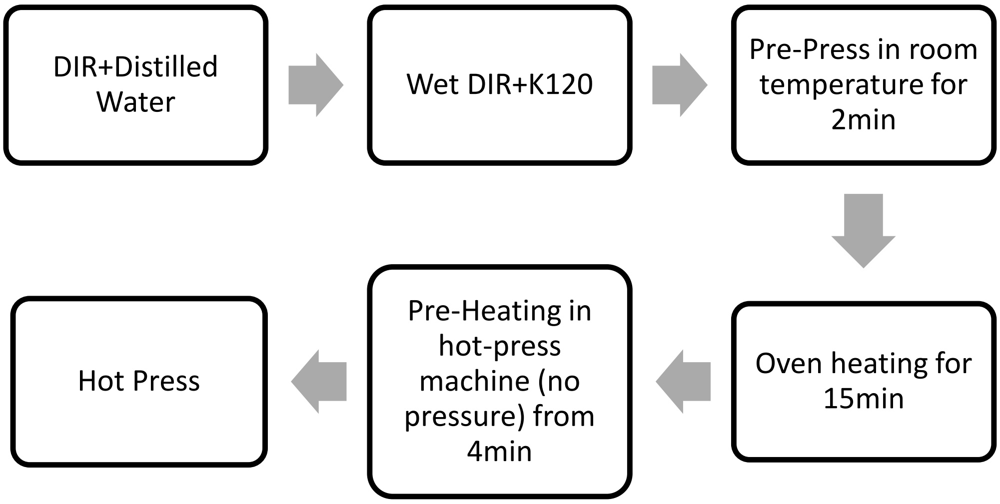

Procedure 4:

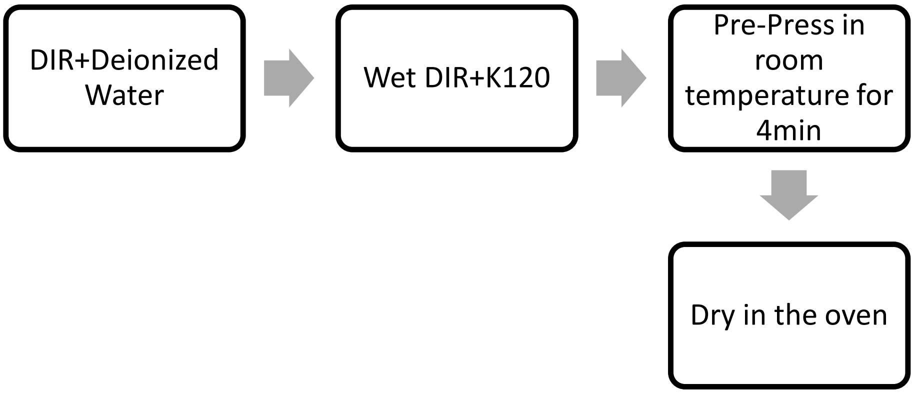

5.14 Analytical methods

pH Analysis

pH values were taken using Fisherbrand pH indicator paper.

Infrared Spectroscopy (IR)

A Bruker Vertex 70 FTIR spectrometer equipped with a MKII Golden Gate Single Reflection ATR System with a 45° diamond crystal was used to obtain infrared spectra. Solid powder samples were placed on the crystal surface and then clamped using a sapphire anvil. A drop of a liquid sample was placed on the crystal surface for analysis. Spectra were taken from 4000 cm^{-1} to 600 cm^{-1} at 64 scans with a spectral resolution of 4

cm^{-1}. A water or blank spectrum was used for the background. Bruker OPUS software was used for analysis of spectra.

Porosimetry

Nitrogen adsorption analyses were carried out at 77 K using a Micromeritics Tristar volumetric adsorption analyser. Prior to analysis, finely ground samples were outgassed at 180 °C for 1 h under nitrogen flow. Specific surface areas (S_{BET}) were analysed using the Brunauer, Emmett and Teller (BET) method and pore size was analysed using the Barrett, Joyner and Halenda method (BJH) method.

XRD

X-Ray diffraction patterns were obtained using a Bruker-AXS D8 Advance diffractometer with a Kristalloflex 760 X-ray generator which produces monochromatic Kα X-rays from a copper source. A powder sample was placed and levelled within a small round hole bevelled out of an aluminium sample holder. Scans were taken across the range 5 - 50 2θ for materials in Chapter 3 and 0.3 – 8 2θ for those in Chapter 2. A 45 kV voltage and 20 mA current were used during analysis.

TEM

Transmission electron microscopy was carried out by Dr Meg Stark at the Department of Biology, University of York. A small sample was suspended in ethanol and dropped onto a carbon grid to evaporate before analysis under vacuum.

NMR

Solid state ^{29}Si NMR was carried out by the Solid State NMR Research Service at the University of York using 400 MHz Bruker Avance III HD spectrometer equipped with a Bruker 4mm H(F)/X/Y triple-resonance probe and 9.4T Ascend® superconducting magnet operating at 79.51 MHz. The spectra with 5 ms contact times and same number of scans for all samples.

Solid-state ^{13}C CP/MAS spectra were acquired using a 400 MHz Bruker Avance III HD spectrometer equipped with a Bruker 4mm H(F)/X/Y triple-resonance probe and 9.4T Ascend® superconducting magnet. The CP experiments employed a 1.5ms linearly-ramped contact pulse, spinning rates of 12000 ± 2 Hz (or 9000 Hz), optimized recycle delays of 3 seconds, spinal-64 heteronuclear decoupling (at vrf=85 kHz) and are a sum of 512 co-added transients. Chemical shifts are reported with respect to TMS, and were referenced using adamantane (29.5 ppm) as an external secondary reference.

ICP

Inductively Coupled Plasma (ICP) analysis was performed using the departmental service utilising Agilent 7700x. Sample & Skimmer Cones was Ni, and analysis was run in He mode.

SEM

Scanning electron microscopy (SEM) was carried out by Dr Meg Stark at the Department of Biology, University of York.

Chapter 6:

Concluding Remarks and Further Work

Low value renewable resources including wheat straw, pea pod waste, DIR, miscanthus (bottom) ash, wheat straw (bottom) ash and cardboard/paper waste were successfully recycled and reused as raw materials to potentially high value materials, chemicals and bio-composites in this thesis.

Initially biomass ash contained high value in silicon had been used as silicon resource to extract biosilicate solutions. Systematic methods for extracting reliable concentrations of silicate were described. Both miscanthus and wheat straw ash proved to be available materials for extracting biosilicate solutions. Biosilicate solutions extracted from miscanthus ash were applied to the process of bioboards. A fully green process to making bioboards was investigated and explored in this project. Biosilicate solutions as the replacement of urea formaldehyde were aimed to reduce the cost of producing boards, eliminate the risk to human health, provide a sustainable developing route and be environmental friendly products. Wheat straw and pea pod also performed the potential value to be the resources in board process. Bioboards under the green process had certain physical and mechanical properties as the considerable internal bond strength. For paper de-inking waste, DIR mixture with high moisture content (>38.7%) can also form hard boards under both oven dry and hot-press. Long-time oven dry successfully formed relative hard DIR boards except the irregular size and structures as the vapour rise during the slow heating. Hot-press gave huge pressure on the mixture in which case the binders (biosilicate solutions) were pressed out. Although high moisture content helps the formation of DIR boards, it also dilutes the concentration of biosilicate solutions and brought issues when using hot-press.

Bio-MCM-41 and bio-SBA-15 were successfully synthesised from wheat straw (bottom) ash extracts named biosilicate solutions. These kinds of mesoporous materials were fully analysed by N_2 Adsorption Porosimetry, XRD, TEM and solid-state ^{29}Si NMR. These mesoporous materials showed considerable large surface area, pore size and pore structure though parts of bio-SBA-15 did not correspond with the typical SBA-15. Also, significant ordered arrangement of pore, structure and the hexagonal arrays were clear found in most bio-MCM-41 and bio-SBA-15 samples.

Wheat straw powder was used as an alternative additive or filler in cardboard/paper sheets to reduce the cost and improve the tensile strength. It was clear that low ratio de-waxed wheat straw powder had a positive influence on the tensile strength of cardboard/paper sheets. De-waxed wheat straw cardboard/paper sheets with the tensile index of 30-34 Nm/g were comparable to the virgin cardboard/paper sheets with a tensile index of 30-32 Nm/g.

Low temperature microwave was successfully to form or produce a sticky surface of cardboard waste. After low temperature microwave low molecular weight organic matter was 'extracted' and stick on the surface of cardboard. FT-IR and solid-state ^{13}C NMR had verified the evidence of organic matter in the aqueous phase and the surface of cardboards. The direction of MW also influenced the efficiency of pyrolysis in this process. Parts of cardboards were burnt if the MW power was higher than 50 W for longer time (> 5 min). But in this case, the yield of bio-oil definitely increased which contained abundant levoglucosan.

Green process of producing bioboards provides an alternative route for reusing and recycling renewable resources. Materials or biomass contained rich silicon were all possibly to be extracted to get biosilicate solutions which was already used as binder in this project. Wheat straw (bottom) ash was successfully used as silicon resource to synthesis mesoporous silica. Other kinds of biomass ash can also to be applied in this synthesis. In contrast to typical MCM-41 and SBA-15, bio-MCM-41 and bio-SBA-15 had significant advantages in surface area and pore size and disadvantages in pore structure. The pore structure and order of bio-mesoporous silica were relatively worse than typical mesoporous silica as the existence of residue and high pH value. If these problems can be solved in future work, then bio-meosporous silica will have a better prospect.

Various biomass and waste materials also can be used as raw materials in bioboards process, such as tea waste, miscanthus and other kinds of paper waste that contained rich cellulosic components. Since cardboards will have a sticky surface after microwave, further work should focus on the development of various approaches to apply MW on cardboards.

Abbreviations

ATCM	Airborne toxic control measure
ATR	Attenuated total reflectance
BET	Brunauer, Emmett and Teller
BJH	Barrett, Joyner and Halenda
CARB	Air Resources Board
CEPI	Confederation of European Paper Industries
CP/MAS	Cross-polarization/magic angle spinning
DIR	De-inked residue
EU	European Union
FT-IR	Fourier transform – Infrared spectroscopy
GC-MS	Gas Chromatography Mass Spectrometry
GSM	Gram per square metre
HDF	Hard fibreboards
HB	Hardboards
HPLC	High-performance liquid chromatography

HWPW	Hardwood plywood
IBS	Internal bond strength
ICP-MS	Inductively coupled plasma – mass spectroscopy
IUPAC	International Union of Pure and Applied Chemistry
MD	Medium boards
MDF	Medium fibreboards
MW	Microwave
NMR	Nuclear Magnetic Resonance
MSDS	Material safety data sheets
PB	Particleboard
TEM	Transmission Electron Microscopy
TEOS	Tetraethyl orthosilicate
TG	Thermogravimetric
TS	Tensile strength
SEM	Scanning electron microscopy
UF	Urea Formaldehyde
UK	United Kingdom
USA	United States of American

VOCs	Volatile organic compounds
WS	Wheat straw
WSA	Wheat straw ash
XRD	X-Ray diffraction

References

1. D. Hoornweg, P. B. Tata and C. Kennedy, *Nature*, 2013, **502**, 615-617.
2. J. Gustavsson and R. V. Otterdijk, presented in part at the Interpack2011, Düsseldorf, Germany, 2011.
3. *Waste or resource? Stimulating a bioeconomy*, London : The Stationery Office Limited, 2014.
4. Commission proposes strategy for sustainable bioeconomy in Europe, http://europa.eu/rapid/press-release_IP-12-124_en.htm (last accessed 01/09/2012).
5. P. T. Anastas and J. C. Warner, *Green Chemistry: Theory and Practice*, Oxford University Press, USA, 2000.
6. Andrew Atkinson and Clint Wheelock, *EXECUTIVE SUMMARY: Green Chemistry Bio-based Chemicals, Renewable Feedstocks, Green Polymers, Less-toxic Alternative Chemical Formulations, and the Foundations of a Sustainable Chemical Industry* 2011.
7. G. Bollero M. Maughan, D. K. Lee, R. Darmody, S. Bonos, L. Cortese, J. Murphy, R. Gaussoin, M. Sousek, D. Williams, L. Williams, F. Miguez and T. Voigt, *GCB Bioenergy*, 2012, **4**, 253-265.
8. J. Copeland and D. Turley, *National and regional supply/demand balance for agricultural straw in Great Britain* C. S. L. Agri-Environment and Land Use Strategy Team, 2008.
9. Cereals and oilseed rape production in the UK 2011 Defra Statistics:, http://www.defra.gov.uk/statistics/foodfarm/food/cereals/cerealsoilseed/ (last accessed 10/06/2014).
10. HGCA, *The wheat growth guide (Spring 2008, second edition)*, 2008.
11. Ely Power Station, http://www.eprl.co.uk/our-sites (last accessed 30/07/2015).
12. E. C. Cooper, Doctor of Philosophy, University of York, 2012.
13. P. Zhao and Q. Shao Y. Shen, *Microporous and Mesoporous Materials*, 2014, **188**, 46-76.
14. S. Jin and H. Chen, *Process Biochemistry*, 2007, **42**, 188-192.
15. D. X. Liu Zhang, and Z. Li, *China Pulp and Paper*, 1990, 16-21.
16. E. Billa and B. Monties, *Cellulose Chem. Technol*, 1995, **29**, 305-314.
17. J.C Roberts, *The Chemistry of Paper*, The Royal Society of Chemistry, 1996.
18. B. Heublein D. Klemm, Hans-Peter Fink and A. Bohn, *Angew. Chem. Int. Ed*, 2005, **44**, 3358-3393.
19. W. T. Mckean and R. S. Jacobs, *Wheat Straw as a Paper Fiber Source*, P. N. E. Region, 1997.
20. Badal C. Saha and Michael A. Cotta Nasib Qureshi, *Bioprocess and Biosystems Engineering*, 2007, **40**, 437-445.
21. J. Carmona A. Barneto, J. E. Alfonso and L. Alcaide, *Bioresour. Technol*, 2009, **100**, 3963-3973.
22. D. Wang and X. S. Sun, *Industrial Crops and Products*, 2002, **15**, 43-50.

23. Report for HGCA_DEFRA, LK0850: *Inorganic Polymer Bio-composites (IPBC),* RD-2007-3368, 2014.
24. B. M. Jenkins D. C. Dayton, S. Q. Turn, R. R. Bakker, R. B. Williams, D. Belle-Oudry and L. M. Hill, *Energ. Fuel*, 1999, **13**, 860-870.
25. D. L. Klass, *Encyclopedia of Energy*, 2004, **1**, 193-212.
26. M. L. Sander and O. Andren, *Water Air Soil Pollut*, 1997, **93**, 93-108.
27. H. Buchtová and M. Rýznarová P. Janos, *Water Res*, 2003, **37**, 4938-4944.
28. L. F. Vilches A. Gómez-Barea, C. Leiva, M. Campoy and C. Fernández-Pereira, *Chem. Eng. J*, 2009, **146**, 227-236.
29. A. Elliott and T. Mahmood, *Tappi J*, 2006, **5**, 9-16.
30. S. Sarenbo, *Biomass Bioenerg*, 2009, **33**, 1212-1220.
31. P. Vesterinen, Wood Ash Recycling: State of the Art in Finland and Swede, http://www.cti2000.it/solidi/WoodAshReport%20VTT.pdf (last accessed 20/03/2011).
32. S. Wang and L. Baxter, presented in part at the Science in Thermal and Chemical Biomass Conversion, ed, 2006.
33. A. Fraaij D. G. Nair, A. A. K. Klaassen and A. P. M. Kentgens, *Cement Concrete Res*, 2008, **38**, 861-869.
34. P. Chindaprasirt and S. Rukzon, *Constr. Build. Mater*, 2008, **22**, 1601-1606.
35. T. Saeting W. Tangchirapat, C. Jaturapitakkul, K. Kiattikomol and A. Siripanichgorn, *Waste Manage*, 2007, **27**, 81-88.
36. S. Y. Wu Y. Q. Wu, Y. Li and J. S. Gao, *Energ. Fuel.*, 2009, **23**, 5144-5150.
37. P. A. Jensen and M. Dam-Johansen S. Arvelakis, *Energ. Fuel.*, 2004, **18**, 1066-1076.
38. D. Belle-Oudry and D. Dayton, *Impact of Mineral Impurities in Solid Fuel Combustion*, Kluwer Academic / Plenum Publishers, New York, 1999.
39. J. R. Dodson, Doctor of Philosophy, University of York, 2011.
40. FAOSTAT, http://faostat.fao.org/site/630/default.aspx (last accessed 01/09/2015).
41. FAOSTAT, Forestry Production and Trade, http://faostat3.fao.org/browse/F/*/E (last accessed 26/09/2015).
42. California Air Resources Board, Fact Sheet: Airborne Toxic Control Measure (ATCM) to Reduce Formaldehyde Emissions from Composite Wood Products.
43. S. I. Aronovsky, A. J. Ernst, H. M. Stucliffe, and G. H. Nelson, *Paper Trade Journal*, 1948, **126**, 78.
44. G. Nemli and I. Öztürk, *Build. Environ*, 2006, **41**, 770-774.
45. A. Ghosh and M. Sain, *Polym. Polym. Compos*, 2006, **14**, 217-227.
46. Bruze M and J. Occup Z. E. Isaksson M, *Environ. Med*, 1999, **41**, 261-266.
47. P. K. Dutta and D. C. Shieh, *Zeolites*, 1985, **5**, 135-138.
48. Environment Protection Agency, An Introduction to Indoor Air Quality, http://www.epa.gov/iaq/formalde.html (last accessed 10/08/2014).
49. L. Zhang S. Shu, F. Ming and M. Xia, *Chinese Academy of Forestry*, 2006, **8**, 41-45.
50. PQ Corporation, *Bulletin 12-31: Bonding and Coating Applications of PQ Soluble Silicates*, 2006.
51. P.M. Gill, PQ Corpration, 1997.
52. A. Rabbii, *Iranian Polymer Journal*, 2001, **10**, 229-235.
53. S. Halvarsson, Doctor of Technology, Mid Sweden University, 2010.
54. SpecialChem, http://www.specialchem4adhesives.com/resources/adhesionguide/index.aspx?id=theory4 (last accessed 10/10/2014).
55. J. Vac, *Sci. Technol. B*, 2003, **21**, 6.

56. B. Bhushan, *Principles and Applications of Tribology, 2nd Edition*, Wiley, 2013.
57. B. Bhushan, *Introduction to Tribology, 2nd Edition*, Wiley, 2013.
58. W. D. Callister, *Materials Science and Engineering--An Introduction, 5th Edition*, Wiley, 1999.
59. M. Hein and S. Arena, *Foundations of College Chemistry, 10th Edition*, Wiley, 2003.
60. G. W. Tormoen E. R. Beach, J. Drelich, and R. Han, *J. Colloid Interface Sci*, 2001, **247**, 81.
61. W. A. Zisman, *Ind. Eng. Chem*, 1963, **55**, 19.
62. J. Mahanty and B. W. Ninham, *Dispersion Forces*, New York : Academic Press, 1976.
63. J. Ferrante D. H. Buckley, M. D. Pashley and J. R. Smith, *Mater. Sci. Eng*, 1986, **83**, 169.
64. J. N. Israelachvili, *Intermolecular and Surface Forces, 2nd Edition*, Academic, San Diego, 1992.
65. Horacio E. Bergna and William O. Roberts, *Colloidal Silica: Fundamentals and Applications*, CRC Press, 2005.
66. K. Tamai and J. F. Ma, *New Phytol*, 2003, **158**, 431-436.
67. S. Hinke J. Mecfel, W. A. Goedel, G. Marx, R. Fehlhaber, E. Bäucker and O. Wienhaus, J. Plant Nutr, *Soil Sci*, 2007, **170**, 769-772.
68. Duy M. Sørensen Le, Hanne R. Knudsen, Niels Ole Meyer and Anne S., *Biofuels, Bioproducts and Biorefining*, 2015, **9**, 109-121.
69. C.J. Brinker, *Journal of Non-Crystalline Solids*, 1998, **100**, 31–50.
70. Stöber W, *Advances in Chemistry*, 1967, **67**, 161–182.
71. B. A. Fleming, *Journal of Colloid and Interface Science*, 1986, **110**, 40-64.
72. G.S Wirth and J.M Gieskes, *Journal of Colloid and Interface Science*, 1979, **68**, 492-500.
73. R. J. Balec and S. D. Kinrade C. T. G. Knight, *Angew. Chem., Int. Ed*, 2007, **46**, 8148-8152.
74. A. P. J. Jansen and R. A. van Santen T. T. Trinh, *J. Phys. Chem. B*, 2006, **110**, 23099-23106.
75. PQ corporation, *Bonding and coating applications of PQ® soluble silicates*, 2010.
76. D. Zeigan G. Engelhardt, H. Jancke, D. Hoebbel and W. Wieker, *A. Anorg. Allg. Chem*, 1975, **418**, 17-28.
77. G. Engelhardt and D. Michel, *High-Resolution Solid-State NMR of Silicates and Zeolites*, John Wiley, New York, 1987.
78. J. L. Bass and G. L. Turner, *J. Phys. Chem. B*, 1997, **101**, 10638-10644.
79. C. F. Weber and R. D. Hunt, *Ind. Eng. Chem. Res*, 2003, **42**, 6970-6976.
80. M. Agarwal I. Halasz, R. Li and N. Miller, *Catal. Lett*, 2007, **117**, 34-42.
81. M. E. Leonowicz C. T. Kresge, W. J. Roth, J. C. Vartuli and J. S. Beck, *Nature*, 1992, **358**, 710-712.
82. J. C. Vartuli J. S. Beck, W. J. Roth, M. E. Leonowicz, C. T. Kresge, K. D. Schmitt, C. T. W. Chu, D. H. Olson, E. W. Sheppard, S. B. McCullen, J. B. Higgins and J. L. Schlenker, *J. Am. Chem. Soc*, 1992, **114**, 10834-10843.
83. A. Corma, *Chemical Reviews*, 1997, **97**, 2373-2242.
84. L. Mercier and T. J. Pinnavaia, *Adv. Mater*, 1997, **9**, 500-503.
85. A. A. Kurganov M. Grün, S. Schacht, F. Schüth and K. K. Unger, *J. Chromatogr. A*, 1996, **740**, 1-9.

86. L. J. Yun M. Bhagiyalakshmi, R. Anuradha and H. T. Jang, *J. Hazard. Mater*, 2010, **175**, 928-938.
87. Q. Huo D. Zhao, J. Feng, B. F. Chmelka and G. D. Stucky, *J. Am. Chem. Soc*, 1998, **120**, 6024-6036.
88. J. L. Feng D. Y. Zhao, Q. S. Huo, N. Melosh, G. H. Fredrickson, B. F. Chmelka and G. D. Stucky, *Science*, 1998, **279**, 548-552.
89. A. Taguchi and F. Schüth, *Microporous Mesoporous Mater*, 2005, **77**, 1-45.
90. J. Cooney and E. Magner S. Hudson, *Angew. Chem. Int. Ed.*, 2008, **47**, 8582-8594.
91. S. J. Gregg and K. S. W. Sing, *Adsorption, surface area, and porosity*, Academic Press, 1991.
92. G. L. Haller, A. V. Neimark and P. I. Ravikovitch, *Adv. Colloid Interface Sci.*, 1998, **76-77**, 203-226.
93. S. Chiarakorn, J. Wittayakun and N. Grisdanurak, *Korean J. Chem. Eng.*, 2003, **20**, 950-955.
94. K. S. Hui and C. Y. H. Chao, *J. Hazard. Mater.*, 2006, **137**, 1135-1148.
95. K.-S. You G. Chandrasekar, J.-W. Ahn and W.-S. Ahn, *Microporous and Mesoporous Materials*, 2008, **111**, 455-462.
96. Particle board, http://www.woodproducts.fi/content/particle-board (last accessed 30/07/2015).
97. European Standard EN 312 : 2003 has the status of a DIN Standard, 2003.
98. F. Fu and H. Pan C. Hse, *Forest Products Journal*, 2008, **58**, 56-61.
99. R. G. Hagens, M.l McDonald and W. Millard, *Adhesive compositions for corrugated boxes, Canada Pat. CA2288808A1,* 2000.
100. I. Mateos-Aparicio and A. Redondo-Cuenca, *LWT-Food Science and Technology*, 2010, **43**, 1467-1470.
101. CEPI, *Production of paper and board in Europe in full transformation* 2015.
102. *Bubbling bed FBC process for the conversion of paper (de-inking)residue*, 2015.
103. Pratima Bajpai, *Management of Pulp and Paper Mill Waste*, Springer, 2015.
104. Jiménez L and García JC, *Bioresource Technology*, 2001, **79**, 23-27.
105. Jiménez L and García JC, *Process Biochemistry*, 2002, **37**, 665-672.
106. Christopher J. Biermann, *Handbook of Pulping and Papermaking, 2nd Edition*, Academic Press, 1996.
107. E. Sjostrom, *Wood Chemistry: Fundamentals and Applications publisher*, Academic Press Inc, 1981.
108. Chemistry Glossary Definition, http://chemistry.about.com/od/chemistryglossary/g/polymerdef.htm (last accessed 30/03/2012).
109. Z. Zhang, MacQuarrie, D. J., De Bruyn, M., Budarin, V. L., Hunt, A. J., Gronnow, M. J., Fan, J., Shuttleworth, P. S., Clark, J. H. and Matharu, A. S, *Green Chemistry*, 2015, **17**, 260-270.
110. M. Foston, *Energy biotechnology*, 2014, **27**, 176-184.
111. V. E. Sokolovich, *Glass and Ceramics*, 1963, **20**, 471-472.